DYNAMICS OF NANOPARTICLES IN POLYMER NANOCOMPOSITES

A Dissertation

Presented to the Faculty of the Graduate School

of Cornell University

In Partial Fulfillment of the Requirements for the Degree of

Doctor of Philosophy

by

Pooja Nath

December 2018

DYNAMICS OF NANOPARTICLES IN POLYMER NANOCOMPOSITES

Pooja Nath, Ph. D.

Cornell University 2018

Polymer nanocomposites are materials comprising of nanometer-sized particles embedded inside polymers. The study of dispersion and dynamics of nanoparticles in polymer matrices has important implications in the processing and long-term stability of polymer nanocomposite materials, which have found application in areas such as packaging, energy storage, and biomedical devices, among others. Another factor guiding our interest in such studies is the occurrence of noncontinuum dynamical behaviors as particle sizes become comparable or smaller than the radius of gyration (R_g) of the host polymers. In simple fluids such as polymer melts and solutions where particle size is much greater than the radius of gyration of the host polymer, the long-time particle dynamics obeys random-walk statistics, and the bulk zero-shear viscosity of the material determines the drag experienced by the particle. In contrast, in polymer liquids (melts or solutions) where particle size is smaller than the radius of gyration of the host, the effective frictional resistance to probe motion arises from localized motion of polymer chain segments with size similar to those of the nanoparticle probes.

We utilize a combination of theoretical and experimental techniques to examine the noncontinuum diffusion of nanoparticles in polymer nanocomposites. Through fluorescence microscopy we track the motion of nanoprobes in aqueous solutions of linear polyethylene oxide and probe particle dynamics in different regimes of particle

diameter (d), with respect to characteristic polymer length scales, viz., the correlation length (ξ), the entanglement mesh size (a), and the radius of gyration (R_g).

We show that in entangled polymer solutions when particle size becomes greater than the entanglement tube diameter, nanoparticle dynamics transition from diffusive to subdiffusive, reminiscent of particle transport in a field with obstructions. This last finding is in stark contrast to the nanoparticle dynamics observed in entangled polymer melts where X-ray photon correlation spectroscopy measurements reveal hyperdiffusive dynamics. The conventional wisdom surrounding hyperdiffusive processes calls for the presence of residual stresses or force fields that can bias particle motion. While this can explain the occurrence of hyperdiffusion in aggregating particles or materials close to their glass transition temperatures, this argument cannot explain the occurrence of hyperdiffusion in non-aging and uniform nanoparticle-laden polymer melts or solutions. We design a simple theoretical framework to understand the origins of diffusive and subdiffusive dynamics observed in entangled polymer solutions against the hyperdiffusive dynamics observed in entangled polymer melts and study the role of solvents in setting structural correlations in polymer nanocomposite systems.

BIOGRAPHICAL SKETCH

Pooja Nath was born in Solan, a scenic town in the state of Himachal Pradesh, India, in 1991. Both her parents held PhD in agricultural sciences and worked as professors in the University of Horticulture and Forestry in Solan district. She grew up in a household where science education was encouraged and since a young age enjoyed reading advanced texts on medicine, plant science and behavioral sciences. After clearing the Joint Entrance Exam (JEE) in 2009, she joined the Indian Institute of Technology Delhi in the field of Chemical Engineering. Here she became exposed to research in Computational Fluid Mechanics and decided to pursue a minor in the field of Applied Mechanics. Through a short summer internship in the Industrial Technology Research Institute (ITRI) in Hsinchu, Taiwan, where she worked on alkaline water electrolyzers, she not only gained a first-hand experience in independent research but also began to understand the role of chemical engineering fundamentals in the development of renewable energy technologies.

Her joint interest in fluid mechanics and renewable energy prompted her to join Prof. Lynden Archer's group in Cornell University in 2013. Here she got the opportunity to work on multiple projects that satisfied both her curiosities and eventually became interested in the question of transport anomalies in polymer nanocomposites.

To the memory of my grandfather, Jaswant Singh Ahluwalia

ACKNOWLEDGMENTS

There are several people who through their contributions, great or small, have made the entirety of this work possible. I would first and foremost acknowledge the efforts and insight provided by my advisor, Prof. Lynden Archer. His comments and critiques have played a critical role in allowing me to develop my identity as a researcher. The vast extent of his intellectual endeavors, his enthusiasm for science, and his curiosity have inspired me to always strive to further my knowledge and not be afraid of undertaking research in new fields of study. I am also thankful to my committee members Prof. Donald Koch and Prof. David Muller for their support during the course of my PhD.

I would also like to thank Prof. Warren Zipfel for his enlightening discussions on microscopy methods and his interest in my research. I also want to thank the Becky, Johanna and Carol at BRC for their kindness and patience. I am also grateful to Ferdinand Kohle and Prof. Uli Wiesner for sharing their expertise on synthesis and imaging of *C dot* probes with me. I also want to thank Suresh Narayanan, and the other staff scientists working at sector 8-ID-I in Argonne National Lab for supporting me during my experiments at the APS. I am also thankful to Detlef Smilgies, Brenda Fischer, Glenn Swan, and Phillip Carubia for their support and expertise.

I also want to thank my collaborators: Lin, Ferdinand, Rahul, Kayla, Deniz, Yalcin, Shuya, Snehashis, Sanjuna, Zhengyuan, Mukul and Mun. I am really thankful for the opportunity to have worked with them and I have learnt a lot from everyone. I would like to thank the Archer group members, both old and new, who I had the pleasure of coming in contact with during my stay in Ithaca. I am especially thankful to Rahul for teaching me hairy nanoparticle synthesis and always being available to discuss about polymer physics. I would also like to thank Lin, for making lab work seem very enjoyable and for always sharing pictures of her adorable cat to cheer me up.

I am really thankful to the friends I made in Ithaca: Apoorva, Taru, Meredith, Pankaj, Abhishek, Himashu and Jinna. Over the course of my stay in Cornell, I obtained several opportunities to develop and hone my teaching skills. I am thankful to all the instructors, and graduate and undergraduate TAs I was able to work with. I am also thankful to Anne Poduska, and the team at Engineering Learning Initiative who gave me the opportunity to work as a TA development consultant. I am especially thankful to my co-facilitator Reece, who I worked with really closely and learnt a lot from, and also my fellow consultants: Brendan, Katherine, Jansen, Aravind, Ana and Xiaoyang. I am also indebted to my family and friends back home for their patience. I am sorry that I had to miss several trips, weddings, and events during these five years. I am eternally grateful to my parents and my brother for always motivating me to be better and stronger. I am also extremely thankful to Ritesh for his encouragement and unwavering support during my PhD journey.

TABLE OF CONTENTS

1. Introduction **1**

1.1 Polymer Nanocomposites 1

1.2 Nanoparticle Dynamics in Polymer Nanocomposites 5

1.3 Outline of Thesis 10

Bibliography 13

2. Theory of Anomalous Diffusion in Polymer Nanocomposites **19**

2.1 Introduction 19

2.2 Theory 20

2.3 Results and Discussion 38

2.4 Conclusions 46

Bibliography 48

3. Effects of Interparticle Correlations on Particle Dynamics in Solutions of Hairy Nanoparticles **53**

3.1 Introduction 53

3.2 Experimental Methods 54

3.3 Results and Discussion 57

3.4 Conclusions 61

Bibliography 63

4. Dynamics of Nanoparticles in Entangled Polymer Solutions **65**

Abstract 65

4.1 Introduction 66

4.2 Experimental Methods 71
4.3 Results and Discussion 76
4.4 Conclusions 89
Bibliography 91

APPENDIX A Modeling Particle Caged in a Polymer Entanglement 102
APPENDIX B Supplementary Information for Chapter 4 110

LIST OF FIGURES

1.1 A schematic of polymer nanocomposites studied in this work. We study the dynamical behavior of polymer grafted nanoparticles: (a) under self-suspended or solvent-free conditions, (b) dispersed in entangled polymer melts, (c) dispersed in solvents, and (d) dispersed in solutions of entangled polymers. 11

2.1 Schematic of the typical mean squared displacement, $\left\langle \Delta r^2(t) \right\rangle$ versus time plot for a particle of size *d*, embedded in a polymer network with tube diameter *a*, given the condition that *d* is greater than *a*, but is smaller than radius of gyration (R_g) of the host polymer. The particle motion follows the scaling $\left\langle \Delta r^2(t) \right\rangle \sim t^2$ up to the ballistic time, τ_{bal}, past which it begins to follow the motion of surrounding chains subdiffusively within the entanglement where it stays till the hopping time τ_{hop}. Scaling theory and MD simulations indicate that beyond this time, nanoparticle hopping and relaxation of surrounding chains can proceed in tandem to allow the nanoparticle to move diffusively. 26

2.2 Plots of the concentration relaxation time normalized by k_{off}^{-1} as a function of the square of length scale $l^2/4\pi^2$ normalized by k_{on}/D_M for $K_{eq} = k_{on}/k_{off}$ = (a) 10, (b) 100, (c) 1000, and (d) 10^4. These plots are based on the association-dissociation model for reversible networks given by Olsen and co-workers. The different curves correspond to different values of the ratio, γ. 33

2.3 Plot of mean squared displacement ($\left\langle \Delta r^2(t) \right\rangle$) normalized by square of the particle radius R_M versus time normalized by the diffusive time for a free particle (R_M^2/D_M) for different values of the ratio of diffusivity of the

cluster and the free particle γ = (a) 0.1, (b) 0.01 (c) 0.001, (d) 0.0001, and (e) 0.00001. Different curves correspond to different values of the parameter K_{eq}. 39

2.4 Mean-squared displacement ($\langle \Delta r^2(t) \rangle$) normalized by the $2D_M t$ plotted against time normalized by the diffusive time for a free particle, R_M^2/D_M for different values of the ratio of diffusivity of the cluster and the free particle γ = (a) 0.1, (b) 0.01 (c) 0.001, (d) 0.0001, and (e) 0.00001. Different curves correspond to different values of the parameter K_{eq}. 41

2.5 Plot of mean squared displacement ($\langle \Delta r^2(t) \rangle$) normalized by square of the particle radius R_M versus time normalized by the diffusive time for a free particle (R_M^2/D_M) for different values of K_{eq} = (a) 0.1, (b) 0.01 (c) 0.001, (d) 0.0001, and (e) 0.00001. Different curves correspond to different values of the parameter γ. 43

2.6 Mean-squared displacement ($\langle \Delta r^2(t) \rangle$) normalized by the R_M^2 for γ = (b) 0.001, (d) 10^{-4} (f) 10^{-5}; and normalized by $2D_M t$ for γ = (b) 0.001, (d) 10^{-4} (f) 10^{-5}. The x-axis corresponds to the time scaled by the diffusive time for the free particle. Different curves correspond to different values of the parameter K_{eq}. 45

3.1 (a) Scattering intensity, *I(q)*, in arbitrary units for PEG5000-SiO_2 particles in DEP for different volume fraction of silica nanoparticles φ at 90 ^oC plotted against the wave vector q (units nm^{-1}). (b) Structure factor, *S(q)*, for PEG5000-SiO_2 particles in DEP for different volume fraction of silica nanoparticles φ at 90 ^oC plotted against the wave vector q (units nm^{-1}) multiplied by the average core radius, *a*. 56

3.2 (a) Scattering intensity, *I(q)*, in arbitrary units for PEG500-SiO_2 particles in ionic liquid for different volume fraction of silica nanoparticles φ at 25

^{o}C plotted against the wave vector q (units nm^{-1}). (b) Structure factor, *S(q)*, for PEG500-SiO_2 particles in ionic liquid for different volume fraction of silica nanoparticles φ at 25 ^{o}C plotted against the wave vector q (units nm^{-1}) multiplied by the average core radius, *a*. (c) The interparticle distance, d_{p-p}, plotted as a function of silica volume fraction φ. 59

3.3 (a) Relaxation time versus wave vector for PEG5000-SiO_2 particles in DEP for different volume fraction of silica nanoparticles φ at 70 ^{o}C plotted against the wave vector *q* (units nm^{-1}). (b) Relaxation time versus wave vector for PEG500-SiO_2 particles in ionic liquid for different volume fraction of silica nanoparticles φ at 25 ^{o}C plotted against the wave vector *q* (units nm^{-1}). The dashed line indicates a q^{-1} scaling and solid line indicates a q^{-2} scaling. 62

4.1 Schematic of C-Dots dispersed in long chain polyethylene glycol solutions in water tracked via both FCS and single particle tracking. 72

4.2 Log-log plots of *D/Ds* (diffusivity scaled by diffusivity of particles in solvent) against the polymer volume fraction ϕ in solution for 35kDa PEG dissolved in water. 78

4.3 D/D_{SE} (diffusivity scaled by the Stokes-Einstein diffusivity calculated using the solution viscosity) for 6.7 nm C dots is plotted against the polymer volume fraction ϕ in solution. *Z* is the entanglement density per chain for the solvated polymer and *d/a* is particle diameter scaled by the solvated polymer's tube diameter. Inset shows viscosity for these samples vs. shear rate – viscosity increases with increasing polymer fraction. All error bars shown are standard error. 80

4.4 D/D_s (diffusivity scaled by diffusivity of particles in solvent) is plotted

against the polymer volume fraction ϕ in solution measurement through FCS for different molecular weights of dissolved polymer corresponding to Rg of ~80 nm (closed symbols) and ~46 nm (open symbols), respectively. The dashed line indicates scaling of $(d/\xi)^{-2}$ and the error bars are standard error. Here, the circles show data for 6.7 nm particles (○), the squares show data for 16.5 nm particles (□), the triangles show data for the 23.7 nm particles (Δ), and the diamonds show data for the 35.5 nm particles (◊). A summary of concentrations used in this figure is provided in Table B2. 82

4.5 D/D_{SE} (diffusivity scaled by the Stokes-Einstein diffusivity calculated using the solution viscosity) is plotted against the host polymer molecular weight for a fixed volume fraction of polymer in solution, φ ~ 0.15, corresponding to d/a ~ 2. Error bars are standard deviation. 84

4.6 Mean square displacement vs. time plotted for 1.352 mil Da Mw polyethylene glycol dissolved in water for φ: (a) 0.04, (b) 0.10, (c) 0.24. (d) Scaling exponent, α, plotted vs. φ, for φ = 0.10 and 0.16 the scaling exponent for the second diffusive step is considered (error bars are standard deviation). 87

4.7 Master curve of diffusivity vs. d/a plotted for 1.352 mil Da Mw PEO solutions in water, here φ varies from 0.01-0.24 and Z varies from 1-89. The open red symbols are the experimental data from FCS, open diamond symbols with star show the data obtained from SPT; the open black symbols with dot are predictions from the Cai-Panyukov-Rubinstein scaling analysis; and the filled green symbols are diffusivities estimated using the Stokes-Einstein formula. The dashed line indicates the modified hopping model given in equation 4.4. The notation used in this figure is

the same as Figure 4.4 where circles are for 6.7 nm particles, squares for 16.5 nm particles, triangles-up for 23.7 nm particles and diamonds for 35.5 nm particles. Error bars for particle-tracking data are standard deviation and FCS data are standard error. 90

A1 (a) A schematic of spherical particle of diameter d, trapped in the entanglement mesh of a polymer with entanglement tube diameter, a. (b) We approximate this case, by considering a particle tethered to a pseudo-spring surrounded by smaller chain segments that act as the solvent. 103

A2 (a)-(c) Plots of mean squared displacement, $<\Delta r^2(t)>$, normalized by $k_BT/m\omega_o^2$ versus time normalized by the momentum relaxation time $\tau_p=\beta^{-1}$ for different values of parameter α by setting the initial coordinate of the particle $x_0 = 0$. The particles transition from ballistic to caged state passing through an intermediate diffusive region. The size of the diffusive regime increases as α increases. 109

B1 (a) Schematic of Cornell dots (C dots) synthesized with ATTO647N dye. (b) Normalized FCS auto-correlation curves for C dots dispersed in DI water. The dashed lines indicate a diffusive fit to the data with fast relaxation correction (equation 4.2) (c) τ_D vs d, dashed line shows fitting with Stokes-Einstein relation (~ d). 111

B2 Absorption (left-axis) and fluorescence emission spectra (right-axis) vs. wavelength for C dots. 113

B3 Photobleaching of C dots in concentrated 1.352 MDa Mw PEO solution in water indicated by (a) drop in fluorescence count rate and (b) changing correlation curves. 116

B4 Fluorescence intensity autocorrelation curves plotted against lag time for 6.7 nm particles dispersed in 35kDa PEG solutions in water. The dashed

lines indicate a diffusive fit to the data with fast relaxation correction (equation 4.2 in Chapter 4). The obtained diffusivity values are plotted in Figure 4.2. 117

B5 Sample fluorescence intensity autocorrelation curves plotted against lag time for 6.7 nm particles dispersed in 1352 kDa PEG solutions in water in varying concentrations. The dashed lines indicate a diffusive fit to the data with fast relaxation correction (equation 4.2 in Chapter 4). 118

B6 Oscillatory rheology measurements for 1352 kDa PEO solutions in water with PEO volume fraction of 0.04 (circles), 0.10 (squares), 0.16 (triangle-up), and 0.24 (diamonds). Closed symbols are for the storage modulus (G') and open symbols are for the loss modulus (G''). The inverse of the crossover frequency between G' and G'' gives the terminal time. 122

B7 XPCS measurements of intensity autocorrelation curves for different wave-vectors for 1 vol% of 80 nm 10kDa PS-functionalized silica NPs in 20 MDa PS dissolved in DEP at different volume fractions (corresponding to different values of d/a). (a) Intensity autocorrelation functions can be fitted by stretched exponential fits (dashed grey lines) at $q = 0.078\ nm^{-1}$, (b) β is the exponent for a stretched exponential fit to the intensity autocorrelation function and is < 1 for all samples at short wave-vectors. (c) Particle relaxation time, τ_p, plotted against wave-vector, q. The dashed line indicates a q-3 scaling for subdiffusion and the solid line indicates a q-2 scaling for diffusion. Based on the scaling particles appear diffusive at longer length scales and subdiffusive at shorter length scales. 123

LIST OF TABLES

4.1	Characterization data for polyethylene oxide (PEO) solutions	79
B1	Characterization of C dots used in this study	114
B2	Particle diameter (d), volume fraction (ϕ), the ratio of particle size to correlation length (d/ξ) for 1352 kDa PEO solutions in water.	119
B3	Particle diameter (d), volume fraction (ϕ), the ratio of particle size to correlation length (d/ξ) for 527.5 kDa PEO solutions in water.	120
B4	Volume fraction (φ) and entanglement density (Z) of PS and the ratio of particle size to tube diameter (d/a) for 80 nm silica probes in PS-DEP solutions.	124

CHAPTER 1

INTRODUCTION

1.1 Polymer Nanocomposites

A composite is a blend of two or more materials, designed with the aim of combining favorable properties and overcoming the inadequacies of its constituents. Polymer nanocomposites are a class of composite materials designed by adding particulates with at least one dimension in the nanoscale, i.e., 1-100 nm, to a polymeric host. It is now well established that addition of particulate fillers of any shape, including platelets, spheres, rods, within a polymeric matrix can create composite materials with desirable mechanical, thermal, and barrier properties, among others[1,2]. These properties are complex function of the characteristics of the particle-polymer interface, depending on the nature of interfacial interactions stemming from the polymer and nanoparticle surface chemistry, interfacial area, and the spatial distribution of the nanoparticles[3]. Adding fillers to polymers is a practice almost as old as the beginning of industrial application of polymers, when polymers were more expensive and fillers could be used as a means for cost-cutting[4]. An additional bonus was that these fillers could also augment the properties of their host polymer. However, compared to larger micron-sized fillers, nanoparticles possess a higher surface area to volume ratio, along with the ability to confine polymers at the nanoscale, due to which nanoparticles can impart similar enhancements to the mechanical properties of polymer as microparticles, albeit at much lower volume fractions[5]. However this enhancement rests on the uniformity and stability of the distribution of nanoparticles in the host polymer[6].

It is generally understood that bare nanoparticles in polymer hosts will either immediately or over time create irreversible aggregates[7]. The factors that drive the transition from their initial state towards a phase-segregated equilibrium are fundamental and present a major challenge in attaining complete experimental control over nanoparticle spatial distribution[7–9]. In addition, composites lacking favorable host polymer-particle interactions[10–12], or comprised of particles with large degree of shape anisotropy[7,13–17] can form percolated networks at lower particle loadings compared to spherical particles that favorably interact with the host. Hence, these filler/host combinations remain best suited for applications that require the formation of volume-spanning particle clusters. For other applications that require a more distributed particle configuration, physical or chemical modifications to the particle polymer interface may be required.

Surface functionalization of bare nanoparticles can provide a simple route to tune particle-particle, and particle-polymer interaction energies to influence particle dispersion and phase behavior. Through either adsorption or ionic and covalent linkage, small species or larger polymer brushes can be attached to particle surfaces. For short-ligands, the relative strength between the aforementioned interaction energies and entropy of surrounding chains is expected to determine the equilibrium particle configuration. As ligands become larger, the entropy of the grafted species also begins to play a role in particle dispersion.

Well-grafted polymer brushes on particle surfaces can sterically inhibit particles from approaching each other closely enough to experience attractive van der Walls forces and undergo "contact aggregation"[18]. Hence, tethering polymers to nanoparticle surfaces seems like an effective route towards forming a stable, and well-dispersed

polymer nanocomposite. Among a wide choice of combinations of grafted and host polymer chemistries and architecture, polymer nanocomposites based on single component host and identical chemistry of tethered polymer (homopolymer nanocomposites) are a well-studied problem and have been the subject of several modeling and experimental works. Kumar et al.[2] and Green[19] provide a detailed summary of these works in their review on dispersion of polymer grafted-nanoparticles in polymer melts. The authors identified the particle size and curvature, polymer grafting density, polydispersity effects, particle volume fraction, and the ratio of degree of polymerization of the host (P) to the degree of polymerization of the grafted chains (N) as important variables in setting the phase behavior of polymer-grafted nanoparticles in homopolymer melts. These factors determine the penetration or exclusion of the host polymer from the grafted polymer brush (also referred to as brush wetting and dewetting), which in turn predicts whether the polymer tethered particles will be phase separated from or dispersed in the host. Thus, the phase boundary of dispersion can be determined through the wetting-dewetting transition of grafted chains and host chains.

For highly grafted particles at low particle loadings, if the P/N ratio is less than 5, polymer grafted spherical nanoparticles have been shown to be well dispersed in homopolymer hosts, irrespective of polymer or particle chemistry[2,9]. Particle size, which affects the curvature, plays a strong role in providing more degrees of conformation to the grafted chains and preventing aggregation[9,21]. Additionally, Mackay et al.[22] found that particles with radius smaller than host R_g could be uniformly dispersed in host of any molecular weight and argued that deviations from this result could be a result of improper sample processing protocols. They attributed this effect to the large number of enthalpically interacting molecular sites available to

long polymer chains, which could offset the loss of their conformational entropy due the presence of the particles.

This stabilizing effect can be amplified by using host and tethered polymer combinations with strong enthalpic attraction and good miscibility, as characterized by negative Flory-Huggins interaction parameter ($\chi < 0$), polymer brushes can be favorably adsorbed on the grafted brush well beyond P/N ratio of 5, as exemplified by the scaling theory of Borukhov and Liebler[23]. This feature has been exploited to disperse particles in high Mw host polymers, up to P/N ~ 140 in the systems based of polyethylene glycol (PEG) grafted silica nanospheres in polymethylmethacrylate (PMMA)[24] and P/N ~ 30 for polystyrene (PS) functionalized gold nanorods in polyphenylene oxide (PPPO)[16] hosts. However, even these dispersions are susceptible to network formation due to polymer bridging as host molecular weight becomes even larger [25].

Another effective route to creating uniform nanocomposites is a bottoms-up approach where the building blocks of the nanocomposites are polymer tethered inorganic particles, void of any free host polymer chains. These materials are typically designed with small to intermediate chain lengths to induce strong stretching of the tethered chains to fill the volume between nanoparticle cores and thereby create highly uniform nanocore distribution. These volume filling constraints also lead to complex flow behavior in these materials, including viscoelasticity, thermal jamming, and shear thinning in the steady shear viscosity at high shear rates[1]. These flow behaviors are set by the rate at which the inherent structures within the composite deform and relax. The structure and dynamics of the core and the tethered polymer chains are highly correlated, however, such that on one hand, the constraints on the polymers are

relaxed when the core moves, and on the other hand, the motion of the core depends on the volume filling constraints on the grafted polymers.

This cyclic causality underpins the interdependent nature of particle dynamics and dispersion quality in polymer nanocomposites. It is also worth noting, that our present discussion has been limited to thermodynamic stability of nanocomposites and that in addition to this physical processing such as shear mixing with co-solvent and its rapid removal, ultrasonication, and melt compounding can be used to create stable dispersions by kinetically trapping particles in a uniform state[26]. However, such materials may be susceptible to aging and reaggregation, which can be identified through particle dynamics measurements.

1.2 Nanoparticle Dynamics in Polymer Nanocomposites

The study of how nanoparticles move in a polymeric host can provide important insight into nanoscale inhomogeneities and other intrinsic length scales of the host medium, as well as about time-dependent properties like viscoelasticity and aging of the host medium. It is well established that the nanoscopic nature of nanocomposites is not only because of the nanoparticles but also in the fact that most common polymer hosts have chain dimensions in the nanoscale (1-100 nm) and one should not expect particles to move through a polymer melt as typical microspheres through a solvent (where molecular dimensions are of the order of few Å). The exception is the case when the particles are relatively large, or in other words when particle radius is much larger than the radius of gyration of the host polymer ($R >> R_g$), where indeed the self-

diffusivity of a spherical particle in a polymer melt follows the Stokes-Einstein relation of diffusivity, D_{SE},

$$D_{SE} = \frac{k_B T}{6\pi\eta_{sys} R}. \quad (1.1)$$

Here, k_B is the Boltzmann constant, T is the temperature, η_{sys} is the zero shear viscosity of the material, and R is the particle radius. However, particles with dimensions around or less than the R_g of the polymer they are embedded in, may exhibit dynamics that deviate from continuum behavior and have been shown to exhibit much higher values of self-diffusivities than what would be expected based on the unfilled polymer viscosity[27–29]. In contrast, the slow down of dynamics is a less common phenomenon, that has been explained in terms of the increase in the effective radius of the core either due to absorption of a layer of host polymer on bare particles[30] or, for polymer-grafted nanoparticles, as a consequence of the increase in the effective particle size due to the tethered polymer[31]. These cases are less interesting primarily because the effective particle radius is typically a few times greater than the polymer R_g. Far more interesting and disputed particle dynamics behavior have been reported when the particle dimensions are smaller or close to polymer R_g.[24, 28-29]

The unexpected speeding-up of particle dynamics in nanoparticle filled polymers at low particle loadings has been consistently observed in polymer nanocomposites and several explanations have been offered to explain this phenomenon. The most common are reduction in material viscosity due to availability of large free-volume for the polymer chains[32–35] and plasticization of polymer chains due to particles acting akin to molecular solvents[36,37]. More complex physical arguments have been advanced to explain lower than expected nanoparticle/polymer composite viscosity and faster than expected nanoparticle dynamics in entangled polymer hosts. Namely, that the

nanoparticle motions could serve to release entanglement constraint on to entangled polymers in a process analogous to what has been reported to occur in bidisperse polymer blends when faster-relaxing, shorter chains release entanglement constraints with their longer neighbors at a higher rate than the long chains can escape the mean-field tube formed by all neighboring chains (long and short)[8,37,38]. Several theoretical works also suggest that polymer slip at nanoparticle surface can impart an additional mechanism for fillers to lower material viscosity[39–41].

Mangal et al.[8] conducted detailed rheological measurements on PEG-tethered silica nanoparticles suspended in PMMA hosts, where the particle size is chosen to be greater than tube diameter, but smaller than the host R_g, and showed that at low concentrations, polymer-functionalized nanoparticles can induce tube-dilation in the host polymer that leads to an earlier onset of reptation relaxation. On longer timescales, the particles being smaller than the polymer R_g can move faster than the surrounding chains and accelerate tube escape via a process similar to constraint release.

These mechanisms lead to an apparent lowering of viscosity in entangled polymers at low nanoparticle concentrations. Thus, the authors found that in these systems the reduction in material viscosity is resultant of faster dynamics of surrounding particles and not the other way around. This observation underscores the importance for studying the dynamics of a single particle in polymer melts to tailor the properties of nanoparticle filled composites. To begin to do this, one must first identify the relationship between nanoparticle transport and its size relative to the polymer R_g.

Theory describes five regimes of transport for self-diffusion of particles in entangled polymers. The analysis is based on the relative ratio of the particle radius R with respect to the host polymer's R_g and two additional length scales, viz., the entanglement length or tube diameter, a, and the size of the kuhn monomer, b, for the host polymer[42–45]. These regimes are: (1) the "penetrant regime", where $2R \sim 1$ nm or smaller, for which the kuhn length is either larger than or comparable to the particle size; (2) the "sieving" regime, $b < 2R < a$; (3) the intermediate crossover regime, where $a \leq 2R << 2R_g$; (4) the macromolecular crossover regime, where $R \sim R_g$; and (5) the well known hydrodynamic regime, characterized by $R >> R_g$, where the Stokes Einstein relation given in equation 1.1 is expected to hold.[44]

Two theoretical approaches are available in the literature that are able to capture these physics, namely, self-consistent mean field theory and scaling analysis based on dynamics of a single polymer chain. The predictions made through both approaches are qualitatively similar and agree (albeit through very dissimilar quantitative expressions) that the particles embedded in entangled polymers may exhibit dynamics much faster than anticipated from SE behavior (in equation 1.1) as long as the size of the particles is smaller than the tube diameter, $2R < a$.

In the penetrant regime, the particle motion is set by the collective density fluctuations of the surrounding monomer beads[46]. As particles become bigger than the kuhn length and enter the sieving regime, their motion begins to follow the segmental motions of the polymer chain[42,44] while still being confined by the polymer entanglements[44]. When particles become comparable to or larger than the tube diameter, they can directly experience the dynamics of the entanglement tubes. It is here that particles can still move around by entanglement hopping from one entanglement cage to another.

The transition to SE behavior happens in regime 4, and the particle size at which this transition occurs shifts to higher values with increasing number of entanglements[44,45]. To-date no single experiment has tracked all five regimes of transport. However, with the development of new experimental techniques enabling measurement of particle dynamics over a range of length scales we have been able to construct a picture of how particles move in polymers piece-by-piece.

The most important experimental finding in this context is the occurrence of anomalous hyperdiffusion for a range of particle sizes in some entangled polymer nanocomposites[27,47–49] and the absence of this behavior in other entangled polymer systems[28,29]. Similar hyperdiffusive dynamics have been observed in self-suspended highly-grafted nanoparticles[50] and are conventionally associated with aging of heterogeneous materials, including colloidal glasses and gels[51–55], and polymer nanocomposites at the glass transition[56]. This dynamical behavior is surprisingly absent from experimental measurements of particle dynamics in polymer solutions. Current theories for single particle dynamics in polymer melts are unable to capture hyperdiffusion.

Among the goals of this thesis is to employ multiple intrusive experimental methods to provide a detailed account of single particle dynamics in highly entangled polymer solutions for different ratios of particle size to intrinsic polymer length scales in solution. We also explore possible origins of hyperdiffusion in some nanocomposites and attempt to explain hyperdiffusion in non-aging, and equilibrated systems such hairy nanoparticles in entangled PMMA[27] and cis-1, 4-polyisoprene[49] melts, and self-suspended hairy nanoparticles[50].

1.3 Outline of Thesis

The dissertation is organized as follows. Chapter 2 begins with a survey of modeling literature on hyperdiffusive dynamics in polymer nanocomposites. We use insights from these studies to build the foundation for a model framework that can describe particle dynamics in jammed polymer nanocomposites (such as those depicted in Figure 1.1a-b). In particular, by solving the Langevin equation for particles in a reversible network, we find the conditions under which average particle trajectories within the nanocomposite can display hyperdiffusive dynamics depending upon the extent of jamming and the strength of the particle-network interactions.

In chapter 3 we systematically tune the nanoparticle correlations in nanocomposites based on hairy nanoparticles using solvents (Figure 1.1 c). We perform simultaneous resolution of nanoparticle distribution and dynamics through X-ray scattering techniques to demystify the strong relationship between particle networks and hyperdiffusion in polymer nanocomposites.

In chapter 4, we study single-particle trajectories in entangled polymer solutions (Figure 1.1d) using fluorescence particle tracking techniques like fluorescence correlation spectroscopy (FCS) and single particle tracking (SPT). We find that these systems are devoid of any hyperdiffusive signatures and conclude that entanglements and entanglement hopping are not responsible for observations of hyperdiffusion in polymer nanocomposite melts.

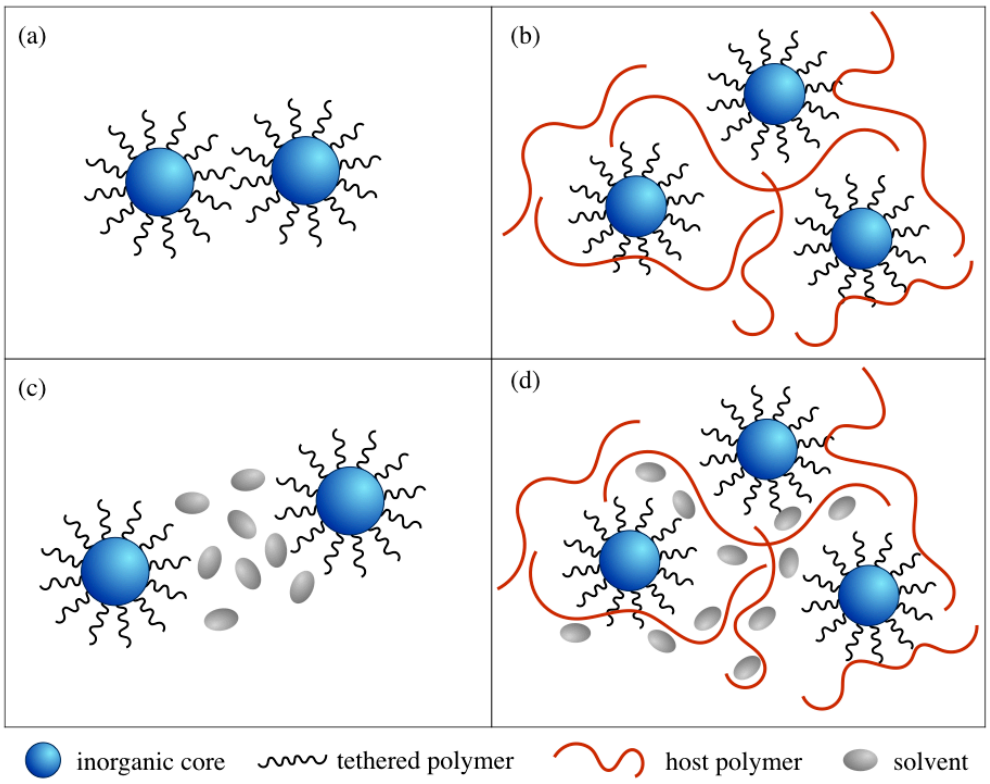

Figure 1.1 A schematic of polymer nanocomposites studied in this work. We study the dynamical behavior of polymer grafted nanoparticles: (a) under self-suspended or solvent-free conditions, (b) dispersed in entangled polymer melts, (c) dispersed in solvents, and (d) dispersed in solutions of entangled polymers.

Our findings are consistent with current theoretical understanding of the self-diffusivity of particles in entangled polymer melts and solutions, which have previously been contradicted by a surge of reports of hyperdiffusion in polymer nanocomposite melts, primarily studied using x-ray photon correlation spectroscopy measurements. The body of work reported in this thesis therefore offers new avenues for particle dynamics research in polymer nanocomposite melts through straightforward tuning of the interaction energies between the particles and their host polymers.

Bibliography

(1) Srivastava, S.; Choudhury, S.; Agrawal, A.; Archer, L. A. Self-Suspended Polymer Grafted Nanoparticles. *Current Opinion in Chemical Engineering*. Elsevier May 1, 2017, pp 92–101.

(2) Kumar, S. K.; Jouault, N.; Benicewicz, B.; Neely, T. Nanocomposites with Polymer Grafted Nanoparticles. *Macromolecules* **2013**, *46* (9), 3199–3214.

(3) Rittigstein, P.; Priestley, R. D.; Broadbelt, L. J.; Torkelson, J. M. Model Polymer Nanocomposites Provide an Understanding of Confinement Effects in Real Nanocomposites. *Nat. Mater.* **2007**, *6* (4), 278–282.

(4) Bhattacharya, M. Polymer Nanocomposites—A Comparison between Carbon Nanotubes, Graphene, and Clay as Nanofillers. *Materials (Basel)*. **2016**, *9* (4), 262.

(5) Zhang, Q.; Archer, L. A. Poly(ethylene oxide)/Silica Nanocomposites: Structure and Rheology. *Langmuir* **2002**, *18* (26), 10435–10442.

(6) Schaefer, D. W.; Justice, R. S. How Nano Are Nanocomposites? *Macromolecules* **2007**, *40* (24), 8501–8517.

(7) Srivastava, S.; Schaefer, J. L.; Yang, Z.; Tu, Z.; Archer, L. A. 25th Anniversary Article: Polymer-Particle Composites: Phase Stability and Applications in Electrochemical Energy Storage. *Adv. Mater.* **2014**, *26* (2), 201–234.

(8) Mangal, R.; Srivastava, S.; Archer, L. A. Phase Stability and Dynamics of Entangled Polymer–nanoparticle Composites. *Nat. Commun.* **2015**, *6* (1), 7198.

(9) Srivastava, S.; Agarwal, P.; Archer, L. A. Tethered Nanoparticle–Polymer Composites: Phase Stability and Curvature. *Langmuir* **2012**, *28* (15), 6276–6281.

(10) Hooper, J. B.; Schweizer, K. S. Theory of Phase Separation in Polymer

Nanocomposites. *Macromolecules* **2006**, *39* (15), 5133–5142.

(11) Filippone, G.; Romeo, G.; Acierno, D. Viscoelasticity and Structure of Polystyrene/Fumed Silica Nanocomposites: Filler Network and Hydrodynamic Contributions. *Langmuir* **2010**, *26* (4), 2714–2720.

(12) Cassagnau, P. Melt Rheology of Organoclay and Fumed Silica Nanocomposites. *Polymer (Guildf).* **2008**, *49* (9), 2183–2196.

(13) Du, F.; Scogna, R. C.; Zhou, W.; Brand, S.; Fischer, J. E.; Winey, K. I. Nanotube Networks in Polymer Nanocomposites: Rheology and Electrical Conductivity. *Macromolecules* **2004**, *37* (24), 9048–9055.

(14) Du, F.; Fischer, J. E.; Winey, K. I. Effect of Nanotube Alignment on Percolation Conductivity in Carbon Nanotube/polymer Composites. *Phys. Rev. B* **2005**, *72* (12), 121404.

(15) Jiang, G.; Hore, M. J. A.; Gam, S.; Composto, R. J. Gold Nanorods Dispersed in Homopolymer Films: Optical Properties Controlled by Self-Assembly and Percolation of Nanorods. *ACS Nano* **2012**, *6* (2), 1578–1588.

(16) Hore, M. J. A.; Composto, R. J. Using Miscible Polymer Blends To Control Depletion–Attraction Forces between Au Nanorods in Nanocomposite Films. *Macromolecules* **2012**, *45* (15), 6078–6086.

(17) Do, N. S. T.; Schaetzl, D. M.; Dey, B.; Seabaugh, A. C.; Fullerton-Shirey, S. K. Influence of Fe 2 O 3 Nanofiller Shape on the Conductivity and Thermal Properties of Solid Polymer Electrolytes: Nanorods versus Nanospheres. *J. Phys. Chem. C* **2012**, *116* (40), 21216–21223.

(18) Hooper, J. B.; Schweizer, K. S. Contact Aggregation, Bridging, and Steric Stabilization in Dense Polymer−Particle Mixtures. *Macromolecules* **2005**, *38* (21), 8858–8869.

(19) Green, P. F. The Structure of Chain End-Grafted Nanoparticle/homopolymer

Nanocomposites. *Soft Matter* **2011**, *7* (18), 7914.

(20) Srivastava, S.; Agarwal, P.; Archer, L. A. Tethered Nanoparticle–Polymer Composites: Phase Stability and Curvature. *Langmuir* **2012**, *28* (15), 6276–6281.

(21) Trombly, D. M.; Ganesan, V. Curvature Effects upon Interactions of Polymer-Grafted Nanoparticles in Chemically Identical Polymer Matrices. *J. Chem. Phys.* **2010**, *133* (15), 154904.

(22) Mackay, M. E.; Tuteja, A.; Duxbury, P. M.; Hawker, C. J.; Van Horn, B.; Guan, Z.; Chen, G.; Krishnan, R. S. General Strategies for Nanoparticle Dispersion. *Science (80-.).* **2006**, *311* (5768), 1740–1743.

(23) Borukhov, I.; Leibler, L. Enthalpic Stabilization of Brush-Coated Particles in a Polymer Melt. *Macromolecules* **2002**, *35* (13), 5171–5182.

(24) Mangal, R.; Nath, P.; Tikekar, M.; Archer, L. A. Enthalpy-Driven Stabilization of Dispersions of Polymer-Grafted Nanoparticles in High-Molecular-Weight Polymer Melts. *Langmuir* **2016**, *32* (41), 10621–10631.

(25) Surve, M.; Pryamitsyn, V.; Ganesan, V. Universality in Structure and Elasticity of Polymer-Nanoparticle Gels. *Phys. Rev. Lett.* **2006**, *96* (17), 177805.

(26) Huang, Y. Y.; Terentjev, E. M. Dispersion of Carbon Nanotubes: Mixing, Sonication, Stabilization, and Composite Properties. *Polymers (Basel).* **2012**, *4* (1), 275–295.

(27) Mangal, R.; Srivastava, S.; Narayanan, S.; Archer, L. A. Size-Dependent Particle Dynamics in Entangled Polymer Nanocomposites. *Langmuir* **2016**, *32* (2), 596–603.

(28) Tuteja, A.; Mackay, M. E.; Narayanan, S.; Asokan, S.; Wong, M. S. Breakdown of the Continuum Stokes−Einstein Relation for Nanoparticle Diffusion. *Nano Lett.* **2007**, *7* (5), 1276–1281.

(29) Grabowski, C. A.; Adhikary, B.; Mukhopadhyay, A. Dynamics of Gold Nanoparticles in a Polymer Melt. *Appl. Phys. Lett.* **2009**, *94* (2), 21903.

(30) Griffin, P. J.; Bocharova, V.; Middleton, L. R.; Composto, R. J.; Clarke, N.; Schweizer, K. S.; Winey, K. I. Influence of the Bound Polymer Layer on Nanoparticle Diffusion in Polymer Melts. *ACS Macro Lett.* **2016**, *5* (10), 1141–1145.

(31) Lin, C.-C.; Griffin, P. J.; Chao, H.; Hore, M. J. A.; Ohno, K.; Clarke, N.; Riggleman, R. A.; Winey, K. I.; Composto, R. J. Grafted Polymer Chains Suppress Nanoparticle Diffusion in Athermal Polymer Melts. *J. Chem. Phys.* **2017**, *146* (20), 203332.

(32) Guzeyev, V. V.; Rafikov, M. N.; Malinskii, Y. M. The Effect of Filler Dispersity of the Melt Viscosity of Polyvinyl Chloride (PVC). *Polym. Sci. U.S.S.R.* **1975**, *17* (4), 923–926.

(33) Merkel, T. C. Ultrapermeable, Reverse-Selective Nanocomposite Membranes. *Science (80-.).* **2002**, *296* (5567), 519–522.

(34) Prokopenko, V. V.; Titova, O. K.; Fesik, N. S.; Malinskii, Y. M.; Bakeyev, N. F. The Nature of the Anomalous Viscosity of Filled Polymers as a Function of Concentration at Low Filler Contents. *Polym. Sci. U.S.S.R.* **1977**, *19* (1), 111–119.

(35) Mackay, M. E.; Dao, T. T.; Tuteja, A.; Ho, D. L.; Van Horn, B.; Kim, H.-C.; Hawker, C. J. Nanoscale Effects Leading to Non-Einstein-like Decrease in Viscosity. *Nat. Mater.* **2003**, *2* (11), 762–766.

(36) Nusser, K.; Schneider, G. J.; Pyckhout-Hintzen, W.; Richter, D. Viscosity Decrease and Reinforcement in Polymer–Silsesquioxane Composites. *Macromolecules* **2011**, *44* (19), 7820–7830.

(37) Tuteja, A.; Duxbury, P. M.; Mackay, M. E. Multifunctional Nanocomposites

with Reduced Viscosity. *Macromolecules* **2007**, *40* (26), 9427–9434.

(38) Tuteja, A.; Mackay, M. E.; Hawker, C. J.; Van Horn, B. Effect of Ideal, Organic Nanoparticles on the Flow Properties of Linear Polymers: Non-Einstein-like Behavior. *Macromolecules* **2005**, *38* (19), 8000–8011.

(39) Kalathi, J. T.; Grest, G. S.; Kumar, S. K. Universal Viscosity Behavior of Polymer Nanocomposites. *Phys. Rev. Lett.* **2012**, *109* (19), 198301.

(40) Ganesan, V.; Pryamitsyn, V.; Surve, M.; Narayanan, B. Noncontinuum Effects in Nanoparticle Dynamics in Polymers. *J. Chem. Phys.* **2006**, *124* (22), 221102.

(41) Wang, M.; Hill, R. J. Anomalous Bulk Viscosity of Polymer-Nanocomposite Melts. *Soft Matter* **2009**, *5* (20), 3940.

(42) Cai, L.-H.; Panyukov, S.; Rubinstein, M. Mobility of Nonsticky Nanoparticles in Polymer Liquids. *Macromolecules* **2011**, *44* (19), 7853–7863.

(43) Yamamoto, U.; Schweizer, K. S. Microscopic Theory of the Long-Time Diffusivity and Intermediate-Time Anomalous Transport of a Nanoparticle in Polymer Melts. *Macromolecules* **2015**, *48* (1), 152–163.

(44) Yamamoto, U.; Schweizer, K. S. Theory of Nanoparticle Diffusion in Unentangled and Entangled Polymer Melts. *J. Chem. Phys.* **2011**, *135* (22), 224902.

(45) Cai, L.-H.; Panyukov, S.; Rubinstein, M. Hopping Diffusion of Nanoparticles in Polymer Matrices. *Macromolecules* **2015**, *48* (3), 847–862.

(46) Bhattacharyya, S.; Bagchi, B. Anomalous Diffusion of Small Particles in Dense Liquids. *J. Chem. Phys.* **1997**, *106* (5), 1757–1763.

(47) Jang, W.; Koo, P.; Bryson, K.; Narayanan, S.; Sandy, A.; Russell, T. P.; Mochrie, S. G. Dynamics of Cadmium Sulfide Nanoparticles within Polystyrene Melts. *Macromolecules* **2014**, *47* (18), 6483–6490.

(48) Narayanan, S.; Lee, D. R.; Hagman, A.; Li, X.; Wang, J. Particle Dynamics in

Polymer-Metal Nanocomposite Thin Films on Nanometer-Length Scales. *Phys. Rev. Lett.* **2007**, *98* (18), 185506.

(49) Kim, D.; Srivastava, S.; Narayanan, S.; Archer, L. A. Polymer Nanocomposites: Polymer and Particle Dynamics. *Soft Matter* **2012**, *8* (42), 10813.

(50) Srivastava, S.; Agarwal, P.; Mangal, R.; Koch, D. L.; Narayanan, S.; Archer, L. A. Hyperdiffusive Dynamics in Newtonian Nanoparticle Fluids. *ACS Macro Lett.* **2015**, *4* (10), 1149–1153.

(51) Cipelletti, L.; Manley, S.; Ball, R. C.; Weitz, D. A. Universal Aging Features in the Restructuring of Fractal Colloidal Gels. *Phys. Rev. Lett.* **2000**, *84* (10), 2275–2278.

(52) Cipelletti, L.; Ramos, L.; Manley, S.; Pitard, E.; Weitz, D. A.; Pashkovski, E. E.; Johansson, M. Universal Non-Diffusive Slow Dynamics in Aging Soft Matter. *Faraday Discuss.* **2003**, *123*, 237–251.

(53) Duri, A.; Cipelletti, L. Length Scale Dependence of Dynamical Heterogeneity in a Colloidal Fractal Gel. *Europhys. Lett.* **2006**, *76* (5), 972–978.

(54) Mazoyer, S.; Cipelletti, L.; Ramos, L. Origin of the Slow Dynamics and the Aging of a Soft Glass. *Phys. Rev. Lett.* **2006**, *97* (23), 238301.

(55) Ramos, L.; Cipelletti, L. Ultraslow Dynamics and Stress Relaxation in the Aging of a Soft Glassy System. *Phys. Rev. Lett.* **2001**, *87* (24), 245503.

(56) Guo, H.; Bourret, G.; Corbierre, M. K.; Rucareanu, S.; Lennox, R. B.; Laaziri, K.; Piche, L.; Sutton, M.; Harden, J. L.; Leheny, R. L. Nanoparticle Motion within Glassy Polymer Melts. *Phys. Rev. Lett.* **2009**, *102* (7), 75702.

CHAPTER 2

THEORY OF ANOMALOUS DIFFUSION IN POLYMER NANOCOMPOSITES

2.1 Introduction

Our understanding of how particles move in a material has significantly grown since Einstein first wrote about Brownian motion in 1905[1]. We have uncovered a range of transport anomalies and developed robust synthetic procedures for creating physical systems that exhibit them. Among these anomalies, hyperdiffusion which is characterized by the mean-squared displacement following a power law relation with time, $\left\langle \Delta r^2(t) \right\rangle \sim t^{\alpha}$ where $\alpha > 1$, is of significant contemporary interest both from a mathematical perspective and because it has been reported in diverse states of matter, including living and non-living systems, with no universal law connecting them.

Of specific relevance to the work reported in this thesis is the existence of a large body of experimental evidence, which confirms hyperdiffusion as the principle mode of transport for nanoparticles in some polymer nanocomposite melts[2–5]. Research in the field of colloidal glasses, where hyperdiffusion is as ubiquitous, has also shown that hyperdiffusion is a result of aging in out-of-equilibrium systems[6]. These physics, however, cannot explain the occurrence of hyperdiffusion in stable polymer nanocomposites such as self-suspended hairy nanoparticles[5] and polymer nanocomposites based on favorably interacting host and tethered polymers,[2] that show no- or minimal evidence of aging.

In search of a unified explanation of the phenomenon, this chapter (sections 2.2.1-2.2.3) reviews the various models for hyperdiffusion in systems, such as well-dispersed and stable polymer nanocomposites, that do not age. In section 2.2.4, we consider a simple model that represent nanocomposites in terms of a two-state structure composed of free particles and clusters to explain hyperdiffusion in physical systems. In this framework, we investigate how disparity in the time scales of motion of the system components can result in hyperdiffusive signatures in the mean particle motion. We present simple scaling relationships in section 2.3, which can be used to predict the occurrence of hyperdiffusion in different physical systems.

2.2 Theory

Langevin Framework

We begin with the 1-D Langevin equation that describes the motion of a spherical particle of mass m in a fluid of viscosity η,

$$m\frac{d\boldsymbol{v}}{dt} = -6\pi\eta R\boldsymbol{v}(t) - \frac{dV}{dx} + F_B(t) \tag{2.1}$$

It is a simple force balance on a single particle, where $\boldsymbol{v}$ is the velocity of the particle, and $6\pi\eta R\boldsymbol{v}$ is the dynamic friction on the particle with the coefficient $6\pi\eta R$, given by the Stokes drag law (R is the radius of the particle), being the coefficient of friction. Here V is a potential field acting on the particle and $\boldsymbol{F_B}$, called the Brownian force, is a random force that arises from thermal fluctuations. This random Brownian force can be approximated using a Gaussian white noise function with zero mean and second moment given by the fluctuation dissipation theorem (FDT),

$\left\langle F_B(t)F_B(t')\right\rangle = 12\pi\eta R k_B T\delta(t-t')$, where $\delta(t)$ is the Dirac delta function, k_B is the Boltzmann constant and T is the temperature.

For a freely diffusing particle, in the absence of any potential field, and in the over-damped limit, i.e., $m/6\pi\eta R << 1$, expected for low-Reynolds number flows where particle inertia term in equation (2.1) can be neglected, we recover Einstein's solution for Brownian motion at long times,

$$\left\langle \Delta r^2(t)\right\rangle = 2D_{SE}t \tag{2.2}$$

where $\left\langle \Delta r^2(t)\right\rangle$ is the time-dependent ensemble-averaged mean squared displacement of the particle from its initial position x_0, and D_{SE} is the particle diffusivity given by the Stokes-Einstein relation $D_{SE} = k_B T / 6\pi\eta R$. Although this equation adequately describes the motion of a single particle in a Newtonian solvent, the interaction of the particle with complex solvents can alter the motion of the particle and yield interesting dynamical behaviors.

2.2.1 Single Particle in an Elastic Polymer Host

In this section we aim to understand the motion of a single particle in an entangled polymer host. X-ray Photon Correlation Spectroscopy (XPCS) measurements in numerous systems comprised of nanoparticles in entangled polymer melts[2-4, 7-8] reveal that the particles exhibit hyperdiffusive dynamics, which has been noticeably absent from the extensive theoretical and modeling literature available on particle diffusion in polymer melts[9-11]. A cursory glance at equation (2.1) with respect to particle motion in a polymer melt might lead one to think that the drag experienced by the particle in a high molecular weight polymer weight polymer melt will be much higher compared to

a Newtonian solvent like water. The real picture, however, is far more complex. Unlike simple solvents, complex solvents like polymer melts are viscoelastic and hence exhibit time-dependent viscosity. Mason and Weitz[12] solved the Langevin equation for such complex materials and showed that one could map the mean squared displacement of nanoparticles from particle tracking experiments to the frequency-dependent linear viscoelastic measurements.

Polymer sizes are in reality much larger than those of molecular solvents, and particularly high molecular weight polymers may be comparable or larger than the nanoparticles, which are embedded in them. In this regime, one can no longer treat the polymer surrounding the particle as a single continuum fluid. Since the time-dependent rheology of polymer melts arises from the hierarchical relaxation of chain segments on a single polymer chain, followed by reptation, and collective relaxation of surrounding chains, how particle sizes compare to the inherent length scales of a polymer chain governs how particles exchange thermal energy with the host polymer and move. Theoretical work based on scaling analysis have been proposed to describe the diffusion of particles in polymer melts in different regimes set by the ratio of particle size to inherent polymer length scales, like Kuhn length, tube diameter, radius of gyration[9,13].

When the particle is smaller than the Kuhn length of the polymer, b, one can treat this regime as equivalent to the motion of a small particle in a dense liquid of larger particles[14]. In the other extreme limit, when the particle is larger than the radius of gyration of the polymer chain, R_g, the polymer chains now become a continuum solvent for the particle to move. In the intermediate regime, when the particle size is larger than the Kuhn length of the polymer, but smaller than the radius of gyration, the

continuum approximation breaks down and the particle might be expected to exhibit anomalous transport and may move much faster than the Stokes-Einstein prediction, D_{SE}, which is based on the total macroscopic polymer viscosity.

When the particle is larger than the Kuhn length, b, and smaller than the radius of gyration of the polymer, R_g, the motion of the particle depends on whether the polymer is entangled or unentangled. For unentangled polymer hosts, the polymer segmental and Rouse chain dynamics should govern the particle motion. It would require a polymer segment similar in size to the particle, $d = 2R$, to relax in order for a single isolated particle to move a distance comparable to the particle size. The presence of entanglements introduces an additional length scale, i.e., the entanglement tube diameter, a beyond which polymer chains can be considered fully coupled on timescales below the reptation time. Thus, in systems with $b < d < a$, theoretical studies based on scaling analysis[9] consider the motion equivalent to that of a particle in an unentangled melt ($d < R_g$). These studies examine the dependence of the particle motion on the segmental and chain relaxation of the polymer and find that the particle diffusivity, D, scales as d^{-3}.

This result is consistent with the diffusivity scaling obtained from molecular dynamics simulations, where a scaling of d^{-3} is also obtained. However the framework used in these simulations is based on collective density fluctuations of surrounding chains, against the Rouse dynamics of a single chain used in the scaling analysis. Molecular dynamics (MD) simulations also indicate that the ratio of D/D_{SE} for a fixed value of d/a grows as a function of increasing entanglement chain density, Z (Z = polymer molecular weight / entanglement molecular weight), and eventually reaches a plateau above $Z \sim$ 5-10 for all values of d/a (for $d < R_g$)[15]. This is a surprising result and

indicates that for highly entangled polymers, D follows a similar dependence on Z as D_{SE}, which scaling analysis based on a single chain is unable to capture!

For particle sizes larger than the tube diameter (i.e. $d > a$, but still smaller than R_g), both analyses account for the effect of entanglements on particle motion. Here, entanglements confine the particles and while particles wait for the surrounding polymer chains to reptate, they move via thermally activated hopping between neighboring entanglements. A simple cartoon of transport in the regime $a < d < R_g$ confirmed through theory and simulations by Rubinstein and co-workers[10,11], is provided in Figure 2.1. This cartoon shows a typical plot of the mean squared displacement, $\left\langle \Delta r^2(t) \right\rangle$, as a function of time for a particle in a highly entangled polymer matrix.

The plot comprises of four regions – an initial ballistic regime where mean squared displacement scales quadratically with time; this transitions to a subdiffusive regime ($\left\langle \Delta r^2(t) \right\rangle \sim t^{\alpha}$, where $\alpha < 1$), where particle and polymer dynamics become coupled; with time, entanglements dampen the coupling and particles become arrested within the entanglement cages until the time τ_{hop}, after which the particles begin to undergo Fickian diffusion, where $\left\langle \Delta r^2(t) \right\rangle$ scales linearly with time. In reality, one may not expect such strong arresting in real systems composed of fluctuating microscopic chains and this region may manifest as a weak extension of the subdiffusive regime. This form of transport is reminiscent of anomalous diffusion during transient caging and hopping in hard-sphere suspensions and, depending on how strongly the particles are arrested, the transition from an arrested to diffusive regime can occur through a weakly superdiffusive intermediate step.[16]

Our interest here is in particle dynamics in the regime *(d > a)*. This interest is motivated in part by recent results from XPCS measurements using polyethylene glycol-grafted silica nanoparticles dispersed in polymethyl methacrylate melts (PEG-SiO_2/PMMA nanocomposites).[2]

The measurements reveal that when the molecular weight of the host polymer exceeds the entanglement molecular weight, a transition from diffusive ($\langle \Delta r^2(t) \rangle \sim t$) to hyperdiffusive ($\langle \Delta r^2(t) \rangle \sim t^{\alpha}$, where $\alpha > 1$)[2] particle dynamics occur. It is also significant that the hyperdiffusion dynamics are sustained through the conditions of measurement, viz., $Z \sim$ 1-25; measurement length scales ranging from 30-200 nm (calculated from $L = 2\pi/q$, where q is the wave vector in XPCS measurements and varies from 0.03-0.2 nm^{-1}); and time scales from 0.1-200s. The physical processes that produce such long-persisting hyperdiffusive motion both in terms of length and time scales are presently not understood.

Based on current understanding of polymer and particle dynamics in systems studied in reference 2, at least two physical arguments can be advanced to rationalize observations of hyperdiffusive ($\langle \Delta r^2(t) \rangle \sim t^{\alpha}$, where $\alpha > 1$) particle relaxations. First, the observed transport corresponds to an extended ballistic regime analogous to that captured in the scaling theory, where $\langle \Delta r^2(t) \rangle$ scales quadratically with time. Alternatively, the configurational relaxation of the polymer and particles could proceed in the presence of residual forces in the material, which would result in driven particle motions. Residual forces can arise in such systems form long-lived external forces during preparation or loading of colloidal particles[17] or may arise from internal forces in the system induced by particle aggregation or aging[18,19].

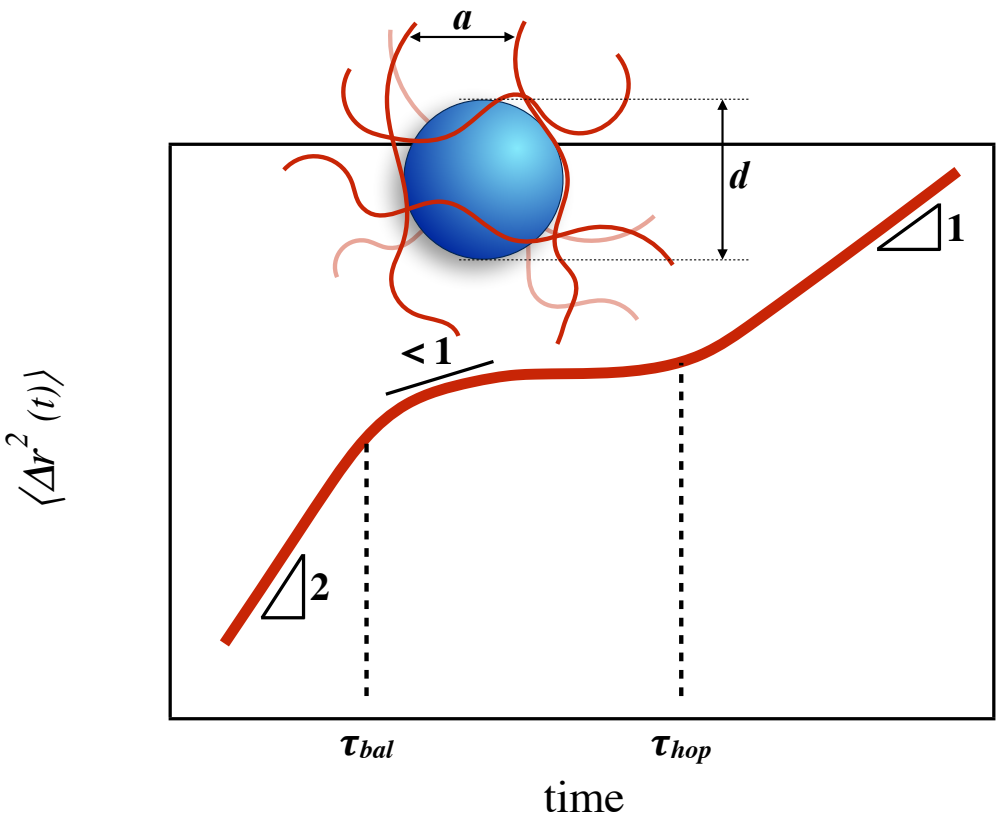

Figure 2.1 Schematic of the typical mean squared displacement, $\langle \Delta r^2(t) \rangle$ versus time plot for a particle of size *d*, embedded in a polymer network with tube diameter *a*, given the condition that *d* is greater than *a*, but is smaller than radius of gyration (R_g) of the host polymer. The particle motion follows the scaling $\langle \Delta r^2(t) \rangle \sim t^2$ up to the ballistic time, τ_{bal}, past which it begins to follow the motion of surrounding chains subdiffusively within the entanglement where it stays till the hopping time τ_{hop}. Scaling theory[10] and MD simulations[11] indicate that beyond this time, nanoparticle hopping and relaxation of surrounding chains can proceed in tandem to allow the nanoparticle to move diffusively.

These physics must be considered in tandem with the fact that hyperdiffusion is also the mechanism of transport in dynamically heterogeneous systems, such as in polymer melts close to the glass temperature[20] or entangled polymer solutions subject to spatial variations in shear rate[21]. Even macroscopically equilibrated systems such as entangled worm-like micelles and "living" polymers with reversible cross-linking have been experimentally and theoretically demonstrated to display hyperdiffusion[22,23]. Hyperdiffusive signatures have also been observed in biological systems such as self-propelled microorganisms[17,24] and in colloidal particles in active environments[25]. However, the systems studied in reference 2 are far above its molecular glass transition, has been reported to show little evidence of aggregation or aging on timescales of days (i.e. well above the time scales of the experiment), and is based neither on "living" particles or host polymers.

To explore the first possibility in greater detail, we begin by estimating the range of characteristic ballistic times, τ_{bal}, for the systems studied in reference 2 using the formula,

$$\tau_{bal} = \left(\frac{bm}{\zeta d} \right)^{2/3} \tau_0^{1/3} \quad , \tag{2.3}$$

where m is the particle mass, ζ is the monomeric friction coefficient, d is the particle diameter, and τ_0 is the Rouse time. For 10 nm SiO_2 particles, in a polymer melt with $\zeta \sim 10^{-7}$, $b \sim 2$ nm and $\tau_0 \sim 10^{-4}$ s, τ_{bal} is of the order of 10^{-11} s. Additionally the length scales over which ballistic motion takes place is of the order of $L_{bal} \sim \left(\sqrt{k_B T / m} \right) \tau_{bal} \sim 10^{-2}$ nm. However, experimental studies of ballistic motion have shown that the transition from ballistic to diffusive is not sudden as expected from Einstein's theory of diffusion and rather occurs over a finite time, which can last over 3 orders of magnitude[26,27]. Even so, the expected time and length scales for the ballistic regime

are still much smaller than those involved in the XPCS measurements for entangled polymer melts such as the PEG-SiO_2/PMMA nanocomposites have been conducted.

Using the Langevin framework described earlier, we explore the transition from ballistic regime for a particle trapped in polymer entanglements in more detail in Appendix A and recover a similar result that particle in polymer entanglements are eventually trapped before additional mechanisms, such as reptation of surrounding chains or cage-to-cage hopping, can allow them to be released from the entanglement cages. These results too yield very small values for the timescales over which ballistic transport might be observed and lend support to the argument that hyperdiffusion in entangled polymer nanocomposites is not due to ballistic transport.

2.2.2 Strain Field Relaxation Model

Srivastava et al.[28] recently studied the occurrence of long-lived hyperdiffusion in self-suspended hairy nanoparticles using the framework of the strain field relaxation (SFR) model formulated by Bouchaud and Pitard[29]. The model is based on the occurrence of random and irreversible "microcollapses" in a contracting gel that can result in creation of long-range force-dipoles, which then bias the transport of surrounding particles. Srivastava et al.[28] extended this analysis to self-suspended hairy nanoparticles where biased hyperdiffusive particle motion is a result strain fields due to the occurrence of slow forming force dipoles that emerge as a result of thermal fluctuations of the nanoparticle building blocks. Here we have "nanocollapses" as the constituent particles and the interparticle spacings are nanoscopic in length (order 1-100 nm). The dynamic structure factor in this limit decays with time, t, as

$\sim \exp(-A(qt)^{3/2})$, where A is a constant and q is the wave vector at which the scattered intensity signal from the sample is collected. Note that the scaling exponent β in $(q\tau)^{\beta}$ determines the nature of transport with β = 1 being diffusive and β > 1 is hyperdiffusive).

An important parameter in this study is the evolution time of the force dipoles. For self-suspended nanoparticles this evolution time was approximated to be of the same order as the material relaxation time obtained from small amplitude shear rheology measurements. However, this approximation is likely invalid when applied to the PEG-SiO_2/PMMA nanocomposites and can provide neither qualitative nor quantitative agreement with the results presented in that study. An additional difficulty with the strain field model is that the "nanocollapses" if irreversible should signal the presence of aging in the system which is inconsistent with observations from the bulk rheology measurements which confirm that macroscopically the self suspended hairy nanoparticles[30,31] and the PEG-SiO_2/PMMA nanocomposites[2] are at equilibrium, as evidence by the fact that their rheological properties change little when measured over days. We propose a different mechanism that could potentially explain hyperdiffusion in polymer nanocomposites based on reversible networks such as self-healing polymers.

2.2.3 The Association-Dissociation Model

Our analysis is inspired by recent work from Olsen and co-workers who provided a simplistic two-state model for the occurrence of so-called *superdiffusion* at intermediate length scales in associating hydrogel networks, such as coiled proteins[32] and polymers linked through metal-ligand bonds[33,34]. These networks are based on

reversible physical cross-links, which means that their building blocks viz., the proteins or polymers, can exist in either of the following two states: as part of the network, which is referred to as the associated state (denoted by subscript *A*); or as isolated elements detached from the network, which is referred to as the molecular state (denoted by subscript *M*). The system on a whole is at dynamic equilibrium and polymer can switch from one state to the other through the equilibrium constant, K_{eq},

$$M \underset{k_{off}}{\overset{k_{on}}{\rightleftharpoons}} A \tag{2.4}$$

Here k_{on} and k_{off} are first order rate constants, with $k_{on}[C_M]$ denoting the rate of association and $k_{off}[C_A]$ denoting the rate of dissociation. Since the reaction is at equilibrium, the macroscopic properties of the material measured via rheology measurement remain fixed, even though microscopically a molecule may consistently be switching from one state to the other. Olsen and co-workers[32–34] solved the coupled reaction-diffusion equations for the two species as,

$$\begin{aligned} \frac{\partial C_M}{\partial t} &= k_{off} C_A - k_{on} C_M + D_M \frac{\partial^2 C_M}{\partial x^2} \\ \frac{\partial C_A}{\partial t} &= -k_{off} C_A + k_{on} C_M + D_A \frac{\partial^2 C_A}{\partial x^2} \end{aligned} \tag{2.5}$$

Here C_i is the concentration of species *i*, and D_i is the diffusivity.

The concentration profile follows the solution for $K_{eq} > 1$, which is the case for most reversible polymer networks,

$$\begin{aligned} & C_i = C_{i,0} \exp(-t/\tau) \\ & \frac{2}{\tau} = (\mathrm{k}_{on} + \mathrm{k}_{off} + \mathrm{D}_M \mathrm{q}^2 + \mathrm{D}_A \mathrm{q}^2) - \\ & \sqrt{(\mathrm{k}_{on} + \mathrm{k}_{off} + \mathrm{D}_M \mathrm{q}^2 + \mathrm{D}_A \mathrm{q}^2)^2 - 4(k_{on} q^2 D_A + k_{off} q^2 D_M + q^4 D_M D_A)} \end{aligned} \tag{2.6}$$

Here $C_{i,0}$ is the initial concentration and τ is the relaxation time, q is frequency in the spatial domain, $q = 2\pi / l$, where l is the length. This functional relationship between τ and q was found to agree well with experimental results obtained via Forced Rayleigh Rayleigh Scattering (FRS) measurements[32–34]. We study the influence of the parameters K_{eq} and γ, where $\gamma = D_A/D_M$ is the ratio of diffusivity of clusters to that of the individual molecules and is always less than 1. In Figure 2.2 we plot the relaxation time τ, normalized by k_{off}^{-1}, and $l^2/4\pi^2$ normalized by D_M / k_{on} by non-dimensionalizing equation 2.6 as given below

$$\frac{2}{\tau} = K_{eq} + 1 + K_{eq}(1+\gamma)\mathrm{q}^2 - \sqrt{[K_{eq} + 1 + K_{eq}(1+\gamma)\mathrm{q}^2]^2 - 4[(K_{eq}^2\gamma + K_{eq})q^2 + q^4 K_{eq}^2\gamma]} \tag{2.7}$$

The curves for the concentration relaxation time (corresponding to the fluorescence intensity relaxation time in a FRS experiments) versus the square of the length-scale of probing can be broken down into three regions. The first of these is the initial linear growth of the normalized relaxation time with respect to the normalized length, $\tau \sim l^2$. Since the diffusion of clusters is much slower than of the components the linear regime observed at short length scales corresponds to the diffusivity of the associated state D_A.

This is followed by the transition region, which can be described with a power-law scaling $\tau \sim l^{2/\alpha}$ with α less than 1; Olsen and co-workers[32–34] describe this as the superdiffusive/hyperdiffusive regime. The third regime is again diffusive and is observed at longer length-scales, where particles can move by dissociating from the network and diffusing as individuals. Here the effective diffusivity can be computed using the expression,

$$D_{eff} = D_M(1+\gamma K_{eq})(1+K_{eq})^{-1} \tag{2.8}$$

As seen in Figure 2.2, for increasing K_{eq}, the value of γ at which the transition from purely diffusive to motion with a hyperdiffusive transition progressively decreases. Additionally, the extent of the length-scales spanned by the hyperdiffusive regime decrease as K_{eq} increases. In fact, the ratio of the squared length demarcating the limits of the hyperdiffusive regime can be shown to be approximately $l^2_{large}/l^2_{small} = (\gamma K_{eq})^{-1}$. Thus, according to this model γK_{eq} should be less than one in order to experimentally observe hyperdiffusion.

Recent Brownian dynamics simulations from the same group cast doubt on the simple framework and in fact indicate that the early time diffusivity in these systems is set by D_M rather than D_A as proposed above. The Brownian dynamics analysis also shows that the transition from the initial diffusive regime to the long-time diffusive regime occurs via a subdiffusive plateau in the mean-squared displacement, without any evidence of hyperdiffusion[35]. Instead the authors attribute the so-called hyperdiffusive regime, which one can observe in Figure 2.2, to the large distribution of displacements due to the multiple diffusion mechanisms in associating network. In the following sections, we attempt to construct a model that can capture hyperdiffusion in particle trajectories in systems, which are macroscopically in equilibrium, by considering the particles as the building blocks of associating networks.

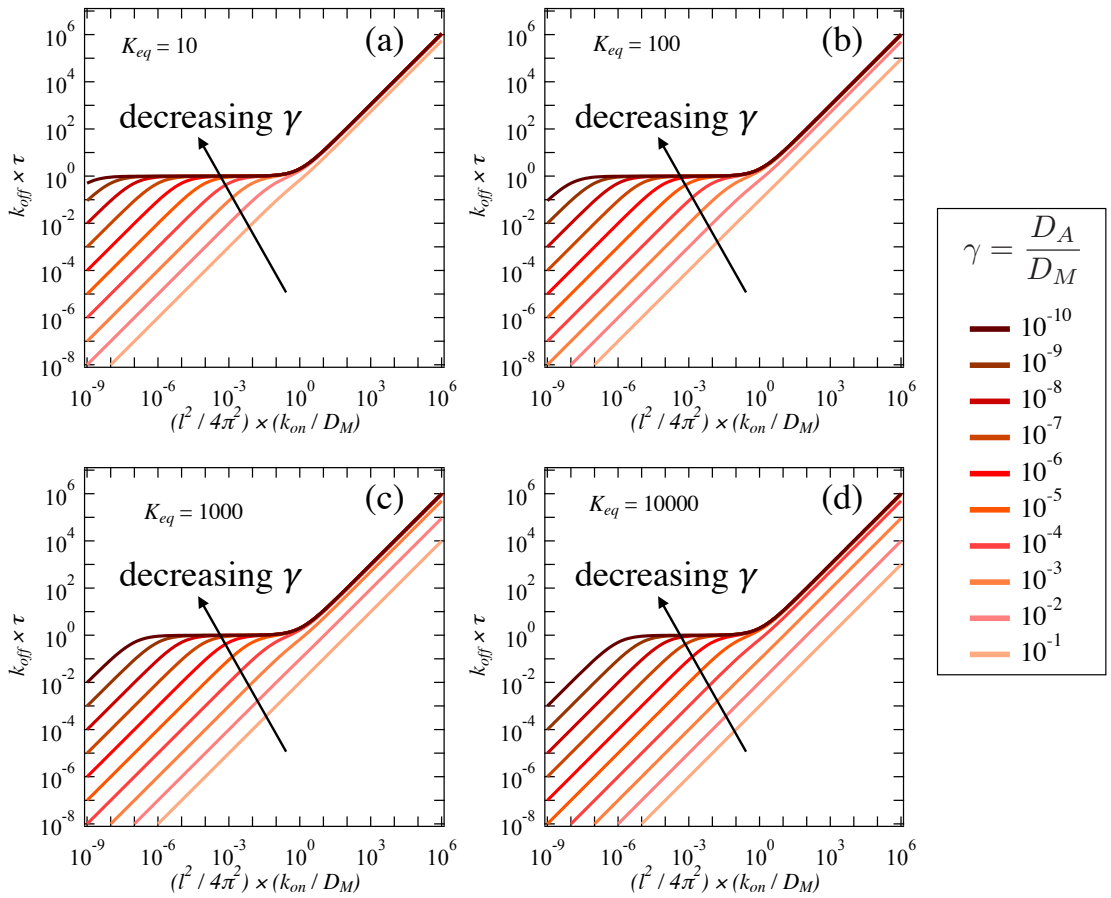

Figure 2.2 Plots of the concentration relaxation time normalized by k_{off}^{-1} as a function of the square of length scale $l^2/4\pi^2$ normalized by k_{on}/D_M for $K_{eq} = k_{on}/k_{off}$ = (a) 10, (b) 100, (c) 1000, and (d) 10^4. These plots are based on the association-dissociation model for reversible networks given by Olsen and co-workers[32–34]. The different curves correspond to different values of the ratio, γ.

2.2.4 Dynamic Cluster Model

Inspired by the analysis given above we create a new model that incorporates the reversible association-dissociation kinetics to predict the trajectory of a single spherical particle, which dynamically switches between being associated with a network of similar particles to being detached and free to move in a solvent of fixed viscosity η. We neglect any hydrodynamic interactions between the particles and the surrounding network.

We utilize the 1D Langevin framework from equation 2.1 in the absence of a surrounding potential ($V = 0$) for the single particle. Using the notation from section 2.2.3 this particle is taken to be the molecular state (represented by subscript M),

$$m_M \frac{d\boldsymbol{v}_M}{dt} = -6\pi\eta R_M \boldsymbol{v}_M(t) + F_{B,M}(t) \tag{2.9}$$

The single particle exists in the overdamped limit where $\tau_{p,M} = m_M / 6\pi\eta R_M << 1$. We have established that this is indeed the case for nanometer-sized particles in solvents such as water, and the more viscous the solvent is, the smaller is the momentum relaxation time τ_p (assuming the continuum approximation holds and the size of solvent molecules is much smaller than the size of the particle). Hence in the molecular state, the particle exhibits random walk trajectories and the mean squared displacement follows the same form as equation 2.2,

$$\left\langle \Delta r^2(t) \right\rangle_M = 2D_M t \ , \tag{2.10}$$

where t is the time, and D_M is the self-diffusivity of the single particle in the solvent with viscosity η.

We assume that the associated state (denoted by subscript *A*) exists as a dense mass fractal of hydrodynamic radius R_A and its diffusivity D_A is given by,

$$D_A = \frac{k_B T}{6\pi\eta R_A} \tag{2.11}$$

The ratio of the diffusivities, $\gamma = D_A / D_M$ can thus be written as $\gamma = R_M / R_A$ and the ratio of the momentum relaxation time of the associated state ($\tau_{p,A}$) to the diffusive time of a single particle or molecular state ($\tau_{D,M}$) is given by

$$\frac{\tau_{p,A}}{\tau_{D,M}} \approx \frac{m_A / 6\pi\eta R_A}{R_M^2 / D_M} = \frac{R_A^2 \rho k_B T}{27\pi\eta^2 R_M^3} = \frac{\rho k_B T}{27\pi\eta^2 R_M \gamma^2} \tag{2.12}$$

where ρ is the density of the fractal. The magnitude of the pre-factor $\rho k_B T / 27\pi\eta^2 R_M$ for a 10 nm radius, density-matched particle in water at room temperature is of the order 10^{-6}. Hence, $\tau_{p,A}$ becomes greater than $\tau_{D,M}$ when γ becomes smaller than 10^{-3}. What this means is that because τ_p is associated with the ballistic time, when $\tau_{p,A}$ is of the same order as $\tau_{D,M}$, the cluster can move ballistically on the order of timescales at which an individual particle is expected to move diffusively.

In an experiment the ensemble-averaged particle trajectory is obtained by averaging the motion of the free particles (particles in state *M*) and the clustered particles (particles in state *A*), which is calculated through center-of-mass displacement of the cluster. While we can separate the ballistic and diffusive times for the molecular state, we cannot separate the diffusive time of the molecular state from the ballistic and diffusive times for the associated state. Thus, we solve the full Langevin equation (equation 2.1) for the associated state, and study the effect of the cluster size and the

fraction of particles in the molecular and associated states on the ensemble averaged particle dynamics of the system.

In the association and dissociation model described in section 2.2.3, $K_{eq} = k_{on}/k_{off}$ denotes the equilibrium rate constant for the reversible reaction given in equation 2.4. Although there is no chemical reaction between the free particles and the cluster in polymer nanocomposites, the number of particles in the free state and the particles in the clustered state form an equilibrium distribution. Therefore, we define equilibrium constant, K_{eq},

$$K_{eq} = \frac{N_A}{N_M} \tag{2.13}$$

which describes the number of particles in the clustered state (N_A) relative to the number of free particles (N_M). This is equivalent to the rate constant discussed in section 2.2.3. Once the equilibrium is attained, the distribution of particles N_A and N_M is fixed on the macroscopic scale, however, the particles can continue to dynamically shift from one state to the other at the microscopic level.

We begin with a network comprising of silica nanoparticles (density of silica ρ_{silica} = 2200 kg/m^3) and the radius of individual particles R_M = 5 nm. For fractal-like aggregates, with a certain value of n, which is the number of particles in a single cluster, n can be related to R_M and R_A via the power law relationship $n = \left(R_A / R_M\right)^{d_f}$, where d_f is the fractal dimension of the cluster and is less than 3. In the case of rapid cluster formation, the clusters are known as diffusion limit aggregates (DLA) with d_f = 1.7-1.8 and in the case of slow cluster formation, d_f = 2.1-2.2 and clusters are called reaction-limited aggregates (RLA)[36]. In this work we assume that the clusters are highly compact and spherical, and the density of the cluster is equal to the density of

the particle, $\rho = \rho_{silica}$ = 2200 kg/m^3. However, the analysis can easily be extended to fractals of different fractal dimensions, and the density of the cluster can be calculated using the expression

$$\rho = \left[R_M^{3-d_f} (\rho_P - \rho_s) + \rho_s \right] \tag{2.14}$$

where ρ_P is density of the particle and ρ_s is the density of the solvent.

We now track the motion of individual particles both in the molecular and associated state, using simulations. The equation of motion for the particle in the molecular state (equation 2.8), after neglecting the inertial term becomes,

$$\frac{dx_M}{dt} = \boldsymbol{F}_{B,M}(t) \tag{2.15}$$

where the position x_M is normalized by the particle radius R_M and the random thermal force $F_{B,M}$ is normalized by k_BT/R_M. For the cluster, the Langevin equation

$$m_A \frac{d^2 x_A}{dt^2} = -6\pi\eta R_A \frac{dx_A}{dt} + F_{B,A}(t) \tag{2.16}$$

Non-dimensionalizing this equation with length scale R_M and timescale R_M^2/D_M we obtain,

$$\frac{\rho k_B T}{27 R\pi (\eta\gamma)^2} \frac{d^2 x_A}{dt^2} = -\frac{dx_A}{dt} + F_{B,A}(t) \tag{2.17}$$

Here the thermal force $F_{B,A}$ is normalized by $k_BT/\gamma R_M$. As shown in equation 2.12, the pre-factor (= $\tau_{P,A}/\ \tau_{D,M}$) to the inertial term becomes larger as γ decreases and hence, the inertial term in this equation cannot be neglected.

We solve equations 2.15 and 2.17 for the trajectories of the cluster (A) and the free particles (M) independent of each other and utilize this to compute the average trajectory of a particle in the given sample volume.

2.3 Results and Discussion

The parameter K_{eq}, which sets the equilibrium between particles associating or dissociating from the clusters in the sample volume, can be interpreted in terms of the ratio of the probability of finding a particle associated with a cluster versus finding a free particle or particle dissociated from the cluster or network. Hence, $K_{eq} = 0$ implies that the particles do not display the tendency to associate into clusters and the sample is primarily composed of free particles. A preference for particles to associate as opposed to staying in the dissociated or molecular state, would mean that $K_{eq} > 1$ and the larger this value is, the larger is the fraction of associated particles in the sample volume. In most associating networks, thermal energy is responsible for dissociating the particles from the network, hence attractive interaction energy between the particles and cluster must be larger than the thermal energy for K_{eq} to be greater than 1.

The normalized mean-squared displacement versus time plots for different γ are shown in Figure 2.3. We treat γ, the ratio of the particle diffusivity to the cluster diffusivity, which can also be written as the ratio of particle size to the cluster size, as an independent parameter from K_{eq} and are not looking at the thermodynamics of cluster formation in the present work.

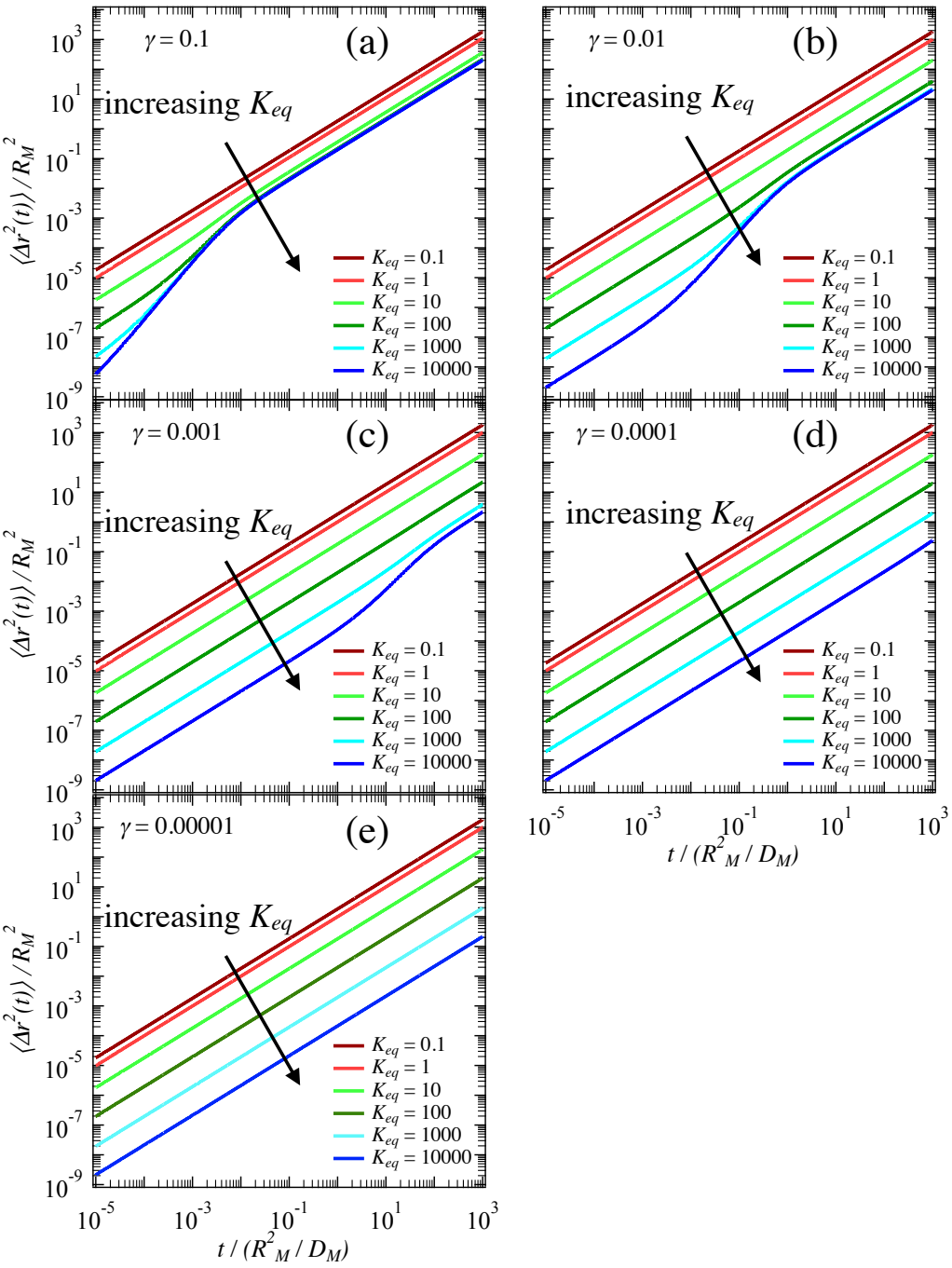

Figure 2.3 Plot of mean squared displacement ($\langle \Delta r^2(t) \rangle$) normalized by square of the particle radius R_M versus time normalized by the diffusive time for a free particle (R_M^2/D_M) for different values of the ratio of diffusivity of the cluster and the free particle γ = (a) 0.1, (b) 0.01 (c) 0.001, (d) 0.0001, and (e) 0.00001. Different curves correspond to different values of the parameter K_{eq}.

In Figure 2.3, irrespective of the size of the cluster, as K_{eq} increases the particle motion slows down. This is intuitive as K_{eq} dictates the contribution of the clusters to the average motion and the cluster moves much more slowly than the free particle. For γ = 0.1 (Figure 2.3a) as K_{eq} increases one can clearly observe two regions to the mean squared displacement curves, viz., an early time hyperdiffusive region ($t < 0.001\ R_M^2/D_M$) and long-time diffusive regime. While smaller values of K_{eq} exhibit only diffusive behavior at all time.

By making the size of the cluster 10 times larger than this case (γ = 0.01 in Figure 2.3b), we observe that mean squared displacement versus time curves have three distinct regions – an initial diffusive, a hyperdiffusive transition and a final diffusive region. The transition from hyperdiffusive region to diffusive region is shifted to longer time ($t_T \approx 1\ R_M^2/D_M$) in comparison to the smaller cluster size and the hyperdiffusive regime would be experimentally accessible. The onset and end of hyperdiffusion is further delayed when we make the cluster size even larger (γ = 0.001 in Figure 2.3c). Here, the transition from the first diffusive to the second hyperdiffusive diffusive step occurs at ($t_T \approx 1\ R_M^2/D_M$) in contrast to $t_T \approx 0.001\ R_M^2/D_M$ in Figure 2.3b. The transition from hyperdiffusive to the second diffusive step occurs at $\sim 100\ R_M^2/D_M$ (not shown in the figure). The curves appear to have no hyperdiffusive regime for $\gamma = 10^{-4}$ and $\gamma = 10^{-5}$ (shown in Figures 2.3d and 2.3e) in the given range of K_{eq}. This shows that as cluster size becomes even larger particles within the cluster are effectively arrested and do not contribute to the average observed dynamics.

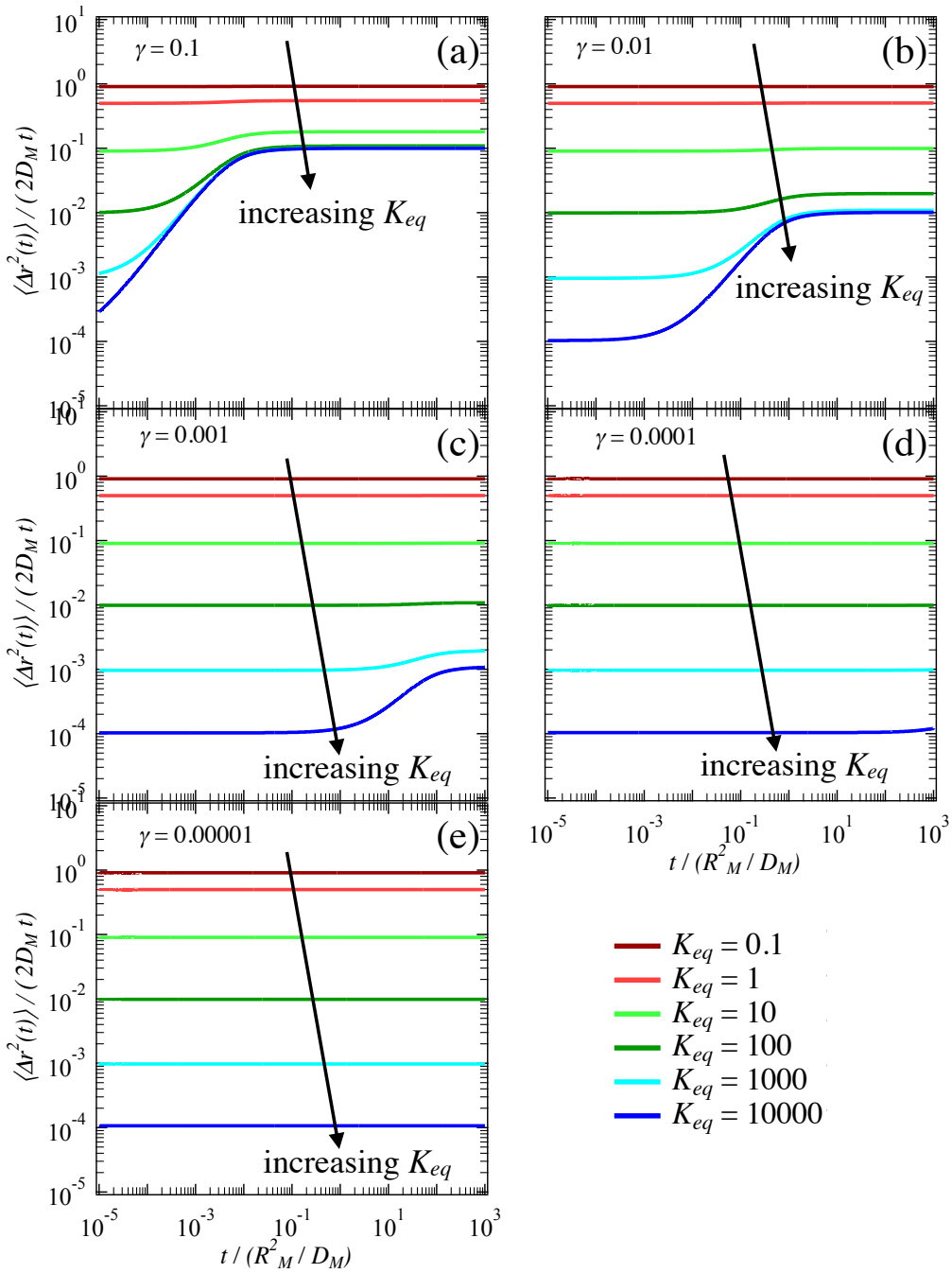

Figure 2.4 Mean-squared displacement ($\langle \Delta r^2(t) \rangle$) normalized by the $2D_M t$ plotted against time normalized by the diffusive time for a free particle, R_M^2/D_M for different values of the ratio of diffusivity of the cluster and the free particle γ = (a) 0.1, (b) 0.01 (c) 0.001, (d) 0.0001, and (e) 0.00001. Different curves correspond to different values of the parameter K_{eq}.

We zoom into the hyperdiffusive transition presented in Figure 2.3, by rescaling the mean-squared displacement by $2D_M\,t$ and plot the result for different values of γ against time normalized by the diffusive time for the free particle (R_M^2/D_M) in Figure 2.4.

A close inspection of Figure 2.4 reveals that the ability to separate timescales and observe ballistic motion of the clusters from the diffusive motion of the free particles is a strong function of K_{eq}. For an arbitrary value of K_{eq}, the probability that one is tracking a free particle at equilibrium is given by $(1+K_{eq})^{-1}$. When the number of free particles in the sample volume are larger than or comparable to the number of associated particles, i.e., K_{eq} = 0.1 and K_{eq} = 1, not only is the average dynamical response diffusive but also the average diffusivity of particles in the sample is given by $\left\langle \Delta r^2(t) \right\rangle / 2D_M t \approx (1+K_{eq})^{-1}$ irrespective of the diffusivity of the cluster (also seen in Figure 2.5 a, b).

For γ = 0.1, and for K_{eq} =10 or higher, the hyperdiffusive regime becomes observable, even though the initial diffusive part of the curves still coincide as seen in Figures 2.5c, 2.5d, 2.5e and the initial diffusivity can still be approximated by $(1+K_{eq})^{-1}$. The time at the hyperdiffusive regime ends for a fixed value of γ coincides with each other and is close to the momentum relaxation time of the cluster $t \approx \tau_{P,A}$. However, the onset of hyperdiffusion is dependent on fraction of associated particles and becomes smaller as K_{eq} increases. In fact for high enough values of K_{eq} the ballistic regime for the clusters will overlap with the ballistic regime of the free particles.

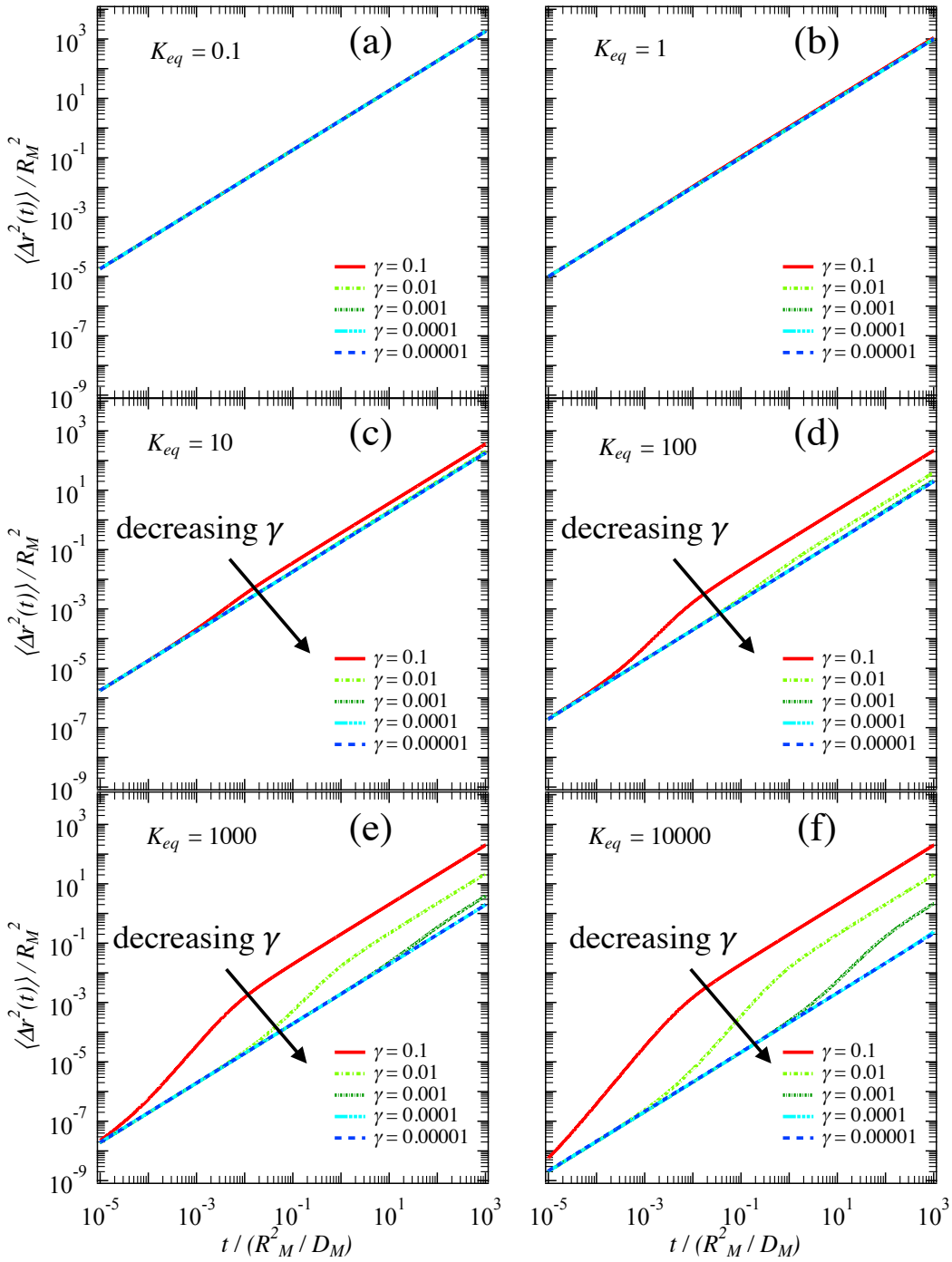

Figure 2.5 Plot of mean squared displacement ($\langle \Delta r^2(t) \rangle$) normalized by square of the particle radius R_M versus time normalized by the diffusive time for a free particle (R_M^2/D_M) for different values of K_{eq} = (a) 0.1, (b) 0.01 (c) 0.001, (d) 0.0001, and (e) 0.00001. Different curves correspond to different values of the parameter γ.

Similar to the short-time diffusivity, the long-time average mean-squared displacement can be approximated by the expression $\left\langle \Delta r^2(t) \right\rangle / 2D_M t \approx p_M D_M + p_A D_A = (1 + K_{eq}\gamma)(1 + K_{eq})^{-1}$, where p_A is probability for finding an associated particle and p_M is the probability of finding a free particle in the sample volume. This matches the expression 2.8 for the effective long-time diffusivity in associating clusters obtained by Olsen and co-workers[32]. We deduce that an appreciable change between the short- and long-time diffusivity exists if $\gamma K_{eq} > 1$.

In the limit of $K_{eq} \to 0$, i.e., in the absence of any associated particles or clusters in the sample volume, the average mean-squared displacement of the particles is given by $\left\langle \Delta r^2(t) \right\rangle = 2D_M t$ and $\left\langle \Delta r^2(t) \right\rangle / 2D_M t = 1$ is a constant in time. In the opposite limit of $K_{eq} \to \infty$, when there are no free particles in the sample volume and at long times the mean squared displacement response is given by $\left\langle \Delta r^2(t) \right\rangle / 2D_M t = \gamma$.

This is an important result and can explain why hyperdiffusion seems to disappear for lower values γ at fixed values of K_{eq} (as seen in Figure 2.5 b, c, d, e). To support this conclusion, we plot the mean-squared displacement normalized by the square of particle radius, R_M, and mean-squared displacement normalized by $2D_M t$ with respect to time for $\gamma = 10^{-3}$, 10^{-4} and 10^{-5} for even longer durations in Figure 2.6. Figures 2.6b and 2.6d clearly indicate that hyperdiffusive regime is visible for $K_{eq} \geq \gamma^{-1}$ and lasts up to roughly the momentum relaxation time of the cluster. On the basis of this analysis, we can predict that even higher values of K_{eq} will exhibit hyperdiffusion in the case where $\gamma = 10^{-5}$, and the overall dynamics will be even slower.

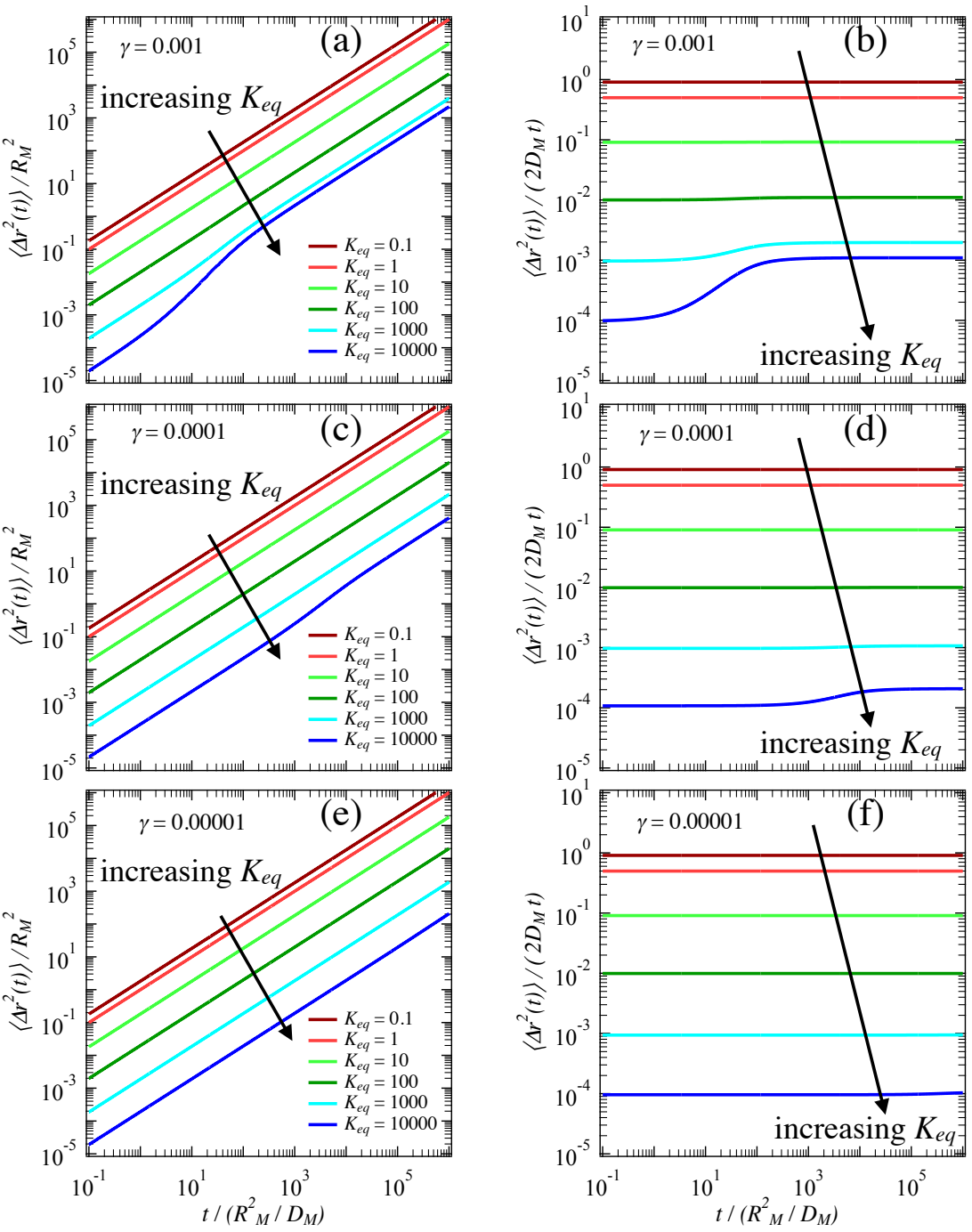

Figure 2.6 Mean-squared displacement ($\langle \Delta r^2(t) \rangle$) normalized by the R_M^2 for γ = (b) 0.001, (d) 10^{-4} (f) 10^{-5}; and normalized by $2D_M t$ for γ = (b) 0.001, (d) 10^{-4} (f) 10^{-5}. The x-axis corresponds to the time scaled by the diffusive time for the free particle. Different curves correspond to different values of the parameter K_{eq}.

2.4 Conclusions

In this work we propose a simple model for explaining hyperdiffusive relaxations in polymer nanocomposites by approximating the composites as reversible physically cross-linked networks, where a fraction of particles are free to move and a fraction are associated with larger structures that form a polymer-particle network. These two phases are in a dynamic equilibrium with each other, allowing the particles to continuously move from one phase to the other based on the relative strength of attractive potential between the particles and network with respect to the repulsive interactions between them, such as those arising from repulsive Brownian forces and steric interactions, among others.

While the long-time transport in these materials is diffusive in nature, it is possible to obtain hyperdiffusion in the average dynamical behavior of particles for some materials under certain length and time scales of observation. These timescales are readily accessible by advanced experiments which have already established that the regime in which hyperdiffusive particle motions are observed can be quite a bit larger than expected from the Langevin prediction[19,27]. These measurements also reveal that the hyperdiffusion regime can be prolonged via memory effects in the host materials stemming from polymer viscoelasticity or hydrodynamic correlations.

It is also well known that strong attractive interactions between the particles and the host polymer are essential to uniformly disperse nanoparticles within the polymer[37]. In fact at sufficiently high particle loadings and large host molecular weights, polymers can form long-range bridges between the particles[38], which do not affect the uniformity of the dispersion[39]. This supports our hypothesis that particles in polymer

nanocomposites exist as part of a large network. In their review titled 'How nano are nanocomposites?' Schaefer and Justice[40] attempted to answer their self-designated question by looking at a number of polymer nanoparticle blends and concluded that a vast majority of nanocomposites may in fact be composed of large clusters unless shown to be not so by ultra-small angle x-ray scattering. However not all nanocomposites where hyperdiffusion is observed satisfy the condition of significant particle bridging described in the literature[38] and are shown to be well-dispersed through small angle x-ray scattering measurements, and hence these materials may not share the same origins for hyperdiffusion as shown in the previous section[2,41].

In contrast a more direct relationship between reversible networks and polymer nanocomposites based on solvent-free, self-suspended hairy nanoparticles was established in a recent work by Agrawal et al.[42], where it was shown that the space filling constraint on the tethered polymers, imposed by the absence of a solvent, creates physical bonds between the chains of neighboring particles that can be likened to reversible cross-links. Since, all particle cores in the sample volume are connected, the presence of long-lived hyperdiffusion in self-suspended hairy nanoparticles is on the basis of the foregoing analysis intuitive since a large portion of sample can behave as one cluster.

More recently, Ramirez et al.[35] have shown through Brownian Dynamics simulations that techniques based on transient structure factor measurements such as Forced Rayleigh Scattering, and X-ray photon correlation spectroscopy are more sensitive to the distribution of diffusivities rather than the mean motion observed in particle tracking experiments. Hence, a bimodal distribution of mean squared displacements can lead to the measurement of pseudo-hyperdiffusive behavior by these techniques.

This result could have significant consequences for the field of nanocomposites, as it highlights that non-ergodicity is not pre-condition for the observation of hyperdiffusion in XPCS measurements.

Bibliography

(1) Einstein, A. Über Die von Der Molekularkinetischen Theorie Der Wärme Geforderte Bewegung von in Ruhenden Flüssigkeiten Suspendierten Teilchen. *Ann. Phys.* **1905**, *322* (8), 549–560.

(2) Mangal, R.; Srivastava, S.; Narayanan, S.; Archer, L. A. Size-Dependent Particle Dynamics in Entangled Polymer Nanocomposites. *Langmuir* **2016**, *32* (2), 596–603.

(3) Narayanan, S.; Lee, D. R.; Hagman, A.; Li, X.; Wang, J. Particle Dynamics in Polymer-Metal Nanocomposite Thin Films on Nanometer-Length Scales. *Phys. Rev. Lett.* **2007**, *98* (18), 185506.

(4) Mangal, R.; Srivastava, S.; Archer, L. A. Phase Stability and Dynamics of Entangled Polymer–nanoparticle Composites. *Nat. Commun.* **2015**, *6*, 7198.

(5) Guo, H.; Bourret, G.; Corbierre, M. K.; Rucareanu, S.; Lennox, R. B.; Laaziri, K.; Piche, L.; Sutton, M.; Harden, J. L.; Leheny, R. L. Nanoparticle Motion within Glassy Polymer Melts. *Phys. Rev. Lett.* **2009**, *102* (7), 75702.

(6) Cipelletti, L.; Manley, S.; Ball, R. C.; Weitz, D. A. Universal Aging Features in the Restructuring of Fractal Colloidal Gels. *Phys. Rev. Lett.* **2000**, *84* (10), 2275–2278.

(7) Jang, W.; Koo, P.; Bryson, K.; Narayanan, S.; Sandy, A.; Russell, T. P.; Mochrie, S. G. Dynamics of Cadmium Sulfide Nanoparticles within Polystyrene

Melts. *Macromolecules* **2014**, *47* (18), 6483–6490.

(8) Tuteja, A.; Mackay, M. E.; Narayanan, S.; Asokan, S.; Wong, M. S. Breakdown of the Continuum Stokes-Einstein Relation for Nanoparticle Diffusion. *Nano Lett.* **2007**, *7* (5), 1276–1281.

(9) Cai, L.-H.; Panyukov, S.; Rubinstein, M. Mobility of Nonsticky Nanoparticles in Polymer Liquids. *Macromolecules* **2011**, *44* (19), 7853–7863.

(10) Cai, L.-H.; Panyukov, S.; Rubinstein, M. Hopping Diffusion of Nanoparticles in Polymer Matrices. *Macromolecules* **2015**, *48* (3), 847–862.

(11) Ge, T.; Kalathi, J. T.; Halverson, J. D.; Grest, G. S.; Rubinstein, M. Nanoparticle Motion in Entangled Melts of Linear and Nonconcatenated Ring Polymers. *Macromolecules* **2017**, *50* (4), 1749–1754.

(12) Mason, T. G.; Weitz, D. A. Optical Measurements of Frequency-Dependent Linear Viscoelastic Moduli of Complex Fluids. *Phys. Rev. Lett.* **1995**, *74* (7), 1250–1253.

(13) Brochard Wyart, F.; de Gennes, P. G. Viscosity at Small Scales in Polymer Melts. *Eur. Phys. J. E - Soft Matter* **2000**, *1* (1), 93–97.

(14) Bhattacharyya, S.; Bagchi, B. Anomalous Diffusion of Small Particles in Dense Liquids. *J. Chem. Phys.* **1997**, *106* (5), 1757–1763.

(15) Yamamoto, U.; Schweizer, K. S. Theory of Nanoparticle Diffusion in Unentangled and Entangled Polymer Melts. *J. Chem. Phys.* **2011**, *135* (22), 224902.

(16) Saltzman, E. J.; Schweizer, K. S. Activated Hopping and Dynamical Fluctuation Effects in Hard Sphere Suspensions and Fluids. *J. Chem. Phys.* **2006**, *125* (4), 44509.

(17) Chen, Y.-F.; Wei, H.-H.; Sheng, Y.-J.; Tsao, H.-K. Superdiffusion in Dispersions of Active Colloids Driven by an External Field and Their Sedimentation Equilibrium. *Phys. Rev. E* **2016**, *93* (4), 42611.

(18) Cipelletti, L.; Manley, S.; Ball, R. C.; Weitz, D. A. Universal Aging Features in the Restructuring of Fractal Colloidal Gels. *Phys. Rev. Lett.* **2000**, *84* (10), 2275–2278.

(19) Cipelletti, L.; Ramos, L.; Manley, S.; Pitard, E.; Weitz, D. A.; Pashkovski, E. E.; Johansson, M. Universal Non-Diffusive Slow Dynamics in Aging Soft Matter. *Faraday Discuss.* **2003**, *123* (1), 237–251.

(20) Guo, H.; Bourret, G.; Corbierre, M. K.; Rucareanu, S.; Lennox, R. B.; Laaziri, K.; Piche, L.; Sutton, M.; Harden, J. L.; Leheny, R. L. Nanoparticle Motion within Glassy Polymer Melts. *Phys. Rev. Lett.* **2009**, *102* (7), 75702.

(21) Shin, S.; Dorfman, K. D.; Cheng, X. Shear-Banding and Superdiffusivity in Entangled Polymer Solutions. *Phys. Rev. E* **2017**, *96* (6), 62503.

(22) Cates, M. E. Reptation of Living Polymers: Dynamics of Entangled Polymers in the Presence of Reversible Chain-Scission Reactions. *Macromolecules* **1987**, *20* (9), 2289–2296.

(23) Ott, A.; Bouchaud, J. P.; Langevin, D.; Urbach, W. Anomalous Diffusion in "'living Polymers'": A Genuine Levy Flight? *Phys. Rev. Lett.* **1990**, *65* (17), 2201–2204.

(24) Ariel, G.; Rabani, A.; Benisty, S.; Partridge, J. D.; Harshey, R. M.; Be'er, A. Swarming Bacteria Migrate by Lévy Walk. *Nat. Commun.* **2015**, *6* (1), 8396.

(25) Vandebroek, H.; Vanderzande, C. The Effect of Active Fluctuations on the Dynamics of Particles, Motors and DNA-Hairpins. *Soft Matter* **2017**, *13* (11), 2181–2191.

(26) Huang, R.; Chavez, I.; Taute, K. M.; Lukić, B.; Jeney, S.; Raizen, M. G.; Florin, E.-L. Direct Observation of the Full Transition from Ballistic to Diffusive Brownian Motion in a Liquid. *Nat. Phys.* **2011**, *7* (7), 576–580.

(27) Pusey, P. N. Brownian Motion Goes Ballistic. *Science (80-.).* **2011**, *332*

(6031), 802–803.

(28) Srivastava, S.; Agarwal, P.; Mangal, R.; Koch, D. L.; Narayanan, S.; Archer, L. A. Hyperdiffusive Dynamics in Newtonian Nanoparticle Fluids. *ACS Macro Lett.* **2015**, *4* (10), 1149–1153.

(29) Bouchaud, J.-P.; Pitard, E. Anomalous Dynamical Light Scattering in Soft Glassy Gels. *Eur. Phys. J. E* **2002**, *9* (3), 287–291.

(30) Agarwal, P.; Qi, H.; Archer, L. A. The Ages in a Self-Suspended Nanoparticle Liquid. *Nano Lett.* **2010**, *10* (1), 111–115.

(31) Agarwal, P.; Srivastava, S.; Archer, L. A. Thermal Jamming of a Colloidal Glass. *Phys. Rev. Lett.* **2011**, *107* (26), 268302.

(32) Tang, S.; Wang, M.; Olsen, B. D. Anomalous Self-Diffusion and Sticky Rouse Dynamics in Associative Protein Hydrogels. *J. Am. Chem. Soc.* **2015**, *137* (11), 3946–3957.

(33) Tang, S.; Habicht, A.; Li, S.; Seiffert, S.; Olsen, B. D. Self-Diffusion of Associating Star-Shaped Polymers. *Macromolecules* **2016**, *49* (15), 5599–5608.

(34) Tang, S.; Olsen, B. D. Relaxation Processes in Supramolecular Metallogels Based on Histidine–Nickel Coordination Bonds. *Macromolecules* **2016**, *49* (23), 9163–9175.

(35) Ramirez, J.; Dursch, T. J.; Olsen, B. D. A Molecular Explanation for Anomalous Diffusion in Supramolecular Polymer Networks. *Macromolecules* **2018**, *51* (7), 2517–2525.

(36) Waite, T. D.; Cleaver, J. K.; Beattie, J. K. Aggregation Kinetics and Fractal Structure of γ-Alumina Assemblages. *J. Colloid Interface Sci.* **2001**, *241* (2), 333–339.

(37) Jayaraman, A. Polymer Grafted Nanoparticles: Effect of Chemical and Physical Heterogeneity in Polymer Grafts on Particle Assembly and Dispersion. *J. Polym. Sci. Part B Polym. Phys.* **2013**, *51* (7), 524–534.

(38) Surve, M.; Pryamitsyn, V.; Ganesan, V. Universality in Structure and Elasticity of Polymer-Nanoparticle Gels. *Phys. Rev. Lett.* **2006**, *96* (17), 177805.

(39) Hooper, J. B.; Schweizer, K. S. Contact Aggregation, Bridging, and Steric Stabilization in Dense Polymer−Particle Mixtures. *Macromolecules* **2005**, *38* (21), 8858–8869.

(40) Schaefer, D. W.; Justice, R. S. How Nano Are Nanocomposites? *Macromolecules* **2007**, *40* (24), 8501–8517.

(41) Mangal, R.; Nath, P.; Tikekar, M.; Archer, L. A. Enthalpy-Driven Stabilization of Dispersions of Polymer-Grafted Nanoparticles in High-Molecular-Weight Polymer Melts. *Langmuir* **2016**, *32* (41), 10621–10631.

(42) Agrawal, A.; Yu, H.-Y.; Sagar, A.; Choudhury, S.; Archer, L. A. Molecular Origins of Temperature-Induced Jamming in Self-Suspended Hairy Nanoparticles. *Macromolecules* **2016**, *49* (22), 8738–8747.

CHAPTER 3

EFFECT OF INTERPARTICLE CORRELATIONS ON PARTICLE DYNAMICS IN SOLUTIONS OF HAIRY NANOPARTICLES

3.1 Introduction

Solvent-free polymer grafted nanoparticles, often referred to by the moniker NOHMs (nanoparticle-organic hybrid materials), comprise of inorganic nanoparticle cores covered by a canopy of polymer chains. These materials are described as self-suspended because they do not contain any solvent, and the only suspending media within these materials are the surface-tethered oligomers. The properties of these materials are a direct function of the grafting density, and the molecular weight of tethered polymers, and the volume fraction of the inorganic core as at low core fractions the materials exhibit similar mechanical properties as the tethered polymers and as the volume fraction of the cores increases complex many body interactions begin to play an important role[1].

Theory, simulations and experiments have conclusively demonstrated the presence of strong space filling constraints on the tethered chains in these hybrid materials, which lead to interesting material properties[2–12]. Previous work by Srivastava et al. showed the profound effect of the space filling constraint on particle dynamics in solvent-free hairy nanoparticles[7] and showed that highly correlated nanoparticles could exhibit hyperdiffusive dynamics due to their collective volumetric fluctuations.

Within this chapter, we study the impact of structure on the dynamics of nanoparticle fluids and demonstrate that loss of interparticle correlation can lead to transition from purely hyperdiffusive dynamics in concentrated solutions to diffusive transport in dilute solutions of hairy nanoparticles in solvents. To systematically study this transition we first create self-suspended hairy nanoparticles and then proceed to dilute them with different amounts of solvent. We prepare a library of hairy nanoparticle fluids doped with solvents and evaluate their structure through small angle x-ray scattering measurements and their dynamics through X-ray photon correlation spectroscopy measurements.

3.2 Experimental Methods

Synthesis: Silane terminated polyethylene glycol methyl ether from Gelest, Inc. (M_w ~ 500 g/mol) and Laysan Bio, Inc. (M_w ~ 5000 g/mol) and covalently coupled to silica nanoparticles (LUDOX SM 30) of diameter (*d*) about 10 nm using a previously described procedure[13,14]. The grafting density for PEG500-SiO_2 and PEG5000-SiO_2 was found to be 2.3 and 1.8 chains/nm^2 respectively, using thermo gravimetric analysis. 1-n-Butyl-3-methylimidazolium chloride was purchased from Alfa Aesar and the halide anion was exchanged with the bis(trifluoromethylsulfonyl)imide anion using lithium bis(trifluoromethylsufonyl)imide salt (purchased for Sigma Aldrich) and following the procedure provided by Camper et al.[15] Pre-weighed amount of the PEG500-SiO_2 was dissolved in 1-n-Butyl-3-methylimidazolium bis(trifluoromethylsulfonyl)imide ionic liquid (IL) using acetonitrile as co-solvent and PEG5000-SiO_2 was dissolved in diethyl phthalate (DEP purchased from Sigma Aldrich) using dichloromethane as co-solvent. Co-solvent removal from PEG500-SiO_2

in IL samples was carried out by heating in a convection oven at 60 ^{o}C followed by annealing in a vacuum oven at 80 ^{o}C for 24 hours. Similarly dichloromethane was removed from PEG5000-SiO_2 samples at room temperature and the resulting samples were annealed for 24 hours under vacuum.

Dynamical Measurements: X-ray Photon correlation spectroscopy measurements were performed at sector 8-ID-I of the Advanced Photon Source at Argonne National Lab using special liquid holders.

Small Angle X-ray Scattering Measurements: Small angle x-ray scattering (SAXS) measurements were performed at station D1 of the Cornell High Energy Synchrotron Source (CHESS). The samples were loaded into aluminum thermal cells with Kapton windows measurements were performed at 25 ^{o}C for the samples comprising of PEG500-SiO_2 in IL and at 90 ^{o}C for samples comprising of PEG5000-SiO_2 in DEP. The scattering intensity, $I(q, \varphi)$, can be described as a function of the wave vector q and nanoparticle volume fraction φ as given below,

$$I(q,\varphi) = P(q) \times S(q,\varphi) \ , \tag{3.1}$$

here $P(q)$ is the particle form factor and $S(q, \varphi)$ is the interparticle structure factor. Because in the limit of infinitely dilution, particles do not have an internal structure, i.e. $S(q,\varphi \to 0) \to 1$, the particle form factor, $P(q)$, was obtained from scattering intensities of dilute aqueous suspensions of SM30 particles. The structure factor for the samples was then obtained by normalizing the scattering intensity with this form factor.

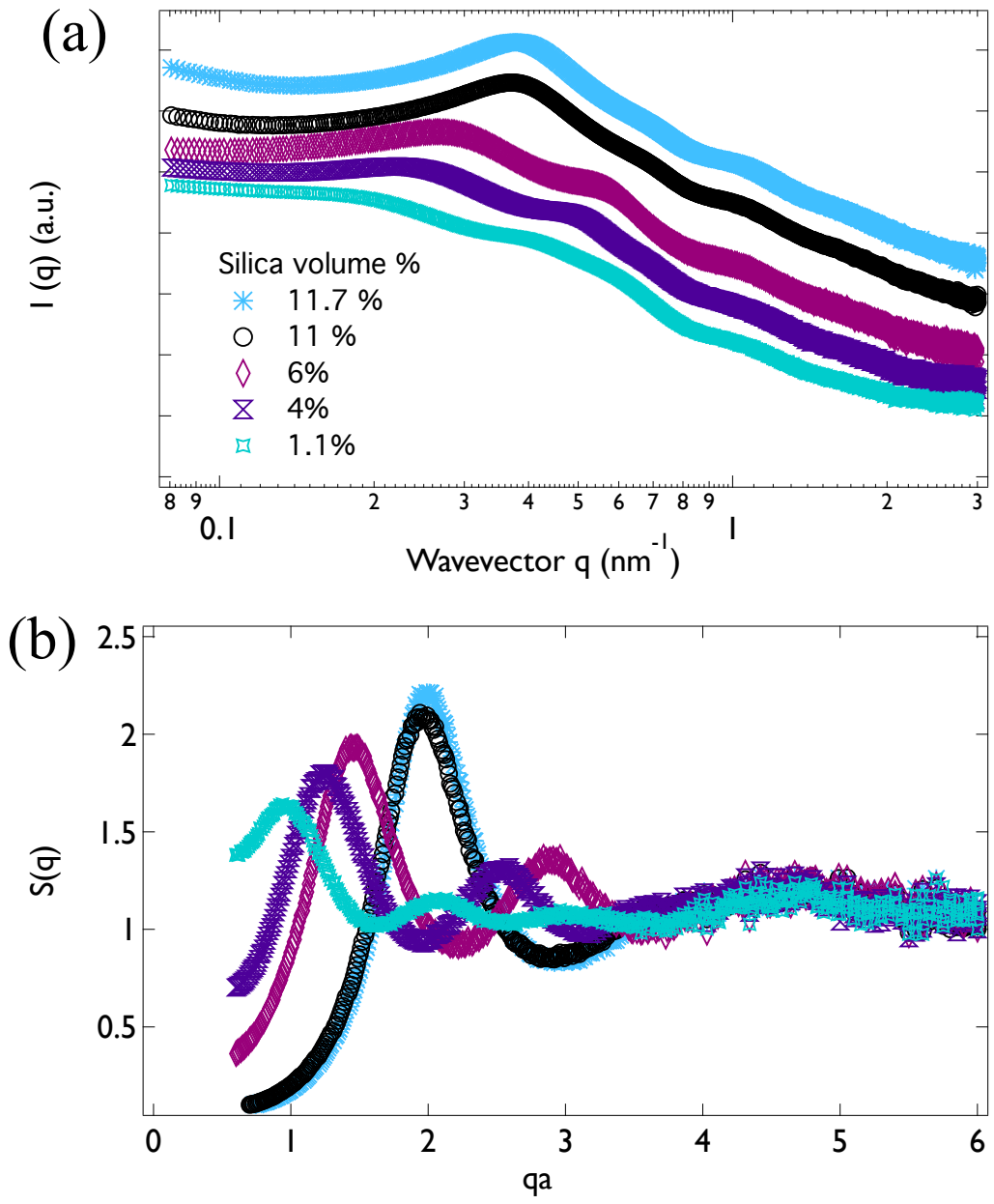

Figure 3.1 (a) Scattering intensity, *I(q)*, in arbitrary units for PEG5000-SiO_2 particles in DEP for different volume fraction of silica nanoparticles φ at 90 ^{o}C plotted against the wave vector q (units nm^{-1}). (b) Structure factor, *S(q)*, for PEG5000-SiO_2 particles in DEP for different volume fraction of silica nanoparticles φ at 90 ^{o}C plotted against the wave vector q (units nm^{-1}) multiplied by the average core radius, *a*.

3.3 Results and Discussion

We plot the scattered intensity *I(q)* from SiO_2 particles grafted with 5000 kDa PEG (diluted with varying amount of DEP) against the scattering wave vector, *q*, for materials with different volume fraction of silica core in Figure 3.1a. The self-suspended particles (containing no DEP) correspond to 11.7 % of silica core volume fraction and the lowest silica core volume fraction (of 1.1%) corresponds to 90% of DEP content in the material. The weak dependence of *I(q)* on *q* for low values of *q* indicates that these materials do not contain large aggregated structures.

To study particle correlations in more detail, we plot the structure factor, *S(q)* for these materials against the wave vector *q* normalized by the core radius *a* (taken to be 5 nm) in Figure 3.1b. Structure factor is the Fourier transform of the radial distribution function, *g(r)*, which represents the average spatial distribution of particles around a reference particle in the material. Thus the height of the first peak S1 is a direct measure of the extent to which the nearest neighbors are correlated to the reference particle. The position of first peak of the structure factor, q_{max}, can be related to the average distance between the particle cores (d_{p-p}) through the relationship $d_{p-p} = 2\pi/q_{max}$.

The loss of correlation with decreasing particle content can thus be deduced from both the height of the peak which progressively decreases and the peak position which continually shifts to the lower values with decreasing core fraction (or increasing solvent content). This result is consistent with previous reports of evaluation of particle structure in suspensions[12]. Another important feature is the distance between the first and the second peaks which is indicative of the interaction between the

particles, with more attractive particles having more closely spaced peaks[1]. We observe that as the volume fraction of the silica cores decreases they develop more affinity for each other. This could be an indicative of a greater tendency for particles to aggregate in solvents compared to the self-suspended case.

We observe a similar trend in the scattering and structure of PEG500-SiO_2 particles in IL, shown in Figure 3.2. For the case of PEG500-SiO_2 particles the solvent-free particles have a silica core volume fraction of about 60% and these particles exist as a solid at 30 ^oC. Hence, we perform structural and dynamical measurements only on the samples that exist as gels or liquids at 30 ^oC. Ionic liquids are known to solvate polyethylene glycol to a much higher degree in comparison to simple solvents like DEP. Since PEG has a higher affinity for ionic liquids compared to itself, the presence of ionic liquid induces a strong stretching of PEG chains[16]. Hence, addition of ionic liquid to hairy nanoparticles must not only lead to the higher interparticle separation but also create an effective repulsion between the PEG chains on neighboring particles. The spacing between the primary and secondary structure factor peaks is shown (in Figure 3.2b) to increase with decreasing core fraction (or increasing IL content). Also similar to the DEP, the presence of ionic liquid increases interparticle spacing as evident in the decreasing value of the wave vector at q_{max}. At the lowest silica volume fraction of 0.06, the structure completely disappears.

The upturn in the structure factor at low q for silica volume fraction of 0.5 suggests that the concentrated blends of NOHMs and ionic liquid are not completely uniform. However this upturn disappears as the solvent content increases, proving that ionic liquid can indeed completely solvate PEG NOHMs.

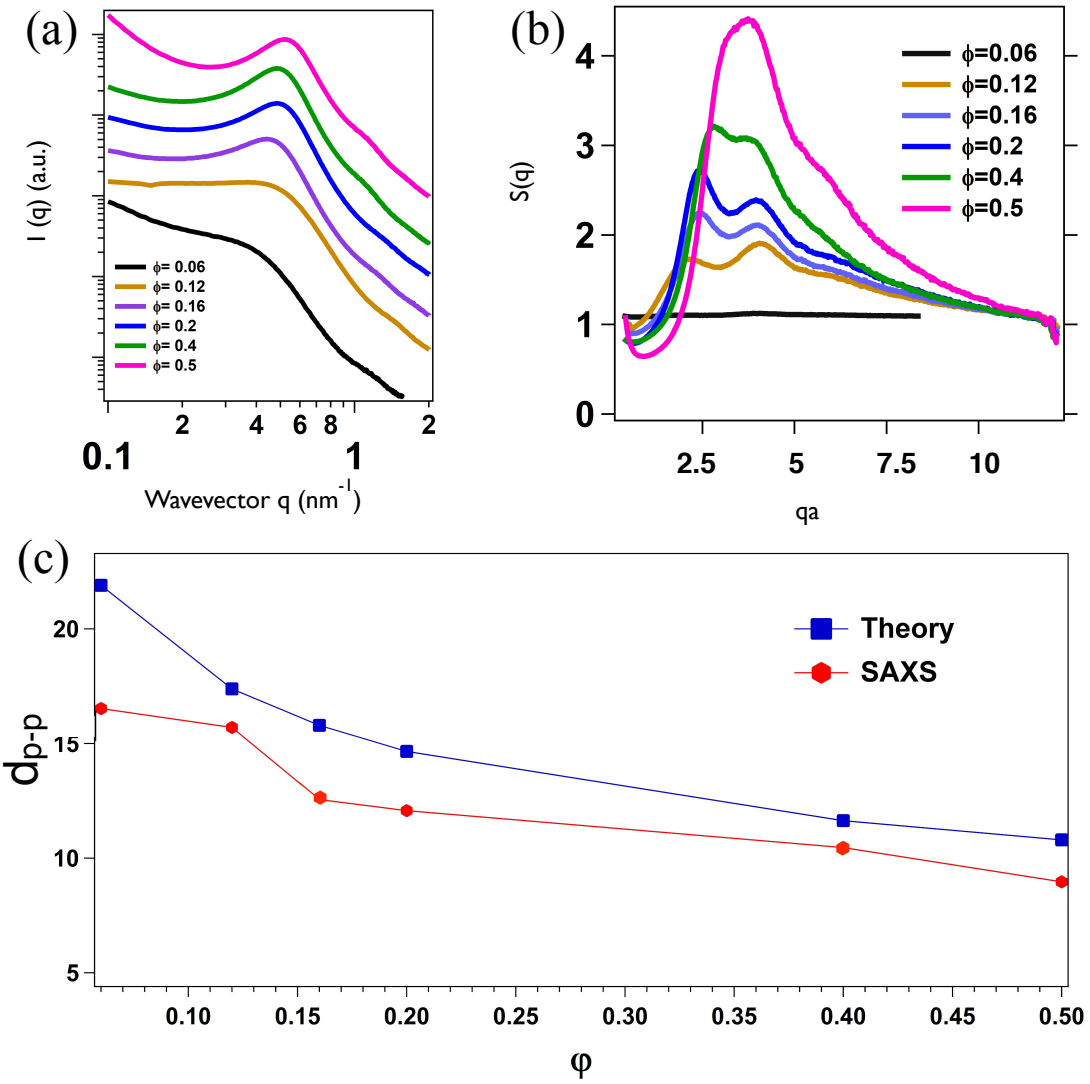

Figure 3.2 (a) Scattering intensity, *I(q)*, in arbitrary units for PEG500-SiO_2 particles in ionic liquid for different volume fraction of silica nanoparticles φ at 25 ^{o}C plotted against the wave vector q (units nm^{-1}). (b) Structure factor, *S(q)*, for PEG500-SiO_2 particles in ionic liquid for different volume fraction of silica nanoparticles φ at 25 ^{o}C plotted against the wave vector q (units nm^{-1}) multiplied by the average core radius, $\underline{a}$. (c) The interparticle distance, $d_{p\text{-}p}$, plotted as a function of silica volume fraction φ.

We compare the value of interparticle separation, $d_{p\text{-}p}$ calculated from the position of primary peak against the theoretical value calculated by assuming a random distribution of silica hard spheres in a suspension as: $d_{p-p} = 2 * a(0.63/\phi)^{1/3}$ in Figure 3.2c. As expected, both these values show a similar trend.

Previously, Srivastava et al. showed that suspensions of PEG-tethered nanoparticles in PEG oligomers exhibit a range of anomalous behaviors beyond a critical volume fraction of particles (φs) where the material viscosity exhibits a sharp increase and the interparticle correlation exhibits a maxima and then decreases[12]. The critical volume fraction could also determine the transition from diffusive to hyperdiffusive transport as silica fraction $\varphi > \varphi s$ in XPCS measurements. However, this transition appeared to be dependent on the size of the silica core for the same dimensions and chemistry of the tethered and free chains, with the silica core of diameter 10 nm not exhibiting the transition while core of diameter 24 nm did[12].

We assess the dynamics of nanoparticles for the two solvent chemistries through XPCS. We obtain and fit intensity-time autocorrelation function, $g_2(q,t)$, with a stretched exponential function:

$$g_2(q,t) = 1 + B * \exp[-2(t/\tau_p(q))^{\beta(q)}] \tag{3.2}$$

Here, B is the experimental contrast factor; τ_p is the wave vector–dependent particle relaxation time; and β is the stretched exponent which is allowed to vary independently as a function of q.

The wave vector dependent relaxation times are plotted against the wave-vector in

Figure 3.3. We confirm our expectation that dynamics become faster as the volume fraction of silica decreases in both cases. The scaling of τ_p with respect to q reveals the nature of the dynamics, with a q^{-1} scaling indicative of hyperdiffusion and q^{-2} scaling indicative of diffusive dynamics. The volume fraction at which this transition occurs is $\varphi_t \sim 0.02$ for PEG5000-SiO_2 in DEP and $\varphi_t \sim 0.16$ for PEG500-SiO_2 in IL (Figure 3.3). The higher value of φ_t for the ionic liquid solvent suggests that a better solvent like ionic liquid can more easily unjam the particle networks in a nanocomposite.

3.4 Conclusions

In this work, we clearly establish a relationship between the structure and dynamics of nanoparticles in polymer nanocomposite fluids. The presence of solvents can reduce particle-particle correlations and allow the particles to move diffusively instead of exhibiting hyperdiffusive network dynamics. Similar findings were reported in a recent work by Russel et al. where they showed that transition from hyperdiffusive to diffusive was related to the jamming-unjamming transition of particle networks at oil-water interfaces[17]. Our findings also underscore that aging or aggregation is not the primary condition for presence of hyperdiffusion in polymer nanocomposites, unlike previous reports of the phenomenon in literature on glassy colloids[18].

*Synthesis and rheology of PEG500-SiO_2 in IL was performed by Sanjuna Stalin.

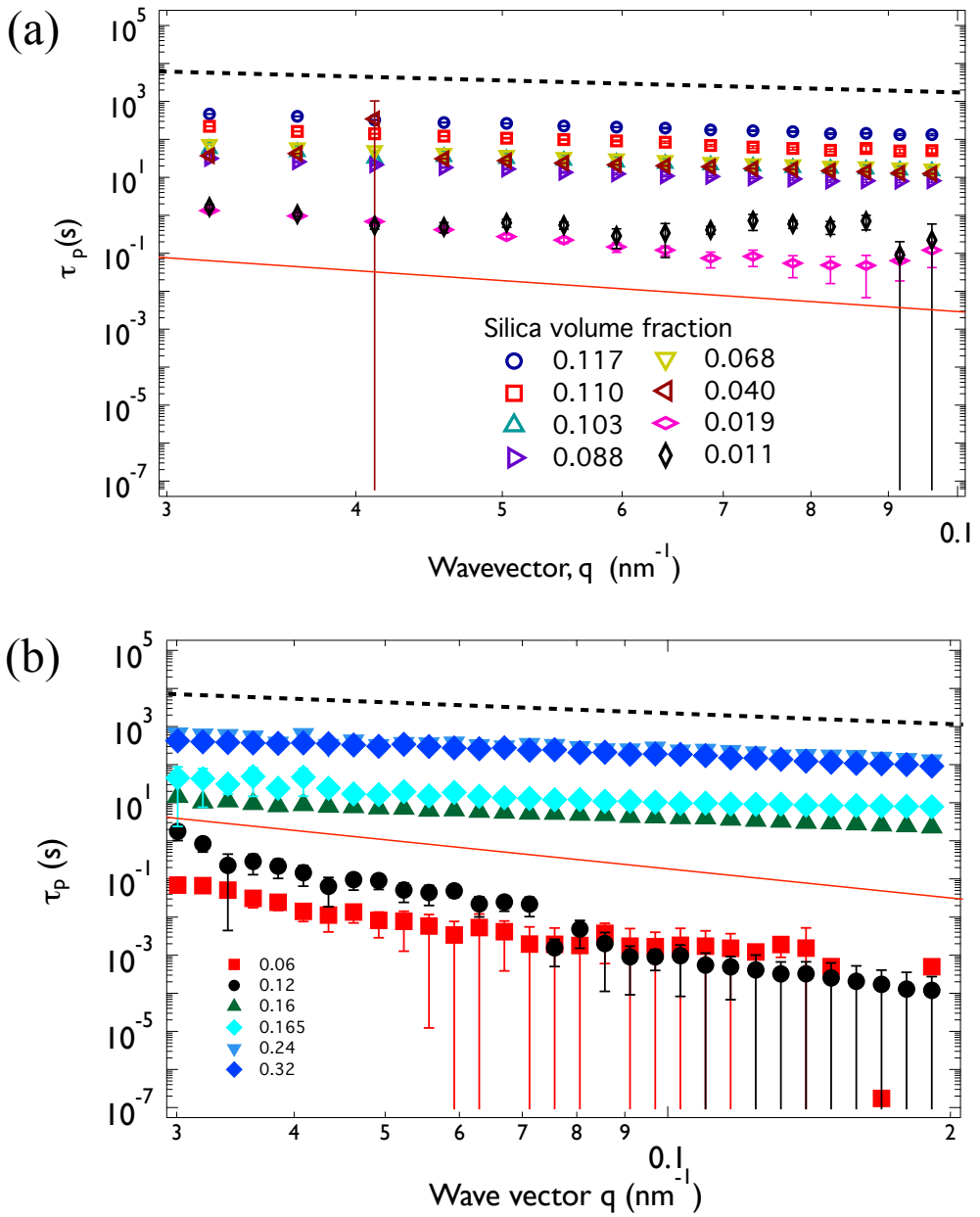

Figure 3.3 (a) Relaxation time versus wave vector for PEG5000-SiO_2 particles in DEP for different volume fraction of silica nanoparticles φ at 70 ^oC plotted against the wave vector q (units nm^{-1}). (b) Relaxation time versus wave vector for PEG500-SiO_2 particles in ionic liquid for different volume fraction of silica nanoparticles φ at 25 ^oC plotted against the wave vector q (units nm^{-1}). The dashed line indicates a q^{-1} scaling and solid line indicates a q^{-2} scaling.

Bibliography

(1) Yu, H.-Y. Density-Functional Theories for Solvent-Free Nanoparticle-Organic Hybrid Materials, Cornell University, 2012.

(2) Agarwal, P.; Kim, S. A.; Archer, L. A. Crowded, Confined, and Frustrated: Dynamics of Molecules Tethered to Nanoparticles. *Phys. Rev. Lett.* **2012**, *109* (25), 258301.

(3) Agarwal, P.; Srivastava, S.; Archer, L. A. Thermal Jamming of a Colloidal Glass. *Phys. Rev. Lett.* **2011**, *107* (26), 268302.

(4) Agrawal, A.; Wenning, B. M.; Choudhury, S.; Archer, L. A. Interactions, Structure, and Dynamics of Polymer-Tethered Nanoparticle Blends. *Langmuir* **2016**, *32* (34), 8698–8708.

(5) Agrawal, A.; Yu, H.-Y.; Sagar, A.; Choudhury, S.; Archer, L. A. Molecular Origins of Temperature-Induced Jamming in Self-Suspended Hairy Nanoparticles. *Macromolecules* **2016**, *49* (22), 8738–8747.

(6) Choudhury, S.; Agrawal, A.; Kim, S. A.; Archer, L. A. Self-Suspended Suspensions of Covalently Grafted Hairy Nanoparticles. *Langmuir* **2015**, *31* (10), 3222–3231.

(7) Srivastava, S.; Agarwal, P.; Mangal, R.; Koch, D. L.; Narayanan, S.; Archer, L. A. Hyperdiffusive Dynamics in Newtonian Nanoparticle Fluids. *ACS Macro Lett.* **2015**, *4* (10), 1149–1153.

(8) Srivastava, S.; Choudhury, S.; Agrawal, A.; Archer, L. A. Self-Suspended Polymer Grafted Nanoparticles. *Curr. Opin. Chem. Eng.* **2017**, *16*, 92–101.

(9) Srivastava, S.; Schaefer, J. L.; Yang, Z.; Tu, Z.; Archer, L. A. 25th Anniversary Article: Polymer-Particle Composites: Phase Stability and Applications in Electrochemical Energy Storage. *Adv. Mater.* **2014**, *26* (2), 201–234.

(10) Yu, H.-Y.; Koch, D. L. Structure of Solvent-Free Nanoparticle−Organic Hybrid Materials. *Langmuir* **2010**, *26* (22), 16801–16811.

(11) Yu, H.-Y.; Srivastava, S.; Archer, L. A.; Koch, D. L. Structure Factor of Blends of Solvent-Free Nanoparticle–organic Hybrid Materials: Density-Functional Theory and Small Angle X-Ray Scattering. *Soft Matter* **2014**, *10* (45), 9120–9135.

(12) Srivastava, S.; Archer, L. A.; Narayanan, S. Structure and Transport Anomalies in Soft Colloids. *Phys. Rev. Lett.* **2013**, *110* (14), 148302.

(13) Zhang, Q.; Archer, L. A. Poly(ethylene oxide)/Silica Nanocomposites: Structure and Rheology. *Langmuir* **2002**, *18* (26), 10435–10442.

(14) Nugent, J. L.; Moganty, S. S.; Archer, L. A. Nanoscale Organic Hybrid Electrolytes. *Adv. Mater.* **2010**, *22* (33), 3677–3680.

(15) Camper, D.; Bara, J.; Koval, C.; Noble, R. Bulk-Fluid Solubility and Membrane Feasibility of Rmim-Based Room-Temperature Ionic Liquids. *Ind. Eng. Chem. Res.* **2006**, *45* (18), 6279–6283.

(16) Mondal, J.; Choi, E.; Yethiraj, A. Atomistic Simulations of Poly(ethylene Oxide) in Water and an Ionic Liquid at Room Temperature. *Macromolecules* **2014**, *47* (1), 438–446.

(17) Cui, M.; Miesch, C.; Kosif, I.; Nie, H.; Kim, P. Y.; Kim, H.; Emrick, T.; Russell, T. P. Transition in Dynamics as Nanoparticles Jam at the Liquid/Liquid Interface. *Nano Lett.* **2017**, *17* (11), 6855–6862.

(18) Cipelletti, L.; Manley, S.; Ball, R. C.; Weitz, D. A. Universal Aging Features in the Restructuring of Fractal Colloidal Gels. *Phys. Rev. Lett.* **2000**, *84* (10), 2275–2278.

CHAPTER 4

DYNAMICS OF NANOPARTICLES IN ENTANGLED POLYMER SOLUTIONS

Adapted with permission from: P. Nath, R. Mangal, F. Kohle, S. Choudhury, S. Narayanan, U. Wiesner, L. A. Archer, Dynamics of Nanoparticles in Polymer Nanocomposites, Langmuir, 2018, 34 (1), 241-249.

Abstract

The mean square displacement $\langle r^2 \rangle$ of nanoparticle probes dispersed in simple isotropic liquids and in polymer solutions is interrogated using fluorescence correlation spectroscopy (FCS) and single particle tracking (SPT) experiments. Probe dynamics in different regimes of particle diameter (d), relative to characteristic polymer length scales, including the correlation length (ξ), the entanglement mesh size (a) and radius of gyration (R_g), are investigated. In simple fluids and for polymer solutions in which $d >> R_g$, long-time particle dynamics obey random walk statistics $\langle r^2 \rangle : t$, with the bulk zero-shear viscosity of the polymer solution determining the frictional resistance to particle motion. In contrast, in polymer solutions with $d < R_g$, polymer molecules in solution exert non-continuum resistances to particle motion and nanoparticle probes appear to interact hydrodynamically only with a local fluid medium with effective drag comparable to that of a solution of polymer chain segments with sizes similar to those of the nanoparticle probes. Under these conditions, nanoparticles exhibit orders of magnitude faster dynamics than those expected from continuum predictions based on the Stokes-Einstein relation. SPT

measurements further show that when $d > a$, nanoparticle dynamics transition from diffusive to subdiffusive on long time scales, reminiscent of particle transport in a field with obstructions. This last finding is in stark contrast to nanoparticle dynamics observed in entangled polymer melts, where X-ray Photon Correlation Spectroscopy (XPCS) measurements reveal faster but hyperdiffusive dynamics. We analyze these results with the help of the hopping model for particle dynamics in polymers proposed by Cai et al. and, on that basis, discuss the physical origins of the local drag experienced by nanoparticles in entangled polymer solutions.

4.1 Introduction

Diffusion of spherical Brownian particles in complex fluids, including polymer solutions, gels, and melts is a topic of interest in multiple fields. It is as important in applications, such as gel electrophoresis[1,2], where the particles move in response to an external driving force, as in situations such as nanoparticle transport in biomacromolecular gels[3,4], where particle motions are unaided by any external forces. Studies of particle motions in crowded biomolecular systems have also emerged as an important area of biophysics research for characterizing mechanics[5], adhesion[6], and for understanding intracellular transport[7], where deviations from Fickian diffusion have been reported[8].

In an effort to understand these findings and to more generally elucidate the underlying physics that govern small particle motions in complex fluids, several recent experimental[9–56] and theoretical works[24,38,57–74] have analyzed particle transport in model polymer-particle composites. Although there is agreement that in the continuum

limit (probe particle sizes much larger than any length scale that determines molecular motions or governs fluid compositional dynamics), the long-time trajectories of particles obey random-walk statistics, with diffusivity set by the bulk fluid viscosity (i.e. the Stokes-Einstein (S-E) law holds), there is significant disagreement about how particles with sizes below continuum limits move in complex fluids. In particular, for particle probes smaller than the radius of gyration (R_g) of their host polymer, experimental and theoretical studies show that particle diffusivities are inconsistent with expectations based on S-E theory and that particles experience a local drag force that can be several orders of magnitude lower than that expected based on the bulk fluid viscosity. These observations remain controversial, however, because in the systems where deviations from S-E diffusion are observed, there is disagreement among the various experimental studies about the nature of particle diffusion in polymers. Experimental results obtained using different analytical tools show *long-time* behaviors spanning the full spectrum of particle diffusion regimes — from subdiffusion[21,32], simple diffusion[14,28,60,61], to hyperdiffusion[12,23,33,36]. Because each of these regimes is associated with qualitatively different balance of forces and fundamentally different dynamic environments surrounding a diffusing particle, it has to-date been difficult to provide a unified understanding for these observations. Here, we analyze diffusion of small probes in linear, water-soluble polymers by means of particle tracking and fluorescence correlation spectroscopy designed to probe particle motions on a wide range of time and length scale. The measurements are designed to elucidate how motions of spherical particles in complex fluids change as one traverses the continuum regime, with respect to all of the relevant length scales in the fluid.

An important starting point for the study are results from early works that consider the range of non-continuum length scales relevant for dynamics of polymer solutions and

where dynamics in polymer solutions are considered as purely diffusive. Among these studies, the work by Phillies et al. stands out in that most diffusion data available at the time could be fitted with an empirical relation of the form of $D/D_s \sim \exp(-\beta\phi^{\upsilon})$ [41-42] and this functional form agreed with models based on hydrodynamic interactions with solvated polymers[43, 62]. Here, D/D_s is the ratio of probe diffusivity in a polymer gel divided by that in the solvent; β is a probe-size dependent constant; υ is a fitting constant, usually in the range of 0.5-1; and ϕ is volume fraction of polymer in the gel or solution. A similar phenomenology has been used to fit polymer self-diffusion and viscosity data in the low concentration regime[75]. As polymer volume fraction increases, polymer chains in solutions can be considered to form immobilized networks through which particles move[62]. In contrast to this hydrodynamic model is the obstruction model[58] created by modifying the Ogston sieving model of transport within porous media.[71] In this framework the particle diffusivity is of the form, $D/D_s = \exp\left[-\pi\left(\frac{r_s + r_f}{a_{monomer}\phi_v^{-0.75}C_\infty^{-0.25}(1-2\chi)^{-0.25} + 2r_f}\right)^2\right]$, where r_f is the radius of the polymer, C_∞ is the characteristic ratio of the polymer, χ is the Flory-Huggins interaction coefficient for the polymer-solvent system and $a_{monomer}$ is the equivalent bond-length of the monomer. A shortcoming of all of these phenomenological network models is that they fail to account for the effects of polymer chain relaxation on probe particle dynamics in polymer solutions and melts.

A recent analysis proposed by Cai *et al.*[60,61] significantly extends earlier work by Brochard-Wyart and de Gennes[59] to provide scaling relations for probe particle dynamics in polymer solutions and melts. For a probe of diameter d dispersed in a polymer solution with correlation blob size ξ, entanglement tube diameter a, and polymer radius of gyration R_g in the solvated state, this analysis is capable of capturing coarse and subtle features of particle motions in polymers. For $d < \xi$, probe particles are argued to experience only the solvent viscosity, η_s. In contrast, for probes in the size range $\xi < d < a$, particles experience segmental viscosity of polymer chain and the self-diffusion coefficient is proportional to $kT\xi^2 / \eta_s d^3$, as the "effective viscosity" experienced by the particle is the Zimm viscosity of a polymer segment with size equal to the particle size. For $d > a$, particles are arrested by the entanglements in the polymer network at short time scales and can move only when the surrounding chains reptate out of their entanglement tubes. The transition from diffusive motions regulated by the segmental viscosity to longer-range particle motions regulated by the bulk viscosity is thought to occur by particle hopping from one entanglement to another.

Fluctuation correlation spectroscopy experiments conducted by Kohli and Mukhopadhyay[25] using mesoscopic gold nanoparticles (d < 20 nm) in solutions of polyethylene glycol in water, for instance, yield behaviors consistent with Cai's scaling model in the $\xi < d < a$ regime, especially for concentrated solutions of moderately entangled polymers where hydrodynamic models are no longer valid.

Other literature studies, however, provide conflicting information about the importance of the hopping regime and about the nature of particle dynamics of polymers on timescales beyond the polymer reptation relaxation time [19,21,33].

Our specific goal in the present study is to use experiments that can probe particle motions in polymers on length scales much larger than the probe particle dimension and on time-scales well above the Brownian configurational relaxation time, t_R. Such experiments are important because they can be used to extend the dynamic range of experimental results recently reported by Mangal *et al.*[33] using X-ray Photon Correlation Spectroscopy (XPCS) for which the maximum probed wavelength to particle size ratio is 17.5:1 and the maximum probed time scale to the Brownian configurational relaxation time is approximately 1:1000. We will use these experiments to elucidate the details of the transition from continuum to non-continuum particle dynamics in complex fluids and, on that basis, provide a more general framework for describing dynamical behaviors of particles under a broad range of regimes of concentration, and probe sizes versus. polymer length-scales. Within these bounds, we focus on high molar mass linear polymers dissolved in a solvent, which can be tuned to obtain a range of polymer dynamics and associated characteristic length and time scales by simply changing the volume fraction of polymer in solution.

4.2 Experimental Methods

Sample preparation:

ATTO647N fluorophore dye with malemide linkage was purchased from Atto-Tec Gmbh. ATTO647N dye labeled silica nanoparticles known as *Cornell dots* (C dots) were synthesized using the protocol provided in Appendix B. The particles were fractionated using gel permeation chromatography to obtain narrowly dispersed polyethylene glycol coated particles and their size characterized using fluorescence correlation spectroscopy (FCS) to reveal particles of average hydrodynamic diameters in the range 6nm – 36 nm. C dots with hydrodynamic diameters 6.7±0.1 nm, 16.5±0.2 nm, 23.7±0.3 nm, and 35.5±0.7 nm were selected for our studies. Polyethylene oxides (PEO) of molar mass 20kDa, 50kDa, 100kDa, 300kDa, 500kDa, and 1500 kDa were purchased from Agilent and of 35kDa was purchased from Polymer Source, Inc. Gels were prepared by mixing stock solutions of PEO in water with the stock aqueous solutions of fluorescent particles, and gently shaking the mixture on an analog shaker for one week at room temperature. Highly viscous nanocomposite gels were prepared by first distributing the particle stock solutions within the dilute PEG-water mixtures, followed by removing the water through freeze-drying and then redispersing the composite into the requisite amount of water using the aforementioned procedure. Particle dynamics in these gels were probed using two dynamic optical microscopy techniques: FCS and 2-D single particle tracking (SPT).

For FCS a particle concentration of ~10 nanomolar was used and for particle tracking the particle concentration was fixed at ~ 1 picomolar. Molarity is calculated by finding particle number density of probes in stock solution using FCS (in L^{-1} units) and dividing it by the Avogadro's number ($N_A = 6.023 \times 10^{23}$). The schematic of the setup is shown in Figure 4.1.

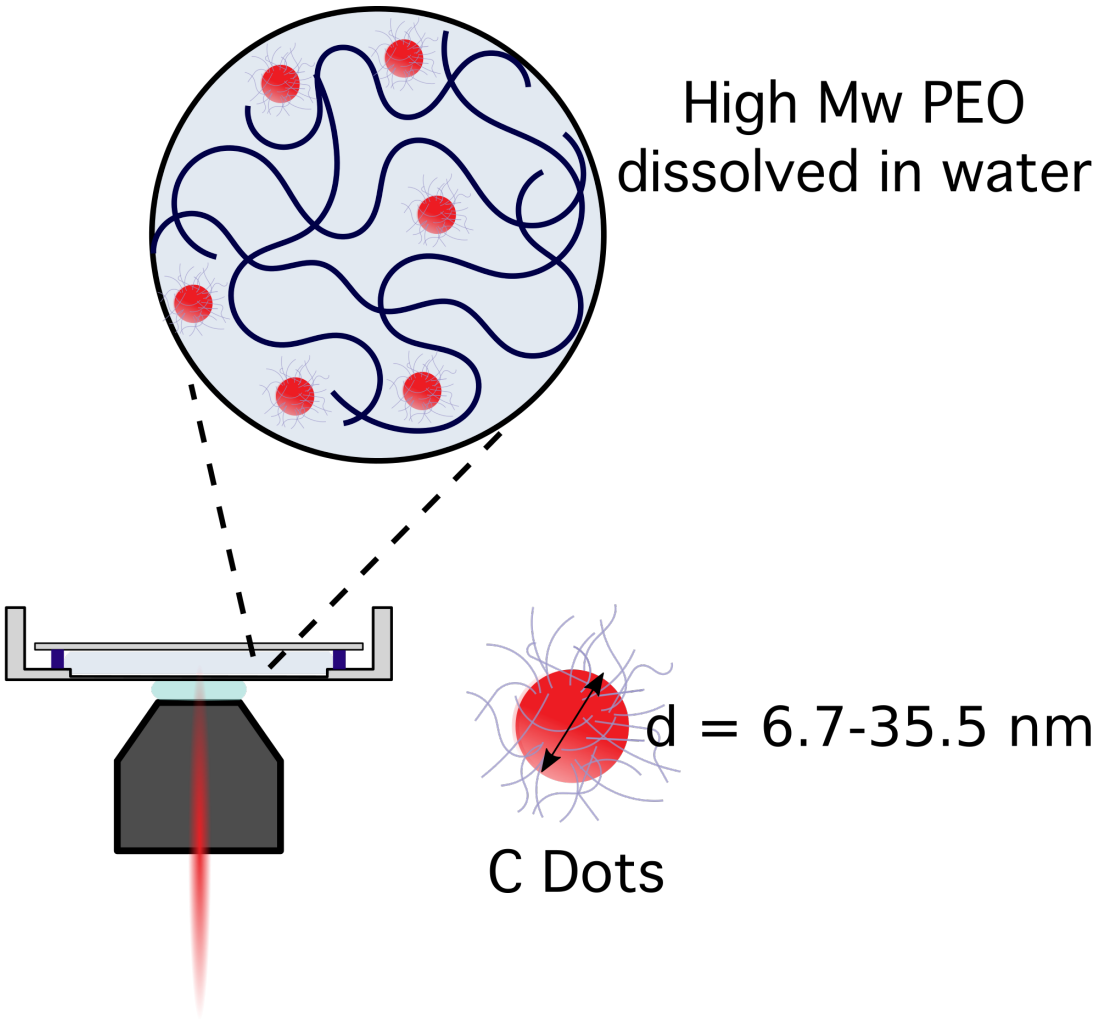

Figure 4.1 Schematic of C-Dots dispersed in long chain polyethylene glycol solutions in water tracked via both FCS and single particle tracking.

To relate our findings from FCS and SPT measurements to earlier results from XPCS measurements, dynamics of particles in high molar mass polystyrene solutions were also investigated using XPCS. Polystyrene with M_w = 20.06 MDa and M_n = 16.72 MDa was purchased from Tosoh Biosciences LLC (F-2000) and dissolved in diethyl phthalate (DEP, purchased from Sigma Aldrich) using dichrolomethane (Sigma Aldrich) as co-solvent. The resultant gels were allowed to stand for periods exceeding six months to ensure homogenous dispersion. Amine-terminated polystyrene (M_w ~ 10kDa, PDI ~ 1.3) was also purchased from Sigma Aldrich and densely grafted to the surface of 80nm silica nanoparticles using a previously reported linking chemistry[76]. These sterically stabilized particles were dispersed in the stock gels at 1 vol% silica concentration using dichloromethane as co-solvent.

FCS measurements:

Measurements were performed using a Zeiss 880 LSM inverted microscope outfitted with 40x water immersion lens (LD-C Apochromat) and used with a 633nm He-Ne (100mW, Thorlabs) source. To prevent water evaporation, samples were sealed between No. 1.5 coverslips using 1.5 cm x 1.6 cm x 250 μm Gene Frames (Thermofischer Scientific). Fluctuations in fluorescence signal as nanoparticles moved in and out of focal volume were recorded and quantified in the form of the fluorescence autocorrelation function (ACF), $G(\tau)$:

$$G(\tau) = \frac{\langle \delta F(t) \delta F(t+\tau) \rangle}{\langle F(t) \rangle^2} \tag{4.1}$$

The ACF function was fitted with a one-component diffusion model corrected for fast relaxation contribution:

$$G(\tau) = 1 + \frac{1}{\langle N \rangle} \cdot \frac{1}{A-1} (1 - Ae^{-\tau/\tau_{trip}}) \frac{1}{1 + \frac{\tau}{\tau_{diffusion}}} \sqrt{\frac{1}{1 + S^2 \frac{\tau}{\tau_{diffusion}}}} \qquad (4.2)$$

For comparison ACF can be plotted as the normalized autocorrelation function $G'(\tau) = \left(G(\tau) - 1\right) \cdot N$. Beam alignment was performed using 10nM Alexa 647 (Fischer Scientific); the diffusivity of Alexa 647 was taken from literature[77] to be 330 $\mu m^2 s^{-1}$, and used to compute the diffusivity of nanoprobes using the formula, $\tau_{diffusion} = \frac{\omega_{xy}^2}{4D}$. Here, N is the number of fluorescent particles in the confocal volume, A is the fraction of particles in the fast relaxation state, τ_{trip} is the triplet relaxation time, $\tau_{diffusion}$ is the diffusion time of the particles through the confocal volume, S is the structure factor for the instrument, ω_{xy} is the width of the confocal volume, and τ is the lag time.

Single Particle Tracking:

2D SPT measurements were performed on an Andor Spinning Disk confocal setup, with 655 nm laser beam and 60X silicon-oil immersion lens. Time-lapse imaging was performed at 100 μm away from the coverslip at intervals 0.4-30s for a period of 4-60 minutes. Particle centers were tracked to obtain mean-squared displacement (MSD) values with time, using the track objects plugin of Metamorph imaging software (Molecular Devices) and analyzed using an in-house MATLAB code. Diffusivities for individual particles were obtained by fitting the MSD vs. time data with a power-law fit in MATLAB. To calculate the mean and standard deviation errors in the diffusivity

values, a Gaussian function was used to fit the diffusivity values obtained for at least 40 particles per sample.

Rheology:

An Anton Paar MCR 301 rheometer outfitted with cone and plate fixtures was used to obtain the viscoelastic response of the nanocomposites. For viscous samples, a plate of 25 mm diameter and 1° cone angle was used. For more liquid like samples, a larger plate of 50 mm diameter with 1° cone angle was used. A solvent trap was attached to the rheometer, which created a water vapor saturated environment to prevent water evaporation during the measurements.

TEM measurements: Transmission electron micrographs (TEM) of C dot dispersions drop casted on carbon-coated grids were collected on a FEI Tecnai Spirit microscope operated at 120kV and particle size analysis was conducted with ImageJ (details in Table B1).

X-ray Photon Correlation Spectroscopy measurements: XPCS measurements on the PS-DEP gels was performed at Sector 8-ID-I of the Advanced Photon Source (APS) at Argonne National Lab (ANL). All measurements were performed at room temperature using special stainless steel holders with Kapton windows. Scattering intensities were collected irradiating the samples with 7.4 keV X-ray beam at different wave vectors, q. A Medipix-3 based LAMBDA (Large Area Medipix Based Detector Array) was used as the photon counting detector. The detector array comprises of 1556 x 516 pixels with a pixel size of 55 μm and can operate at a maximum frame rate of 2000 frames/sec[78]. We consider a q-range of 0.018 nm^{-1} to 0.16 nm^{-1} for our analysis, which translates to wavelength in the range of $39\text{nm} \le \lambda(=2\pi/q) \le 339\text{nm}$,

and fit the intensity-time autocorrelation function, $g_2(q,t)$, with a stretched exponential function:

$$g_2(q,t) = 1 + B * \exp\left[-2(t/\tau_p(q))^{\beta(q)}\right] \quad (4.3)$$

Here, B is the experimental contrast factor; τ_p is the wave vector–dependent particle relaxation time; and β is the stretched exponent which is allowed to vary independently as a function of q. The XPCS results for particle dynamics in PS solutions are provided in Appendix B.

4.3 Results and Discussion

FCS measurements were performed using polymer solutions in the semi-dilute entangled regime and for probe particle sizes ($d < R_g$). By varying the concentration of the polymer in solution, particle dynamics in suspensions in the small-particle ($d < \xi$) and intermediate-particle ($\xi < d < a$) size ranges could be investigated. Figure 4.2 reports the measured tracer particle diffusivity (D) in solutions of 35 kDa PEG in water normalized by corresponding tracer's diffusivity measured in pure water, D_s. The corresponding correlation curves and fits can be found in Appendix B, Figure B4. The figure includes a comparison of our results for particles with diameter of 6.7 nm dispersed in aqueous solutions of 35kDa PEG with those obtained from fluctuation correlation spectroscopy measurements reported by Kohli and Mukhopadhyay[25] for unfunctionalized gold nanoparticles of diameter 5 nm, 10 nm and 20 nm in 35 kDa polyethylene glycol solutions in water. Based on the scaling model proposed by Cai *et*

al.[60-61], D/D_s for diffusing particles experiencing the polymer segmental viscosity should be of the form: $\frac{D}{D_s} \sim \frac{\xi^2}{d^2}$ at long times. The dependence of correlation length on polymer volume fraction (equation B1) gives that the scaled diffusivity must vary as $\phi^{-2\upsilon/(3\upsilon-1)}$, where the exponent (ν) is -1.52 for a good solvent and -2 for a poor solvent. A power law fit, hence, must identify the dependence of D on ϕ as $D \sim \phi^{-2\upsilon/(3\upsilon-1)}$.

The scaling exponent of -2.91 observed for the 6.7 nm C Dots agrees well with the scaling of -2.28 found in complementary measurements using 10 nm particles in ref. 25 (also given in Figure 4.2) but is higher than the expected scaling of -1.56. This discrepancy can suggest additional slower modes of transport other than polymer segmental viscosity as the particle size approaches the polymer R_g (reported in Table 4.1).

Kohli and Mukhopadhyay[25] also showed that their 20 nm probe particles ($d > R_g$) experienced the solution viscosity (found both via rheology measurements and the scaling exponent which is close to the bulk viscosity scaling of ~3.93 with polymer volume fraction); in contrast, our 6.7 nm probes experience a viscosity that is approximately 8-20 times lower than the bulk solution viscosity, shown in Figure 4.3, and are still smaller than the tube diameter (*a*) in the entangled polymer solution, estimated by equation B2. The observation that particles approach from faster than Stokes-Einstein diffusivity to the Stoke-Einstein diffusivity as the particle diameter approaches the solvated polymer's R_g is consistent with previous reports[22,69,74].

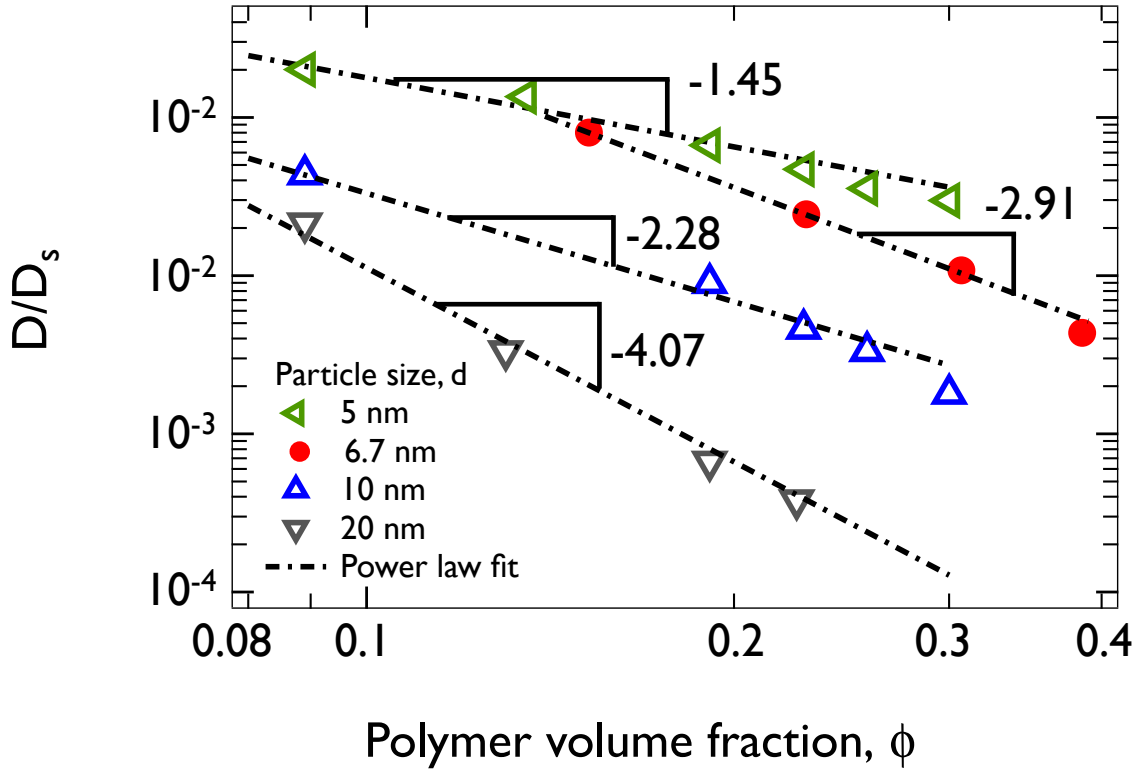

Figure 4.2 Log-log plots of *D/Ds* (diffusivity scaled by diffusivity of particles in solvent) against the polymer volume fraction ϕ in solution for 35kDa PEG dissolved in water. The data for 5, 10, and 20 nm particles is taken from Ref 25.

Table 4.1. Characterization data for polyethylene oxide (PEO) solutions

M (kDa)	Mw (kDa)	PDI	$R_g = 0.02 M_w^{0.588}$ nm	$\phi^* = \frac{M_w}{4/3 \pi R_g^3 N_A \rho_{PEO}}$	$\phi_e = \left(\frac{N}{N_e} \right)^{-3/4}$
20	20.22	1.04	6.81	0.0227	0.18
35	37.8	1.08	9.83	0.0141	0.12
50	48.49	1.05	11.38	0.0116	0.09
100	92.9	1.05	16.68	0.0071	0.06
300	256. 2	1.05	30.29	0.0033	0.03
500	527.5	1.05	46.31	0.0019	0.02
1500	1352	1.13	80.55	0.0009	0.01

R_g is the radius of gyration of the polymer in the melt state.

ϕ^* is the overlap volume fraction of polymer at which the solution transitions from dilute to semi-dilute regime.

ϕ_e is the volume fraction of polymer at which the solution transitions from semi-dilute unentangled to semi-dilute entangled regime.

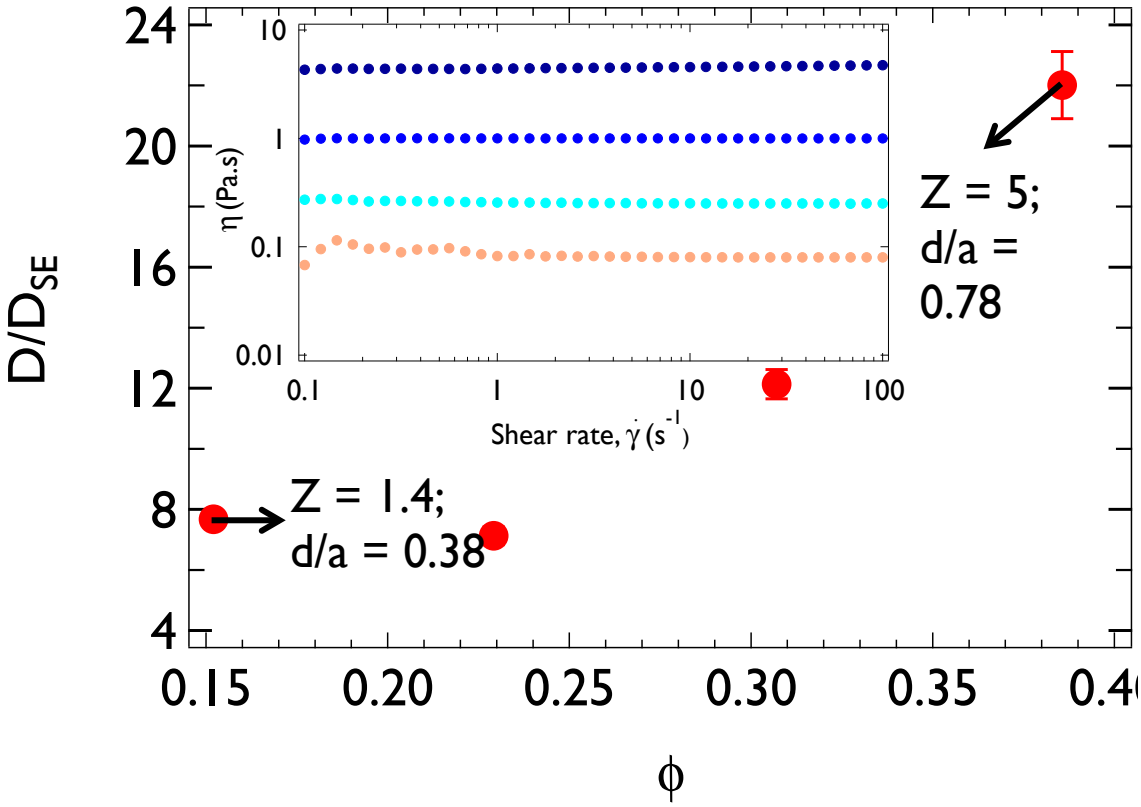

Figure 4.3 D/D_{SE} (diffusivity scaled by the Stokes-Einstein diffusivity calculated using the solution viscosity) for 6.7 nm C dots is plotted against the polymer volume fraction ϕ in solution. Z is the entanglement density per chain for the solvated polymer and d/a is particle diameter scaled by the solvated polymer's tube diameter. Inset shows viscosity for these samples vs. shear rate – viscosity increases with increasing polymer fraction. All error bars shown are standard error.

Thus, particle dynamics in the regime $d < a << R_g$ were studied in solutions containing higher molar mass polymers (Mw 527.5 kDa and 1352 kDa). We plot the values for D/D_s obtained through FCS for the given regime of particle sizes (for PEO Mw 527.5 kDa and 1352 kDa) in Figure 4.4 against the particle diameter, *d*, scaled by the correlation length, ξ. These solutions are entangled and the full range of d/ξ accessed is from 0.5-2. For different particle diameters when particle diameter is close to the correlation length, the particles follow the scaling of proposed by Cai *et al*. of $\frac{D}{D_s} \sim \frac{\xi^2}{d^2}$ based on polymer segmental viscosity[60]. The details of the concentrations used for the measurements shown in this figure are provided in Table B2 and Table B3**.** Sample correlation curves are also reported in Figure B5, where it is shown that an analysis based on simple diffusive motions of the particles fits the data well.

The scaling model predicts that particles smaller than ξ diffuse under the influence of the solvent viscosity; however, we find that the transition from the regime in which particle motion is resisted by the solvent viscosity to that in which polymer segmental viscosity resists motion is less abrupt than predicted by Cai *et al*.[60,61]

For polymer solutions with higher PEG concentrations (ϕ) and probe sizes approaching the entanglement mesh size of the polymer, the time taken by the nanoparticles to travel through the confocal volume approaches the photo-bleaching time of the C dots.

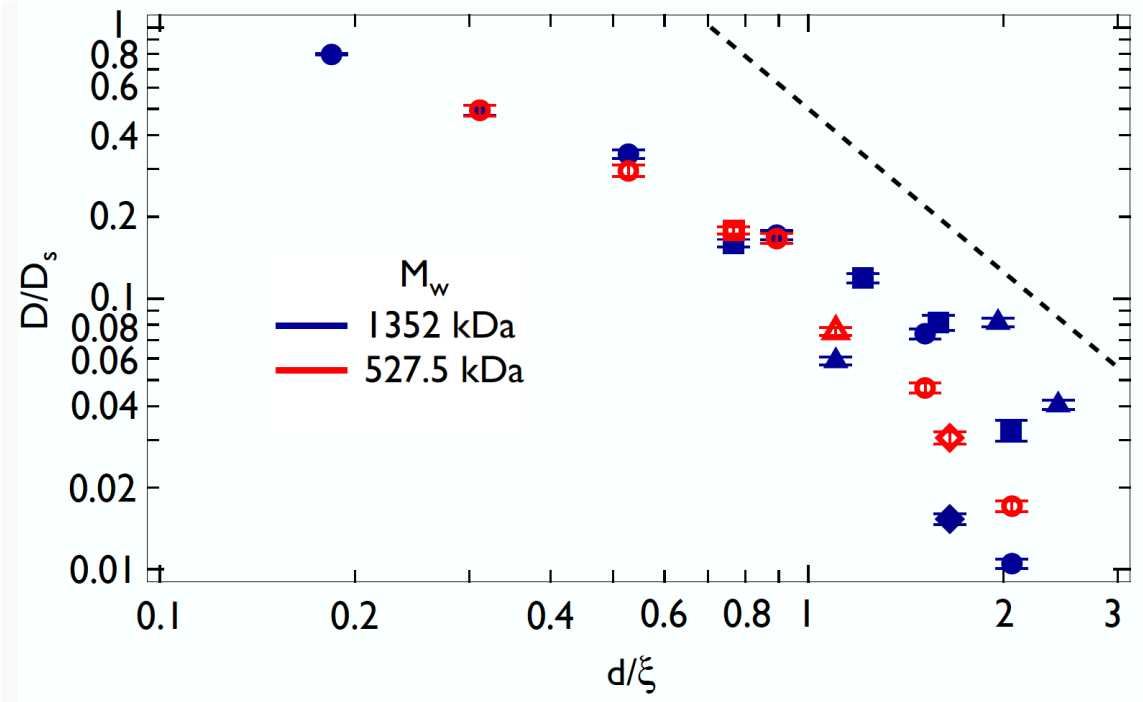

Figure 4.4. D/D_s (diffusivity scaled by diffusivity of particles in solvent) is plotted against the polymer volume fraction ϕ in solution measurement through FCS for different molecular weights of dissolved polymer corresponding to Rg of ~80 nm (closed symbols) and ~46 nm (open symbols), respectively. The dashed line indicates scaling of $(d/\xi)^{-2}$ and the error bars are standard error. Here, the circles show data for 6.7 nm particles (○), the squares show data for 16.5 nm particles (□), the triangles show data for the 23.7 nm particles (Δ), and the diamonds show data for the 35.5 nm particles (◊). A summary of concentrations used in this figure is provided in Table B2.

This complicates measurement of particle dynamics using FCS (Figure B3) even under conditions where the photo-bleaching time of the C dots is much larger than that of the free fluorophore in solution[79]. SPT measurements were more fruitful for such systems. In Figure 4.5, we report results from these experiments in terms of D/D_{SE} for PEG with varying molar mass. The ratio of particle size to tube diameter is fixed at d/a ~ 2 (by fixing the particle diameter at 35.5 and selecting the concentration of ~15 vol%) for all polymer molecular weights. In the regime of d > a, the Cai-Panyukov-Rubenstein scaling model[60, 61] predicts that the nanoparticles can either diffuse following the total viscosity of the system, or via hopping caused by entanglement fluctuations, where the hopping diffusivity D_{hop} is given by $D_{hop} = \frac{\xi^2}{\tau_e}\exp(-d/a)$.

A key assumption is that above a critical entanglement density (Z_c) nanoparticles move by hopping in contrast to simply undergoing random diffusion under the influence of the drag force produced by the bulk viscosity of the surrounding polymer fluid and Z_c is given by the expression: $Z_c = \left[\left(\frac{a^2}{\xi d}\right)\exp(d/a)\right]^{1/3}$. For PEO solutions with d/a ~ 2, this value comes out to be 2.32. It is worth noting that the smallest molecular weight used, i.e., 20kDa will form an unentangled solution and the 48.49 kDa as well as 92.9 kDa polymers also form a modestly entangled solution where entanglement density below 3.5 (using M_e = 2000 g/mol).

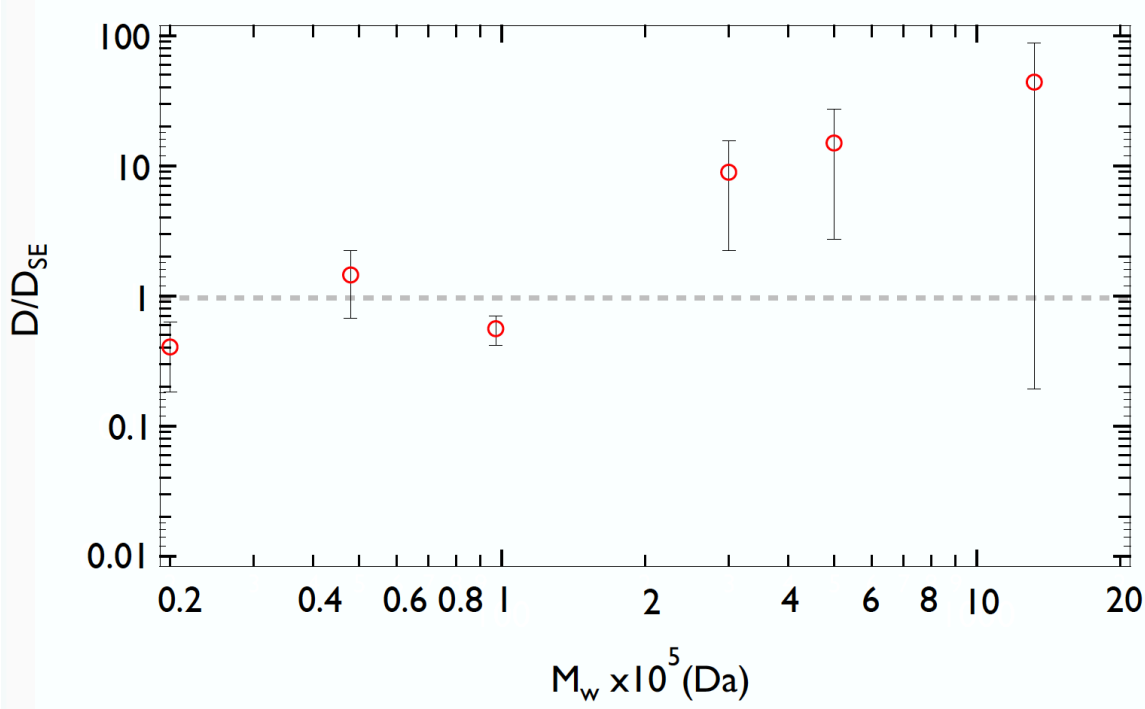

Figure 4.5. D/D_{SE} (diffusivity scaled by the Stokes-Einstein diffusivity calculated using the solution viscosity) is plotted against the host polymer molecular weight for a fixed volume fraction of polymer in solution, $\varphi \sim 0.15$, corresponding to $d/a \sim 2$. Error bars are standard deviation.

Hence, both the entanglement density criterion and the R_g criteria (previously found in the experiments by Holyst et al. for unentangled or modestly entangled solutions and simulations of Yamamoto and Schweizer and Liu et al. [22,69,74] as the length scale below which faster than S-E dynamics can be observed in polymer solutions) suggest that the lower molecular weight polymer solutions must exhibit S-E behavior. Evidently, as the PEG molar mass is increased beyond ~ 200 kDa, a positive deviation of probe diffusion coefficient with respect to the Stokes-Einstein diffusivity is again observed and this effect becomes more amplified with increasing polymer molar mass, indicating that the probes are undergoing hopping motion.

Consistent with our conclusions from the FCS measurements, SPT measurements on probes smaller than the tube diameter, reveal long-time diffusive dynamics, as seen for d/a = 0.82 in Figure 4.6a. Recent XPCS experiments on particle diffusion in entangled polymer melts have associated the limit of $d/a \geq 1$ with observations of anomalous, hyperdiffusion[23,33,36]. This phenomenon has been explained in terms of local strain-fields produced by probe particle motions in elastic media which produces ballistic motions at the small length scales probed by XPCS[80]. Our SPT results are inconsistent with this conclusion and in fact show no evidence of hyperdiffusive motion for particles in entangled solutions with $d/a \sim 2$. To more rigorously evaluate this conclusion, materials with larger d/a were created using the same probe size (35.5 nm) as in Figure 4.5, but in solutions with higher polymer concentration. For $d/a > 1$, a characteristic two-step diffusion process is observed in all materials studied, with an initial subdiffusive (MSD ~ $t^{0.5}$) regime followed by a long-time diffusive step, as seen

in Figure 4.6b. Results reported in Figure 5c show that the initial subdiffusive step is significantly extended at higher polymer concentration. The occurrence of subdiffusion in highly entangled polymer gels, previously observed by Mason and Weitz[34], has been disputed, with Ochab-Marcinek and Holyst[37] offering an alternate explanation in terms of a two step process wherein the particle initially moves in a confined space comprised of the polymer depletion layer formed in the vicinity of the particle and then encounters the polymer in the second step. Their confined walking diffusion model carries the approximate functional form of $\left\langle r^2 \right\rangle = 6D_M t + \frac{6}{5}a^2\left(1 - e^{-5D_m t/a^2}\right)$. Hence, within the framework of their model, the analytical limits of at short and long times are diffusive, while the intermediate solution can give the appearance of subdiffusion. This can explain the apparent transition from two-step to a single-step regime observed in our data (Figure 4.5c) as our measurements fall somewhere in the intermediate to long time regime.

The occurrence of intermediate time subdiffusion in polymer gels has also been reported in XPCS measurements[21] of polystyrene-grafted gold nanoparticles in entangled solutions of polystyrene in xylene, where it was shown that increasing the entanglement density (Z) leads to more pronounced subdiffusive behavior. We performed similar XPCS measurements using 10 kDa grafted 80 nm silica nanoparticles in 20 MDa PS solution in DEP and observed that the intensity correlation curves are fitted best with stretched exponential functions and that the particle motion is diffusive and subdiffusive but never hyperdiffusive (see Figure B7 and Table B3).

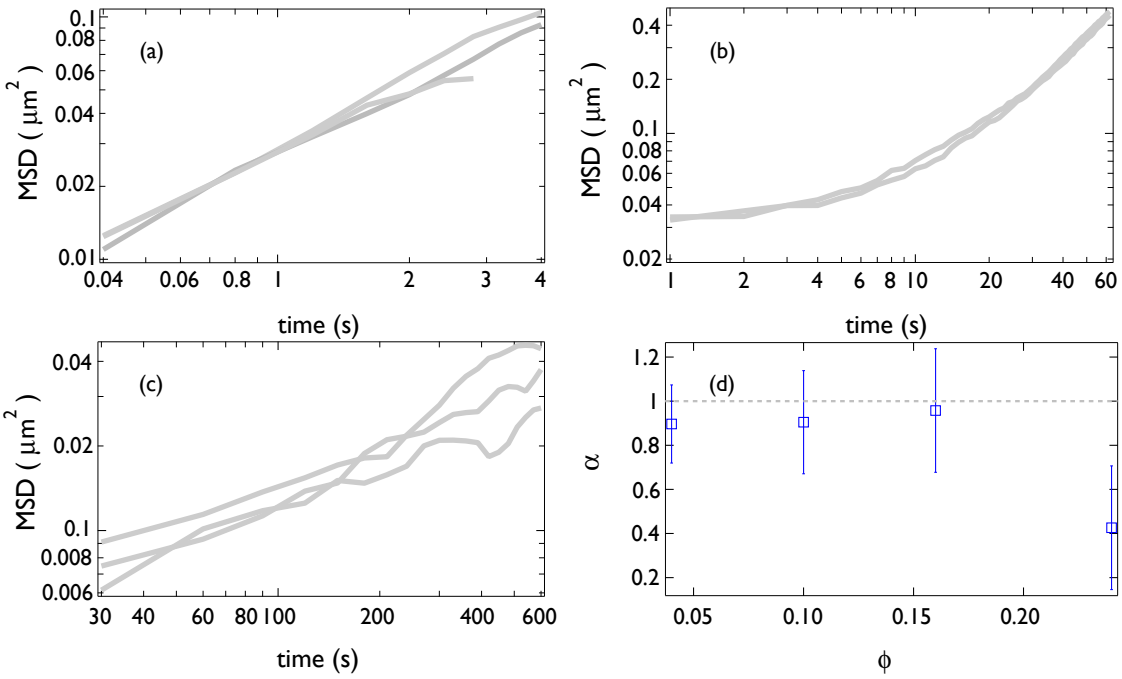

Figure 4.6. Mean square displacement vs. time plotted for 1.352 mil Da Mw polyethylene glycol dissolved in water for φ: (a) 0.04, (b) 0.10, (c) 0.24. (d) Scaling exponent, α, plotted vs. φ, for φ = 0.10 and 0.16 the scaling exponent for the second diffusive step is considered (error bars are standard deviation).

In Figure 4.7 we consider the effect of d/a on D obtained from experiments, using Cai's scaling analysis, and computed from the solution viscosities using the Stokes-Einstein analysis. We find that for d/a < 0.7, the measured D decreases with increasing d/a and is three or more orders of magnitude larger than values predicted by the S-E equation. For d/a > 0.7, D undergoes an abrupt transition to a regime where it is essentially independent of d/a. In contrast, diffusivities computed using the S-E formula, decrease strongly with d/a > 0.7 and by $d/a \approx 3$ are more than three orders of magnitude lower than the experimentally measured D. Our results therefore show that diffusivities of small particles in polymers are markedly faster than those expected from Stokes-Einstein analysis over the entire range of d/a studied. Comparison of the measured diffusivities with those obtained using the analysis of Cai et al. leads to a very different set of conclusions. At low d/a, the measured and predicted values are within a factor of 2-3 of each other over the full range of d < 0.7. For d/a > 0.7 the calculated diffusivities are orders of magnitude larger than the measured values, but both are nearly independent of d/a. Both aspects of our observations are strikingly similar to those reported by Mangal et al.[33] from XPCS studies of PEG grafted nanoparticles in PMMA melts, which exhibit hyperdiffusive relaxations on the timescales probed by the experiments. Remarkably, as reported by Mangal et al., we also find that a simple amendment to Cai's hopping model to account for the fact that stretching of multiple (approximately 5) chain entanglements must occur simultaneously for a particle to escape its entangled surroundings, could fit the diffusive step of the two-step diffusion process. The diffusive step of the faster hopping-type diffusivity data was fitted with the model:

$$D \approx D_{SE} + D_{hop} \approx \frac{k_B T}{3\pi d \eta_{sys}} + \frac{\xi^2}{\tau_e} \exp(-Ad/a) \qquad (4.4)$$

where the pre-factor A was found to be ~4.303. The data value at the volume fraction of 0.24 does not follow this correction, as the transport is arrested and subdiffusive. This is in contrast to a recent report on XPCS measurements for nanorod diffusion in entangled worm-like micelle solutions (WLMs) where it was found that the low aspect ratio nanorods (with lengths larger than the mesh size, and diameters smaller than the mesh size) remarkably followed Cai's original hopping model sans correction[81]. More experiments on motion of nanoparticles of varying geometries in the regime $a \sim d < R_g$ will provide further insights on how topological constraints posed by entanglement network act and influence particle motion.

4.4 Conclusions

We study diffusion of nano-sized, highly stable fluorescent C dots in polyethylene oxide solutions in different regimes of particle diameter (d) with respect to characteristic polymer length scales (correlation length (ξ), the entanglement mesh size (a) and radius of gyration (R_g) of the polymer). Through, fluorescence correlation spectroscopy in the regime $d/a < 1$ and single particle tracking in the regime $d/a > 1$ we find that dynamics in these regimes are diffusive, and tend to be subdiffusive in concentrated polymer solutions for $d/a > 1$. While subdiffusion in these systems is intuitive and is a well-known signature of caged particle dynamics, it is not captured in most theoretical studies of nanoparticle dynamics in polymeric hosts.

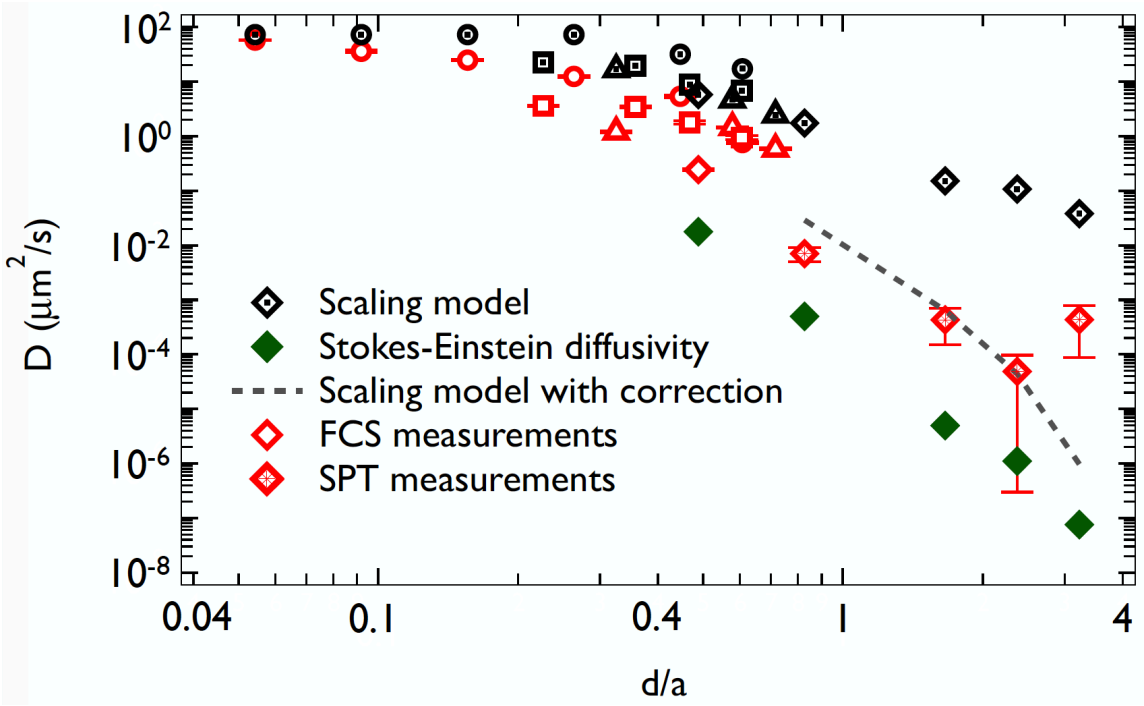

Figure 4.7. Master curve of diffusivity vs. d/a plotted for 1.352 mil Da Mw PEO solutions in water, here φ varies from 0.01-0.24 and Z varies from 1-89. The open red symbols are the experimental data from FCS, open diamond symbols with star show the data obtained from SPT; the open black symbols with dot are predictions from the Cai-Panyukov-Rubinstein scaling analysis [Ref 60-61]; and the filled green symbols are diffusivities estimated using the Stokes-Einstein formula. The dashed line indicates the modified hopping model given in equation 4.4. The notation used in this figure is the same as Figure 4.4 where circles are for 6.7 nm particles, squares for 16.5 nm particles, triangles-up for 23.7 nm particles and diamonds for 35.5 nm particles. Error bars for particle-tracking data are standard deviation and FCS data are standard error.

The average viscosity that the particle experiences in this regime is neither the bulk solution viscosity nor the calculated viscosity from pure hopping motion. We find instead that the resistance to probe particle motions can be captured by the hopping model proposed by Cai only when an additional prefactor is included to account for the fact that relaxation of around 4-5 or more entanglements are needed to release a particle from its entangled cage.

In disagreement with previous X-ray Photon Correlation Spectroscopy (XPCS) studies of nanoparticle dynamics in entangled melts, we find no evidence of hyperdiffusive particle dynamics in entangled solutions. This absence of hyperdiffusion in solvated polymers is in qualitative accord with expectations from a recent theory[80] that attributes hyperdiffusive nanoparticle dynamics to dynamic strain dipoles formed by increased interparticle correlations in crowded systems.

Bibliography

1. Hill, R. J. Electrokinetics of nanoparticle gel-electrophoresis. *Soft Matter* **2016**, *12*(38), 8030-8048.

2. Fichtner, A.; Jalil A.; Pyell, U. Determination of the Exact Particle Radius Distribution for Silica Nanoparticles via Capillary Electrophoresis and Modeling the Electrophoretic Mobility with a Modified Analytic Approximation. *Langmuir*. **2017**, *33*(9), 2325-2339.

3. Lai, S. K.; O'Hanlon, D. E.; Harrold S.; Man, S. T.; Wang, Y.; Cones, R.; Hanes, J. Rapid transport of large polymeric nanoparticles in fresh undiluted human mucus. *Proc. Natl. Acad. Sci. U.S.A*. **2007**, *104*(5), 1482-1487.

4. Lieleg, O.; Vladescu, I.; Ribbeck, K. Characterization of particle translocation through mucin hydrogels. *Biophys. J*. **2010**, *98*(9), 1782-1789.

5. Moeendarbary E.; Harris, A. R. Cell mechanics : principles, practices, and prospects. *Wiley Interdiscip. Rev.: Sys. Biol. Med*. **2014**, *6*(5), 371-388.

6. Gumbiner, B. M. Cell Adhesion : The Molecular Basis of Tissue Architecture and Morphogenesis. *Cell* **1996**, *84*(3), 345-357.

7. Reverey, J. F.; Jeon, J.; Bao, H.; Leippe, M.; Metzler, R.; Selhuber-Unkel, C. Superdiffusion dominates intracellular particle motion in the supercrowded cytoplasm of pathogenic Acanthamoeba castellanii. *Sci. Rep*. **2015**, *5*, 1-14.

8. Sokolov, I. M. Models of anomalous diffusion in crowded environments. *Soft Matter* **2012**, *8*, 9043-9052.

9. Banks, D.; Tressler, C.; Peters, R.; Höfling, F.; Fradin, C. Characterizing anomalous diffusion in crowded polymer solutions and gels over five decades in time with variable-lengthscale fluorescence correlation spectroscopy. *Soft Matter* **2016**, *4*(8), 1166-1169.

10. Bremmell, K. E.; Wissenden, N.; Dunstan, D. E. Diffusing probe measurements in Newtonian and elastic solutions. *Adv. Colloid Interface Sci*. **2001**, *89-90*, 141-154.

11. Brown W.; Rymden, R. Comparison of the translational diffusion of large spheres and high-molecular-weight coils in polymer solutions. *Macromolecules*. **1988**, *21*(3), 840-846.

12. Carnis, J.; Cha, W.; Wingert, J.; Kang, J.; Zhang, J.; Song, S.; Sikorski, M.; Robert, A.; Gutt, C.; Chen, S.; Dai, Y.; Ma, Y.; Guo, H.; Lurio, L. B.; Shpyrko,

O.; Narayanan, S.; Cui, M.; Kosif, I.; Emrick, T.; Russell, T. P.; Lee, H. C.; Yu, C.; Grübel, G.; Sinha, S. K.; Kim, H. Demonstration of Feasibility of X-Ray Free Electron Laser Studies of Dynamics of Nanoparticles in Entangled Polymer. *Sci. Rep*. **2014**, *4*, 6017.

13. Cheng, Y.; Prud'homme, R. K.; Thomas, J. L. Diffusion of Mesoscopic Probes in Aqueous Polymer Solutions Measured by Fluorescence Recovery after Photobleaching. *Macromolecules* **2002**, *35*(21), 8111-8121.

14. de Kort, D. W.; Rombouts, W. H.; Hoeben, F. J. M.; Janssen, H. M.; As, H. V.; van Duynhoven, J. P. M. Scaling Behavior of Dendritic Nanoparticle Mobility in Semidilute Polymer Solutions. *Macromolecules* **2015**, *48*(20), 7585-7591.

15. Fatin-Rouge, N.; Starchev, K.; Buffle, J. Size effects on diffusion processes within agarose gels. *Biophys. J*. **2004**, *86*(5), 2710-2719.

16. Ge, T.; Kalathi, J. T.; Halverson, J. D.; Grest, G. S.; Rubinstein, M. Nanoparticle Motion in Entangled Melts of Linear and Nonconcatenated Ring Polymers. *Macromolecules* **2017**, *50*(4), 1749-1754.

17. Gold, D.; Onyenemezu, C.; Miller, W. G. Effect of Solvent Quality on the Diffusion of Polystyrene Latex Spheres in Solutions of Poly(methyl methacrylate). *Macromolecules* **1996**, *29*(17), 5700-5709.

18. Grabowski, C. A.; Mukhopadhyay, A. Diffusion of Polystyrene Chains and Fluorescent Dye Molecules in Semidilute and Concentrated Polymer Solutions Diffusion of Polystyrene Chains and Fluorescent Dye Molecules in Semidilute and Concentrated Polymer Solutions. *Polymer* **2008**, *41*(16), 6191-6194.

19. Grabowski, C. A.; Mukhopadhyay, A. Size effect of nanoparticle diffusion in a

polymer melt. *Macromolecules* **2014**, *47*(20), 7238-7242.

20. Guo, H.; Bourret, G.; Corbierre, M. K.; Rucareanu, S.; Lennox, R. B.; Laaziri, K.; Piche, L.; Sutton, M.; Harden, J. L.; Leheny, R. L. Nanoparticle Motion within Glassy Polymer Melts. *Phys. Rev. Lett*. **2009**, *102*(7), 75702.

21. Guo, H.; Bourret, G.; Lennox, R. B.; Sutton, M.; Harden, J. L.; Leheny, R. L. Entanglement-Controlled Subdiffusion of Nanoparticles within Concentrated Polymer Solutions. *Phys. Rev. Lett*. **2012**, *109*(5), 55901.

22. Holyst, R.; Bielejewska, A.; Szymański, J.; Patkowski, A.; Gapiński, J.; Żywociński, A.; Kalwarczyk, E.; Tabaka, M.; Ziębacz, N.; Wieczorek, S. A. Scaling form of viscosity at all length-scales in poly(ethylene glycol) solutions studied by fluorescence correlation spectroscopy and capillary electrophoresis. *Phys. Chem. Chem. Phys*. **2009**, *11*(40), 9025-9032.

23. Jang, W.; Koo, P.; Bryson, K.; Narayanan, S.; Sandy, A.; Russell, T. P.; Mochrie, S. G. Dynamics of Cadmium Sulfide Nanoparticles within Polystyrene Melts. *Macromolecules* **2014**, *47*(18), 6483-6490.

24. Kang, K.; Gapinski, J.; Lettinga, M. P.; Buitenhuis, J.; Meier, G.; Ratajczyk, M.; Dhont, J. K. G.; Patkowski, A. Diffusion of spheres in crowded suspensions of rods. *J. Chem. Phys*. **2005**, *122*(4), 44905.

25. Kohli, I.; Mukhopadhyay, A. Diffusion of Nanoparticles in Semidilute Polymer Solutions: Effect of Different Length Scales. *Macromolecules* **2012**, *45*(15), 6143-6149.

26. Landers, J.; Roeder, L.; Salamon, S.; Schmidt, A. M.; Wende, H. Particle–Matrix Interaction in Cross-Linked PAAm-Hydrogels Analyzed by Mössbauer

Spectroscopy. *J. Phys. Chem. C* **2015**, *119*(35), 20642-20648.

27. Langevin, D.; Rondelez, F. Sedimentation of large colloidal particles through semidilute polymer solutions. *Polymer* **1978**, *19*(8), 875-882.

28. Lin, C.; Griffin, P. J.; Chao, H.; Hore, M. J. A.; Ohno, K.; Clarke, N.; Riggleman, R. A.; Winey, K. I.; Composto, R. J. Grafted polymer chains suppress nanoparticle diffusion in athermal polymer melts. *J. Chem. Phys*. **2017**, *146*(20), 203332.

29. Lin, T. H.; Phillies, G. D. J. Probe diffusion in poly(acrylic acid)-water. Effect of probe size. *Macromolecules* **1984**, *17*(9), 1686-1691.

30. Liu, S.; Senses, E.; Jiao, Y.; Narayanan, S.; Akcora, P. Structure and Entanglement Factors on Dynamics of Polymer- Grafted Nanoparticles. *ACS Macro Lett*. **2016**, *5*(5), 569-573.

31. Lu, Q.; Solomon, M. J. Probe size effects on the microrheology of associating polymer solutions. *Phys. Rev. E: Stat., Nonlinear, Soft Matter Phys*. **2002**, *66*(6), 61504.

32. Lungova, M.; Krutyeva, M.; Pyckhout-Hintzen, W.; Wischnewski, A.; Monkenbusch, M.; Allgaier, J.; Ohl, M.; Sharp, M.; Richter, D. Nanoscale Motion of Soft Nanoparticles in Unentangled and Entangled Polymer Matrices. *Phys. Rev. Lett*. **2016**, *117*(14), 147803.

33. Mangal, R.; Srivastava, S.; Narayanan, S.; Archer, L. A. Size-Dependent Particle Dynamics in Entangled Polymer Nanocomposites. *Langmuir*. **2016**, *32*(2), 596-603.

34. Mason, T. G.; Weitz, D. A. Optical Measurements of Frequency-Dependent

Linear Viscoelastic Moduli of Complex Fluids. *Phys. Rev. Lett*. **1995**, *74*(7), 1250-1253.

35. Michelman-Ribeiro, A.; Horkay, F.; Nossal, R.; Boukari, H. Probe diffusion in aqueous poly(vinyl alcohol) solutions studied by fluorescence correlation spectroscopy. *Biomacromolecules* **2007**, *8*(5), 1595-1600.

36. Narayanan, S.; Lee, D. R.; Hagman, A.; Li, X.; Wang, J. Particle Dynamics in Polymer-Metal Nanocomposite Thin Films on Nanometer-Length Scales. *Phys. Rev. Lett*. **2007**, *98*(18), 185506.

37. Ochab-Marcinek, A.; Hołyst, R. Scale-dependent diffusion of spheres in solutions of flexible and rigid polymers: mean square displacement and autocorrelation function for FCS and DLS measurements. *Soft Matter* **2011**, *7*(16), 7366-7374.

38. Ochab-Marcinek, A.; Wieczorek, S. A.; Ziębacz, N.; Hołyst, R. The effect of depletion layer on diffusion of nanoparticles in solutions of flexible and polydisperse polymers. *Soft Matter* **2012**, *8*(43), 11173.

39. Omari, R. A.; Aneese, A. M.; Grabowski, C. A.; Mukhopadhyay, A. Diffusion of nanoparticles in semidilute and entangled polymer solutions. *J. Phys. Chem. B* **2009**, *113*(25), 8449-8452.

40. Onyenemezu, C. N.; Gold, D.; Roman, M.; Miller, W. G. Diffusion of polystyrene latex spheres in linear polystyrene nonaqueous solutions. *Macromolecules* **1993**, *26*(15), 3833-3837.

41. Phillies, G. D. J.; Gong, J.; Li, L., Rau, A.; Zhang, K.; Yu, L.; Rollings, J. Macroparticle diffusion in dextran solutions. *J. Phys. Chem*. **1989**, *93*(16),

6219-6223.

42. Phillies, G. D. J.; Clomenil, D. Probe diffusion in polymer solutions under theta and good conditions. *Macromolecules* **1993**, *26*(1), 167-170.

43. Altenberger, A. R.; Tirrell, M. On the theory of self-diffusion in a polymer gel. *J. Chem. Phys.* **1984**, *80*(5), 2208-2213.

44. Pluen, A.; Netti, P. A.; Jain, R. K.; Berk, D. A. Diffusion of macromolecules in agarose gels: comparison of linear and globular configurations. *Biophys J.* **1999**, *77*(1), 542-552.

45. Rathgeber, S.; Beauvisage, H.; Chevreau, H.; Willenbacher, N.; Oelschlaeger, C. Microrheology with fluorescence correlation spectroscopy. *Langmuir* **2009**, *25*(11), 6368-6376.

46. Schnurr, B.; Gittes, F.; Mackintosh, F. C.; Schmidt, C. F. Determining Microscopic Viscoelasticity in Flexible and Semiflexible Polymer Networks from Thermal Fluctuations. *Macromolecules* **1997**, *30*(25), 7781-7792.

47. Seiffert, S.; Oppermann, W. Diffusion of linear macromolecules and spherical particles in semidilute polymer solutions and polymer networks. *Polymer* **2008**, *49*(19), 4115-4126.

48. Sozański, K.; Wiśniewska, A.; Kalwarczyk, T.; Hołyst, R. Activation energy for mobility of dyes and proteins in polymer solutions: from diffusion of single particles to macroscale flow. *Phys. Rev. Lett*. **2013**, *111*(22), 228301.

49. Sprakel, J.; van der Gucht, J.; Cohen Stuart, M. A.; Besseling, N. A. M. Brownian particles in transient polymer networks. *Phys. Rev. E.: Stat. Nonlinear, Soft Matter Phys*. **2008**, *77*(6), 61502.

50. Tokita, M.; Miyoshi, T.; Takegoshi, K.; Hikichi, K. Probe diffusion in gels. *Phys. Rev. E*. **1996**, *53*(2), 1823-1827.

51. Tong, P.; Ye, X.; Ackerson, B. J.; Fetters, L. J. Sedimentation of Colloidal Particles through a Polymer Solution. *Phys. Rev. Lett*. **1997**, *79*(12), 2363-2366.

52. van Zanten, J. H.; Amin, S.; Abdala, A. A. Brownian Motion of Colloidal Spheres in Aqueous PEO Solutions. *Macromolecules* **2004**, *37*(10), 3874-3880.

53. Wiśniewska, A; Sozański, K.; Kalwarczyk, T.; Kędra-Królik, K.; Pieper, P.; Wieczorek, S. A.; Jakieła, S.; Enderlein, J; Hołyst, R. Scaling of activation energy for macroscopic flow in poly(ethylene glycol) solutions: Entangled – Non-entangled crossover. *Polymer* **2014**, *55*(18), 4651-4657.

54. Won, J.; Onyenemezu, C.; Miller, W. G.; Lodge, T. P. Diffusion of Spheres in Entangled Polymer Solutions: A Return to Stokes-Einstein Behavior. *Macromolecules* **1994**, *27*(25), 7389-7396.

55. Wong, I. Y.; Gardel, M. L.; Reichman, D. R.; Weeks, E. R.; Valentine, M. T.; Weitz, D. A. Anomalous diffusion probes microstructure dynamics of entangled F-actin networks. *Phys. Rev. Lett*. **2004**, *92*(17), 178101.

56. Tuteja, A.; Mackay, M. E.; Narayanan, S.; Asokan, S.; Wong, M. S. Breakdown of the continuum stokes-einstein relation for nanoparticle diffusion. *Nano. Lett*. **2007**, *7*(5), 1276-1281

57. Amsden, B. An Obstruction-Scaling Model for Diffusion in Homogeneous Hydrogels. *Macromolecules*. **1999**, *32*(3), 874-879.

58. Amsden, B. Modeling solute diffusion in aqueous polymer solutions. *Polymer* **2002**, *43*(5), 1623-1630.

59. Brochard-Wyart, F.; de Gennes, P. G. Viscosity at small scales in polymer melts. *Eur. Phys. J. E: Soft Matter Biol. Phys.* **2000**, *1*(1), 93-97.

60. Cai, L.-H.; Panyukov, S.; Rubinstein, M. Hopping Diffusion of Nanoparticles in Polymer Matrices. *Macromolecules*. **2015**, *48*(3), 847-862.

61. Cai, L.-H.; Panyukov, S.; Rubinstein, M. Mobility of Nosticky Nanoparticles in Polymer Liquids. *Macromolecules*. **2011**, *44*(19), 7853-7863.

62. Cukier, R. I. Diffusion of Brownian spheres in semidilute polymer solutions. *Macromolecules*. **1984**, *17*(2), 252-255.

63. Dong, Y.; Feng, X.; Zhao, N.; Hou, Z. Diffusion of nanoparticles in semidilute polymer solutions: A mode-coupling theory study. *J. Chem. Phys*. **2015**, *143*(2), 24903.

64. Egorov, S. A. Anomalous nanoparticle diffusion in polymer solutions and melts: a mode-coupling theory study. *J. Chem. Phys*. **2011**, *134*(8), 84903.

65. Fan, T.-H.; Dhont, J. K. G.; Tuinier, R. Motion of a sphere through a polymer solution. *Phys. Rev. E: Stat., Nonlinear, Soft Matter Phys*. **2007**, *75*(1), 11803.

66. Fan, T.-H.; Xie, B.; Tuinier, R. Asymptotic analysis of tracer diffusivity in nonadsorbing polymer solutions. *Phys Rev E: Stat., Nonlinear, Soft Matter Phys*. **2007**, *76*(5), 51405.

67. Kalwarczyk, T.; Sozanski, K.; Ochab-Marcinek, A.; Szymanski, J.; Tabaka, M., Hou, S.; Hołyst, R. Motion of nanoprobes in complex liquids within the framework of the length-scale dependent viscosity model. *Adv. Colloid Interface Sci*. **2015**, *223*, 55-63.

68. Kuldová, J.; Uhlík, F.; Košovan, P. The drag of the tails: Diffusion of sticky nanoparticles in dilute polymer solutions. *J. Chem. Phys*. **2015**, *143*(24), 243129.

69. Liu, J.; Cao, D.; Zhang, L. Molecular Dynamics Study on Nanoparticle Diffusion in Polymer Melts: A Test of the Stokes−Einstein Law. *J. Phys. Chem. C* **2008**, *112*(17), 6653-6661.

70. Masaro, L.; Zhu, X. Physical Models of Diffusion for Polymer Solutions, Gels and Solids. *Prog. Polym Sci.* **1999**, *24*(5), 731-775.

71. Ogston, A. G.; Preston, B. N.; Wells, J. D. On the Transport of Compact Particles Through Solutions of Chain-Polymers. *Proc. R. Soc. A* **1973**, *333*(1594), 297-316.

72. Solomon, M. J.; Lu, Q. Rheology and dynamics of particles in viscoelastic media. *Curr. Opin. Colloid Interface Sci*. **2001**, *6*(5-6), 430-437.

73. Tuinier, R.; Fan, T.-H. Scaling of nanoparticle retardation in semi-dilute polymer solutions. *Soft Matter* **2008**, *4*(2), 254-257.

74. Yamamoto, U.; Schweizer, K. S. Theory of nanoparticle diffusion in unentangled and entangled polymer melts. *J. Chem. Phys*. **2011**, *135*, 224902.

75. Phillies, G. D. J. Dynamics of polymers in concentrated solutions: the universal scaling equation derived. *Macromolecules* **1987**, *20*(3), 558-564.

76. Choudhury, S.; Agrawal, A.; Kim, S. A.; Archer, L. A. Self-Suspended Suspensions of Covalently Grafted Hairy Nanoparticles. *Langmuir* **2015**, *31*(10), 3222-3231.

77. Fields, A. P.; Cohen, A. E. Electrokinetic trapping at the one nanometer limit. *Proc. Natl. Acad. Sci. U.S.A.* **2011**, *108*(22), 8937–8942.

78. Pennicard, D.; Lange, S.; Smoljanin, S; Hirsemann, H.; Graafsma, H.; Epple, M; Zuvic, M.; Lampert, M-O; Fritzsch, T.; Rothermund, M. The LAMBDA photon-counting pixel detector. *J. Phys. Conf. Ser.* **2013**, *425*(6), 62010.

79. Ma, K.; Zhang, D.; Cong, Y.; Wiesner, U. Elucidating the mechanism of silica nanoparticle PEGylation processes using Fluorescence Correlation Spectroscopies. *Chem. Mater.* **2016**, *28*(5), 1537-1545.

80. Srivastava, S.; Agarwal, P.; Mangal, R.; Koch, D. L.; Narayanan, S.; Archer, L. A. Hyperdiffusive Dynamics in Newtonian Nanoparticle Fluids. *ACS Macro. Lett.* **2015**, *4*, 1149-1153.

81. Lee, J.; Grein-Iankovski, A.; Narayanan, S.; Leheny, R. L. Nanorod mobility within entangled wormlike micelle solutions. *Macromolecules* **2017**, *50*, 406-415.

APPENDIX A

MODELING PARTICLE CAGED IN A POLYMER ENTANGLEMENT

In this section we model the particle caged in a polymer entanglement as a particle in a harmonic potential well, where the potential field surrounding the particle is given by $V(x) = (1/2)kx^2$, where k is the spring constant and x is the extent to which the spring has been stretched from its equilibrium position. This is a valid assumption as an ideal elastic polymer chain in three dimensions can be modeled as a spring with spring constant $k = 3k_BT / Nb^2$, where k_B is the Boltzmann constant, T is the temperature, N is the number of kuhn monomers making up the spring and b is the kuhn length. Hence, the polymers become stiffer as the temperature increases or the size of the chain decreases. As the particles move by stretching the polymer entanglements, we assume that the particle is tethered to pseudo polymer segment, which we treat as a spring, and is surrounded by a sea of smaller polymer segments which act as solvent, depicted in Figure A.1.

We begin by considering the 1D Langevin equation,

$$m\frac{d\boldsymbol{v}}{dt} = -\gamma \boldsymbol{v}(t) - \frac{dV}{dx} + \boldsymbol{F}_B(t) \tag{A.1}$$

It is a simple force balance on a single particle, where $\boldsymbol{v}$ is the velocity of the particle, and $\gamma=6\pi\eta R$, given by the Stokes drag law (in which η is the surrounding medium's viscosity and R is the radius of the particle), V is the potential field surrounding the particle and $\boldsymbol{F_B}$, called the Brownian force, is a random force that arises from thermal fluctuations. This random Brownian force is Gaussian in nature with a zero mean and the second moment given by the fluctuation dissipation theorem (FDT), $\left\langle F_B(t)F_B(t')\right\rangle = 2\gamma k_BT\delta(t-t')$, where $\delta(t)$ is the Dirac delta function.

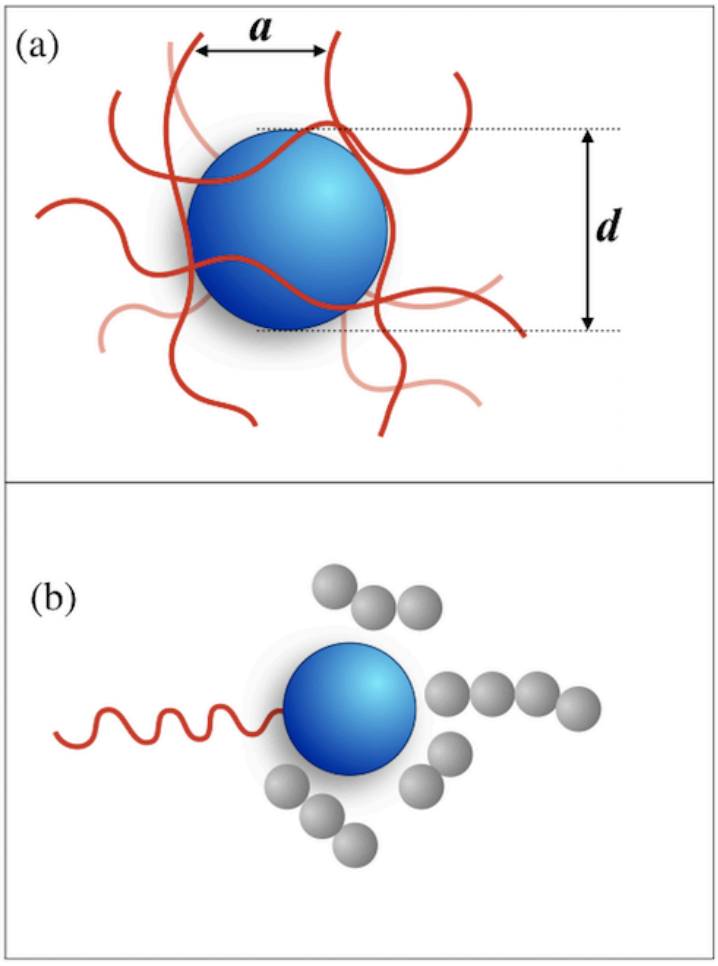

Figure A1. (a) A schematic of spherical particle of diameter *d*, trapped in the entanglement mesh of a polymer with entanglement tube diameter, *a*. (b) We approximate this case, by considering a particle tethered to a pseudo-spring surrounded by smaller chain segments that act as the solvent.

The solution to this equation for particle in a harmonic potential well, $V(x) = \frac{1}{2}kx^2$ (where k is the spring constant and x is the extent to which the spring has been stretched from its equilibrium position) is well described in the works of Uhlenbeck and Ornstein[1] and Chandrasekhar[2]. They provided the expression for the mean-squared displacement of a particle from its initial position x_0 at time t, $\langle \Delta r^2(t) \rangle$, that could be written down as,

$$\langle \Delta r^2(t) \rangle = \frac{k_B T}{m\omega_o^2} + \left(x_0^2 - \frac{k_B T}{m\omega_o^2} \right) e^{-\beta t} \left(\cosh \frac{1}{2}\beta_1 t + \frac{\beta}{\beta_1} \sinh \frac{1}{2}\beta_1 t \right)^2$$

$$\beta_1 = \sqrt{\beta^2 - 4\omega_o^2} \qquad \text{(A.2)}$$

$$\omega_o^2 = \frac{k}{m}$$

$$\beta = \frac{\gamma}{m}$$

Here ω_o is the natural frequency of the spring. There are three relevant timescales that can be extracted from this equation, viz., the momentum relaxation timescale $\tau_P = \beta^{-1}$ which is the time taken by a freely diffusing particle to relaxes its velocity, a restoring timescale $\tau_{res} = \gamma / k$ associated with damping of a stretched spring back to its equilibrium length, and $T = \omega_o^{-1}$ known in classical mechanics as the period of a harmonic oscillator. The value of β_1 determines the nature of dynamics with positive, real values corresponding to the overdamped limit, where particle inertia can be neglected, and zero or imaginary values corresponding to the underdamped case, where particle motion is Non-Markovian or in other words correlated. The condition for underdamping of a particle in a harmonic potential well can also be written down

in terms of the momentum relaxation and restoring timescales as $\tau_{res} \leq 4\tau_p$. We define the ratio of $\tau_{res} / \tau_p = \beta^2 / \omega_o^2$ as α, so that the transition from underdamping to overdamping takes place at $\alpha = 4$.

Now, equation (A.2) can be simplified for the underdamped periodic ($\beta^2 < 4\omega_o^2$) and underdamped aperiodic ($\beta^2 = 4\omega_o^2$) conditions respectively as given below[2],

$$\left\langle \Delta r^2(t) \right\rangle = \frac{k_B T}{m\omega_o^2} + \left(x_0^2 - \frac{k_B T}{m\omega_o^2} \right) e^{-\beta t} \left(\cos \omega_1 t + \frac{\beta}{2\omega_1} \sin \omega_1 t \right)^2$$
$$\omega_1 = \sqrt{\omega_o^2 - \frac{\beta^2}{4}} \qquad \text{(A.3)}$$

$$\left\langle \Delta r^2(t) \right\rangle = \frac{k_B T}{m\omega_o^2} + \left(x_0^2 - \frac{k_B T}{m\omega_o^2} \right) e^{-\beta t} \left(1 + \frac{\beta}{2} t \right)^2 \qquad \text{(A.4)}$$

The long time response in all these cases, equation (A.2), (A.3), (A.4) is similar, that is, the particle eventually attains the equipartition condition where $\left\langle \Delta r^2(t) \right\rangle = k_B T / m\omega_o^2 = k_B T / k$. The short time behavior depends on whether the spring is overdamped or underdamped, and shows how the particle moves in the harmonic well before it attains the equilibrium at long times.

We study the effect of damping on dynamics of a particle in a harmonic potential, by plotting the mean squared displacement normalized by $k_B T / m\omega_o^2$ against time normalized by the momentum relaxation time $\tau_p = \beta^{-1}$ for different values of α in Figure A.2. When $\alpha < 2$, the mean squared displacement in Figure A.2(a) oscillates and the frequency of oscillations decreases with increasing α. The oscillations die down at $\sim 10\tau_p$ at which the particle reaches the equipartition condition or in other words becomes trapped in the harmonic well. These oscillations disappear for higher

values of α as seen in Figure A.2 (b) and (c). As oscillations die down, for the curves α = 2-10, the mean squared displacement exhibits the ballistic scaling, i.e. $\left\langle \Delta r^2(t) \right\rangle \sim t^2$ which then transitions directly to the arrested regime, where $\left\langle \Delta r^2(t) \right\rangle = k_B T / m\omega_o^2$. However as α becomes even higher, as seen in Figure A.2(c), there exist three clear regimes of transport. Physically speaking for a fixed value of τ_p, increasing α means that the spring attached to the particle becomes less stiff as τ_{res} is inversely proportional to the spring constant *k*. Under these conditions, the restoring force of the spring weakens and the particle becomes free to perform random walk. This is evident in Figure A.2(c) for α = 10 and beyond, where we clearly observe a transition from ballistic to diffusive with mean squared displacement $\left\langle \Delta r^2(t) \right\rangle$ growing linearly with time after $\sim 10\tau_p$. The particle is now free to move via random walk up until τ_{res} when it becomes arrested. In the asymptotic limit of $k \to 0$, $\tau_{res} \to \infty$ and $\alpha \to \infty$ the particle exhibits random walk indefinitely.

Hence the non-Markovian region (or the ballistic region) of mean squared displacement persists roughly for $\sim 10\tau_p$ irrespective of the strength of damping. We estimate this timescale using the parameters provided in the work of Mangal et al [3]. Within this work, the authors studied the dynamics of polyethylene glycol (PEG) tethered silica nanoparticles in highly entangled polymethyl methacrylate melts (PMMA). The particle diameter *d* = 10 nm, and entanglement tube diameter for PMMA *a* ≈ 7 nm. We estimate the effective viscosity η_{eff} of the chain segment that interacts with the particle as,

$$\eta_{eff} \sim \frac{1}{6} G_N^0 \tau_e \left(\frac{N}{N_e^3} \right) \left(\frac{d}{b} \right)^4 \tag{A.5}$$

Here G_N^0 is the high-frequency plateau modulus and τ_e is the entanglement relaxation time. By treating the polymer entanglement as a spring with spring constant

$$k = \frac{3k_BT}{N_e b^2} = \frac{3k_BT}{a^2} \tag{A.6}$$

For PMMA k comes out to be ~ 3.7x10^{-4} J/m. Hence the η_{eff} for the 10 nm silica particle tethered to a pseudo-PMMA spring in 260kDa PMMA host (G_N^0 ~ 10^5 Pa, τ_e ~ 0.01 s, b ~ 1.5 nm, N_e ~ 18) can be calculated to be ~ 3.7x10^4 Pa s and the parameter α is of the order of 10^{17} making the system highly overdamped and the ballistic motion extremely difficult to detect, as the time $10\tau_p$ is very small being of the order of 10^{-18} s. Making the spring longer will only decrease the spring constant and make this number even smaller.

We must note that this analysis is based on harmonic traps where the spring constant is invariant in time, and the final arrested state where mean squared displacement of the particle becomes fixed can last indefinitely. However, polymer entanglements are transient traps and can only last as long as the polymers surrounding the particle do not reptate out of the tube. Hence this analysis is only valid as long as $\tau_{res}, \tau_p << \tau_{rep}$ (reptation time for the polymer melt or solution). This seems to be the case in the above-described example where reptation time τ_{rep} is of the order of 10^4 s. Several authors have recognized hopping as viable mechanism through which particles can move from one entanglement tube to the other as they wait for the surrounding polymers to reptate[4] and using this transport mechanism particles can break out of arrested state much earlier.

While hopping steps are small, being of the order of a kuhn length, and are challenging to measure in tracking experiments where thermal fluctuations are larger than the size of the kuhn length; a realistic treatment of particle motion in entanglements would include these considerations. Currently molecular dynamics (MD) simulations are being developed which can be used to study nanoparticle motion both within the entanglement tube and outside beyond the reptation time[5].

REFERENCES

(1) Uhlenbeck, G. E.; Ornstein, L. S. On the Theory of the Brownian Motion. *Phys. Rev.* **1930**, *36* (5), 823–841.

(2) Chandrasekhar, S. Stochastic Problems in Physics and Astronomy. *Rev. Mod. Phys.* **1943**, *15* (1), 1–89.

(3) Mangal, R.; Srivastava, S.; Narayanan, S.; Archer, L. A. Size-Dependent Particle Dynamics in Entangled Polymer Nanocomposites. *Langmuir* **2016**, *32* (2), 596–603.

(4) Cai, L.-H.; Panyukov, S.; Rubinstein, M. Hopping Diffusion of Nanoparticles in Polymer Matrices. *Macromolecules* **2015**, *48* (3), 847–862.

(5) Ge, T.; Kalathi, J. T.; Halverson, J. D.; Grest, G. S.; Rubinstein, M. Nanoparticle Motion in Entangled Melts of Linear and Nonconcatenated Ring Polymers. *Macromolecules* **2017**, *50* (4), 1749–1754.

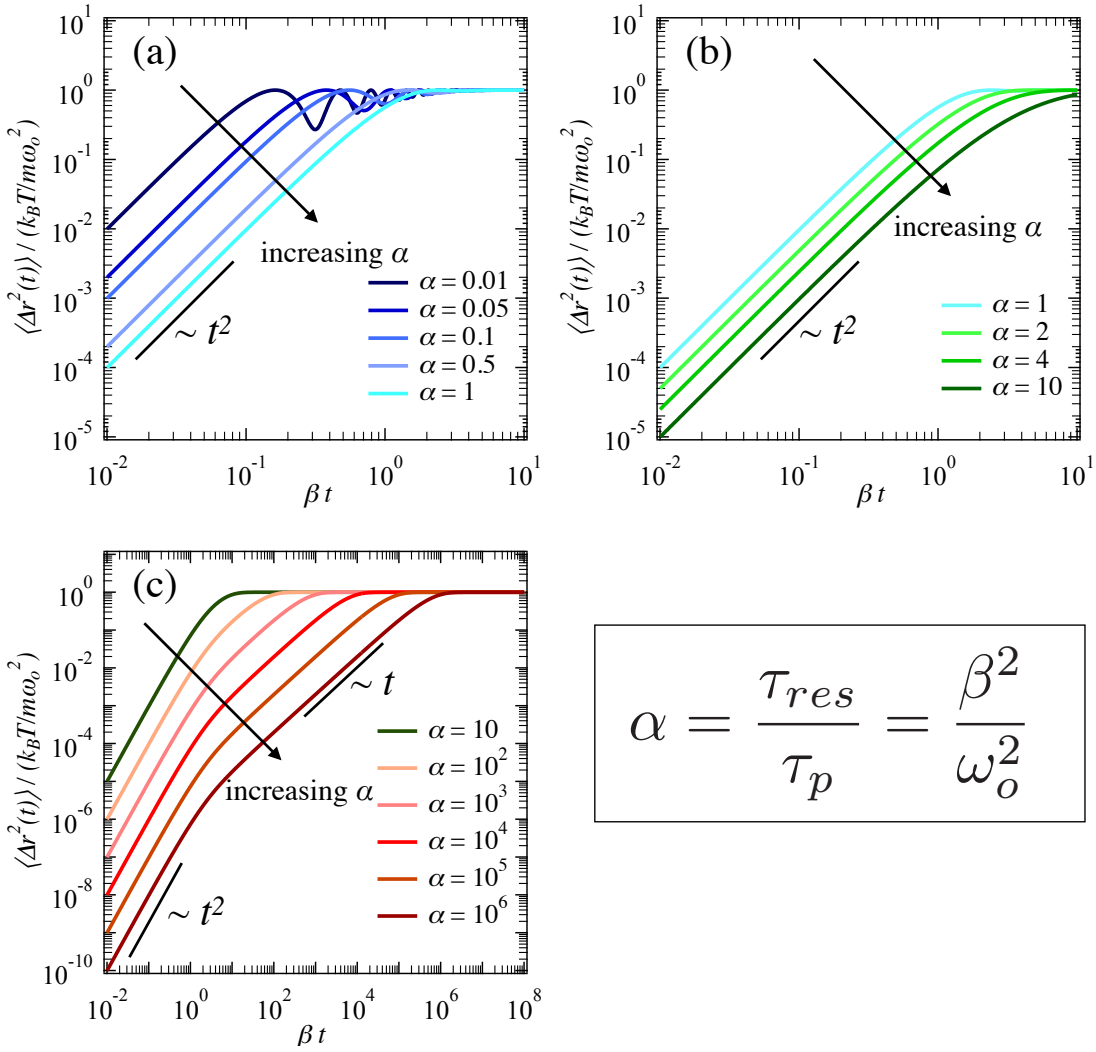

Figure A2. (a)-(c) Plots of mean squared displacement, $\langle \Delta r^2(t) \rangle$, normalized by $k_B T / m\omega_o^2$ versus time normalized by the momentum relaxation time $\tau_p = \beta^{-1}$ for different values of parameter α by setting the initial coordinate of the particle $x_0 = 0$. The particles transition from ballistic to caged state passing through an intermediate diffusive region. The size of the diffusive regime increases as α increases.

APPENDIX B

SUPPLEMENTARY INFORMATION FOR CHAPTER 4

C Dot Synthesis and Characterization

Chemicals and Reagents: All chemicals were used as purchased. Dimethyl sulfoxide (DMSO), (3-mercaptopropyl) trimethoxysilane (MPTMS), tetramethyl orthosilicate (TMOS), tetraethyl orthosilicate (TEOS), ammonium hydroxide were purchased from Sigma-Aldrich. 2-[Methoxy-(polyethyleneoxy)propyl] trimethoxysilane (PEG-silane, molar mass ~500 g/mol) was purchased from Gelest. Maleimide-functionalized ATTO647N organic dye was purchased from ATTO-Tec. DI water (18.2MΩ.cm^{-1}) was obtained from a Millipore Milli-Q system.

Sample Preparation: Sub-10nm fluorescent silica nanoparticles (C dots) were synthesized according to Ma *et al.*[1] In short, 0.25 μmol maleimide-functionalized ATTO647N dye were reacted with MPTMS in DMSO at a molar ratio of 1:25 under nitrogen atmosphere. Then, 0.43 mmol TMOS were added to a solution of 10 mL DI water at pH 9 under vigorous stirring, immediately followed by ATTO647N-silane (shown in Figure B1). Next, 0.21 mmol PEG-silane were added followed by heating at 80 °C for 12 hours.

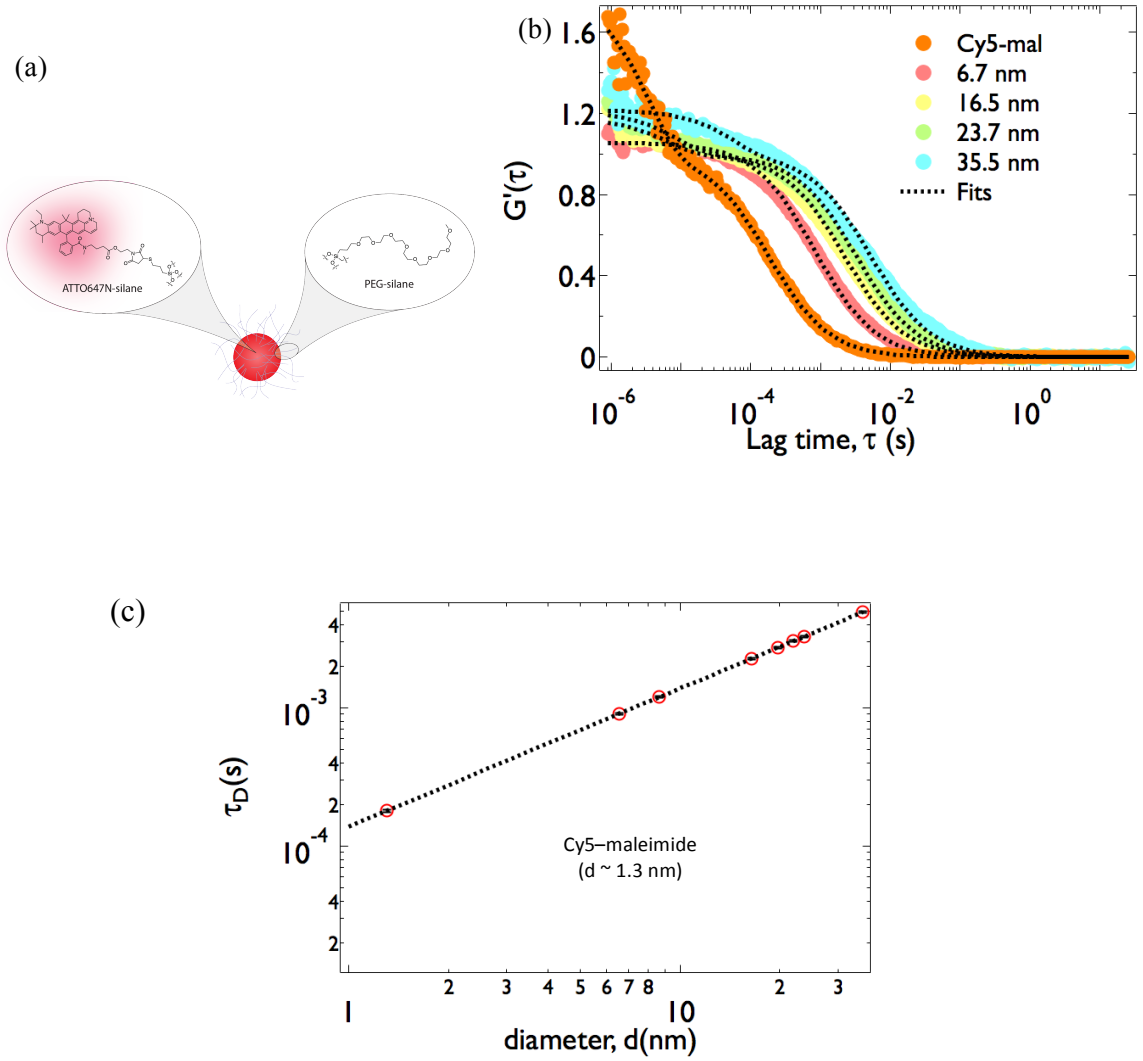

Figure B1. (a) Schematic of Cornell dots (C dots) synthesized with ATTO647N dye. (b) Normalized FCS auto-correlation curves for C dots dispersed in DI water. The dashed lines indicate a diffusive fit to the data with fast relaxation correction (equation 4.2) (c) τ_D vs. d, dashed line shows fitting with Stokes-Einstein relation (~ d).

Fluorescent silica nanoparticles larger than 10 nm were synthesized according to Hartlen *et al*. and Schübbe *et al*.[2,3] In this approach particle growth is achieved by stepwise dosing of TEOS to a seed particle solution under the influence of L-arginine as a catalyst for the hydrolysis of TEOS. First, 0.60 mmol TEOS are deposited on the water air interface of 9.32 mL water containing 66.6 µmol L-argenine and 0.06 µmol ATTO647N-silane, at 60 ºC to form a seed particle. Then, dye-silane and TEOS are added twice per day until the desired particle sizes are achieved. Finally, particles are PEGylated using 0.21 mmol PEG-silane and heated to 80°C for 12 hours.

To remove excess materials, all particles were dialyzed in a dialysis membrane tube (Pierce, molecular weight cutoff, MWCO 10 000) in 2 L of DI water for three days with three water exchanges. To remove all possible excess dye and obtain narrowly dispersed nanoparticles, all samples were filtered through a 0.2 um syringe filter (Fisher) and fractionated using gel permeation chromatography (GPC). Size of the fractioned particles was characterized via FCS by comparing the particle size and diffusion times of the synthesized particles with the diffusion time and diameter for Cy-5 dye molecules as seen in Figure B2 and Figure B3. Particles with hydrodynamic diameters of 6.7 ± 0.1 nm, 16.5 ± 0.2 nm, 23.7 ± 0.3 nm, and 35.5 ± 0.7 nm were obtained for further experiments. The emission and absorption spectra of these particles, shown in Figure B2, indicates that the fluorescence response of the particles is similar to Cy5 dye.

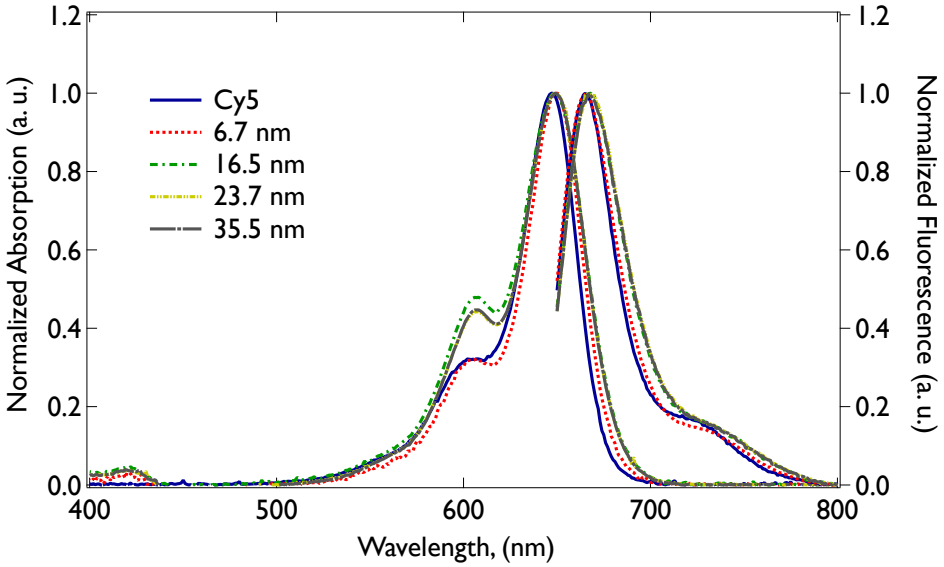

Figure B2. Absorption (left-axis) and fluorescence emission spectra (right-axis) vs. wavelength for C dots.

Table B1: Characterization of C dots used in this study

d (nm) obtained from FCS	d (nm) obtained from TEM
6.7±0.1	4.1±1.2
16.5±0.2	16.4±2.6
23.7±0.3	26.3 ±2.3
35.5±0.7	37.5±3.5

FCS measurements in aqueous solutions of PEO in water:

We use aqueous solutions of linear polyethylene oxide (PEO) as model systems for study of length scale dependent probe dynamics in polymer solutions. The density of PEO is assumed to be constant at 1.12 g cm^{-3} and M_e = 2000 g mol^{-1} and M_c = 5870 g mol^{-1}. For the purpose of our calculations we have considered water to be a good solvent for PEO (irrespective of polymer molecular weight).

Hence the values of characteristic length scales are:

$$\xi = b * \phi^{-0.76} \tag{B1}$$

$$a(\phi) = a(1)\phi^{-0.76} \tag{B2}$$

The Kuhn length, *b*, is taken to be 1.1 nm and the melt tube diameter, *a(1)*, is 3.73 nm.

We limit the use of FCS to measurements of particle dynamics for d/a < 1 as in the regime where particle size becomes comparable or larger than the tube diameter in the polymer solution, time taken by the particle to diffuse out of the confocal volume becomes longer than the photo-bleaching time of dye molecules. As a result, we observed a drop in the fluorescence intensity with time and were unable to obtain reproducible correlation curves for *d/a* around or greater than 1 (shown in Figure B3). The normalized fluorescence autocorrelation curves for 6.7 nm C Dots dispersed in solutions of 35 kDa PEO in water is given in Figure B4. The corresponding diffusivity data is plotted in Figure 4.2 and Figure 4.3 in Chapter 4. Similarly sample autocorrelation curves for 6.7 nm C Dots dispersed in 1352 kDa PEO solutions are given in Figure B5.

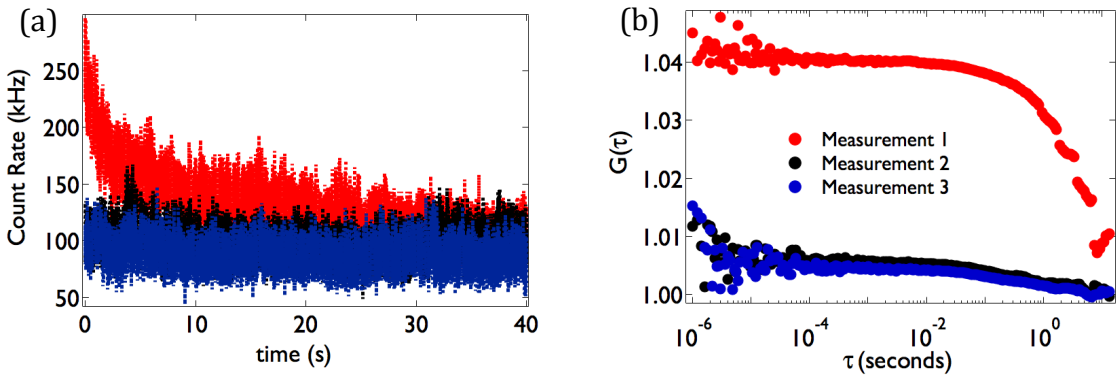

Figure B3. Photobleaching of C dots in concentrated 1.352 MDa M_w PEO solution in water indicated by (a) drop in fluorescence count rate and (b) changing correlation curves

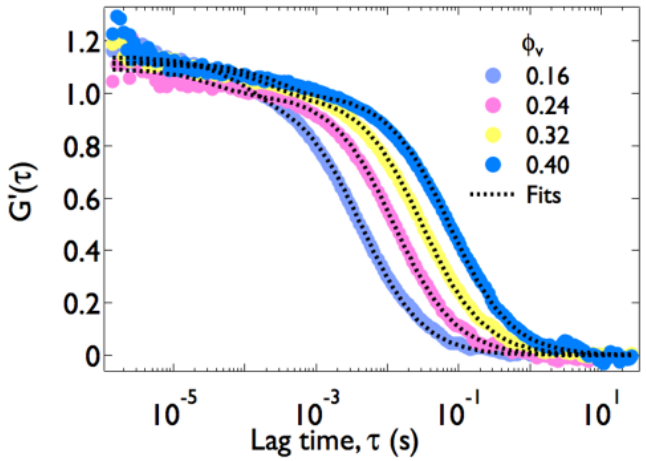

Figure B4. Fluorescence intensity autocorrelation curves plotted against lag time for 6.7 nm particles dispersed in 35kDa PEG solutions in water. The dashed lines indicate a diffusive fit to the data with fast relaxation correction (equation 4.2 in Chapter 4). The obtained diffusivity values are plotted in Figure 4.2.

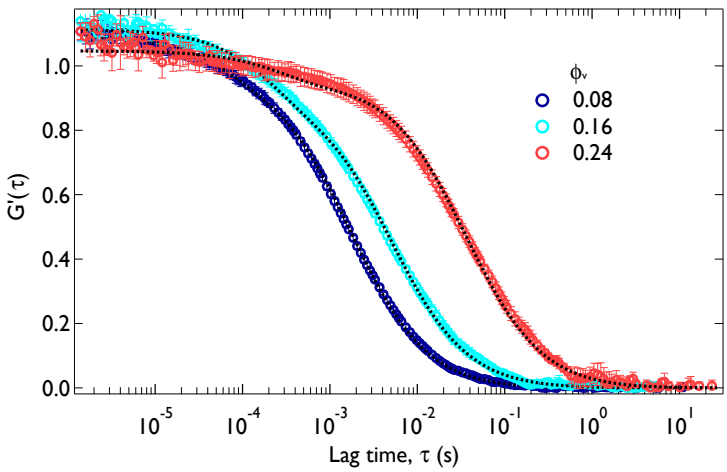

Figure B5. Sample fluorescence intensity autocorrelation curves plotted against lag time for 6.7 nm particles dispersed in 1352 kDa PEG solutions in water in varying concentrations. The dashed lines indicate a diffusive fit to the data with fast relaxation correction (equation 4.2 in Chapter 4).

Table B2: Particle diameter (d), volume fraction (ϕ), the ratio of particle size to correlation length (d/ξ) for 1352 kDa PEO solutions in water.

Mw	*d*	ϕ	d/ξ	*D/Ds*	*D/Ds error*
1352 kDa	6.7 nm	0.01	0.18	0.794	0.005
	6.7 nm	0.02	0.31	0.495	0.022
	6.7 nm	0.04	0.53	0.341	0.012
	6.7 nm	0.08	0.89	0.171	0.007
	6.7 nm	0.16	1.51	0.074	0.003
	6.7 nm	0.24	2.06	0.011	0.0004
1352 kDa	16.5 nm	0.02	0.77	0.160	0.005
	16.5 nm	0.03	1.21	0.119	0.005
	16.5 nm	0.05	1.59	0.082	0.005
	16.5 nm	0.07	2.05	0.033	0.003
1352 kDa	23.7 nm	0.02	1.10	0.059	0.002
	23.7 nm	0.02	1.96	0.082	0.003
	23.7 nm	0.04	2.42	0.040	0.002
1352 kDa	35.5 nm	0.02	1.65	0.015	0.001

Table B3: Particle diameter (d), volume fraction (ϕ), the ratio of particle size to correlation length (d/ξ) for 527.5 kDa PEO solutions in water.

527.5 kDa	6.7 nm	0.02	0.31	0.495	0.022
	6.7 nm	0.04	0.53	0.296	0.014
	6.7 nm	0.08	0.89	0.166	0.007
	6.7 nm	0.16	1.51	0.047	0.002
	6.7 nm	0.24	2.06	0.017	0.001
527.5 kDa	16.5 nm	0.02	0.77	0.178	0.006
527.5 kDa	23.7 nm	0.02	1.10	0.076	0.003
527.5 kDa	35.5 nm	0.02	1.65	0.031	0.002

The diffusivity values for different probes sizes for d/a < 1 in solutions of 1352 kDa and 527.5 kDa PEO are given in Table B2 and Table B3 and these diffusivity values are plotted in Figure 4.4 in Chapter 4.

SPT measurements of C Dots in aqueous solutions of PEO

Oscillatory rheology measurements for were performed to obtain the terminal relaxation times using The crossover frequencies obtained through oscillatory rheology measurements (shown in Figure B6) for 1352 kDa PEO solutions at polymer volume fractions of: $\phi = 0.04$ is 23.7 s-1, $\phi = 0.10$ is 1.9275 s^{-1}, $\phi = 0.16$ is 0.8796 s^{-1}, and $\phi = 0.24$ is 0.2687 s^{-1}. We observed in Figure 4.6 that the transition time from subdiffusive to diffusive behavior for concentrated entangled polymer solutions can last well beyond the terminal time obtained from rheology.

XPCS measurements in PS-DEP solutions

Linear polystyrene of molecular weight 20 MDa has an R_g of ~119.9 nm. We disperse particles of 80 nm diameter (smaller than the polymer R_g) in solutions of 20 MDa PS in DEP and study their dynamics through XPCS (results in Figure B7). The tube diameter of PS melt is taken to be 8.52 nm and the M_e of PS used is 18000 Da. The polymer volume fraction and corresponding values entanglement density and ratio of particle size to tube diameter are reported in Table B4.

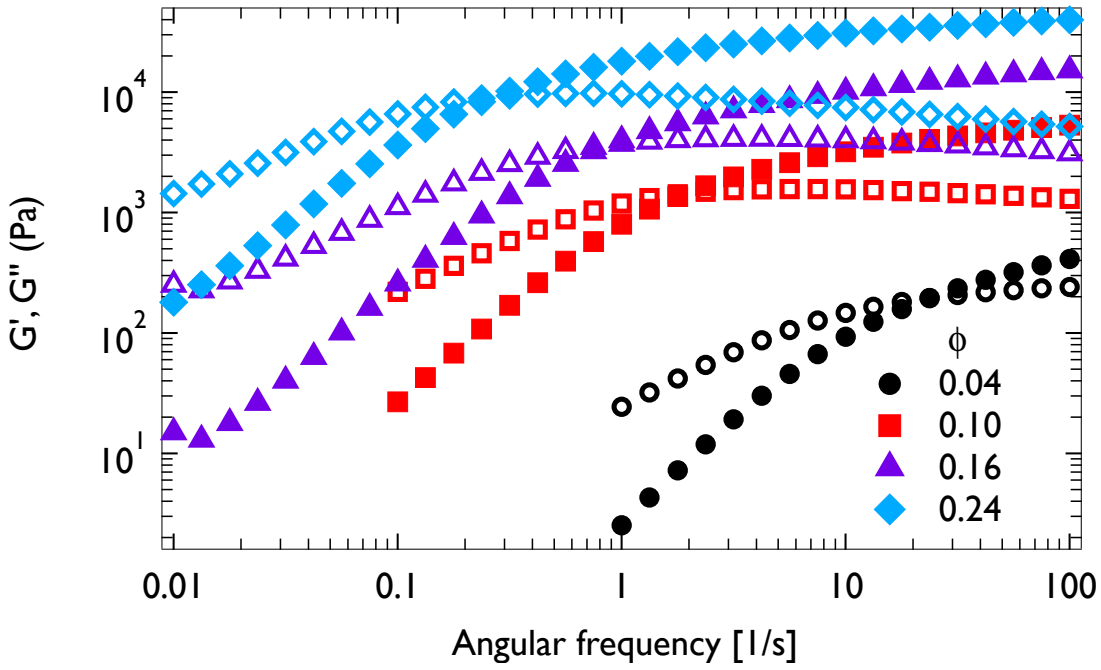

Figure B6. Oscillatory rheology measurements for 1352 kDa PEO solutions in water with PEO volume fraction of 0.04 (circles), 0.10 (squares), 0.16 (triangle-up), and 0.24 (diamonds). Closed symbols are for the storage modulus (G') and open symbols are for the loss modulus (G''). The inverse of the crossover frequency between G' and G'' gives the terminal time.

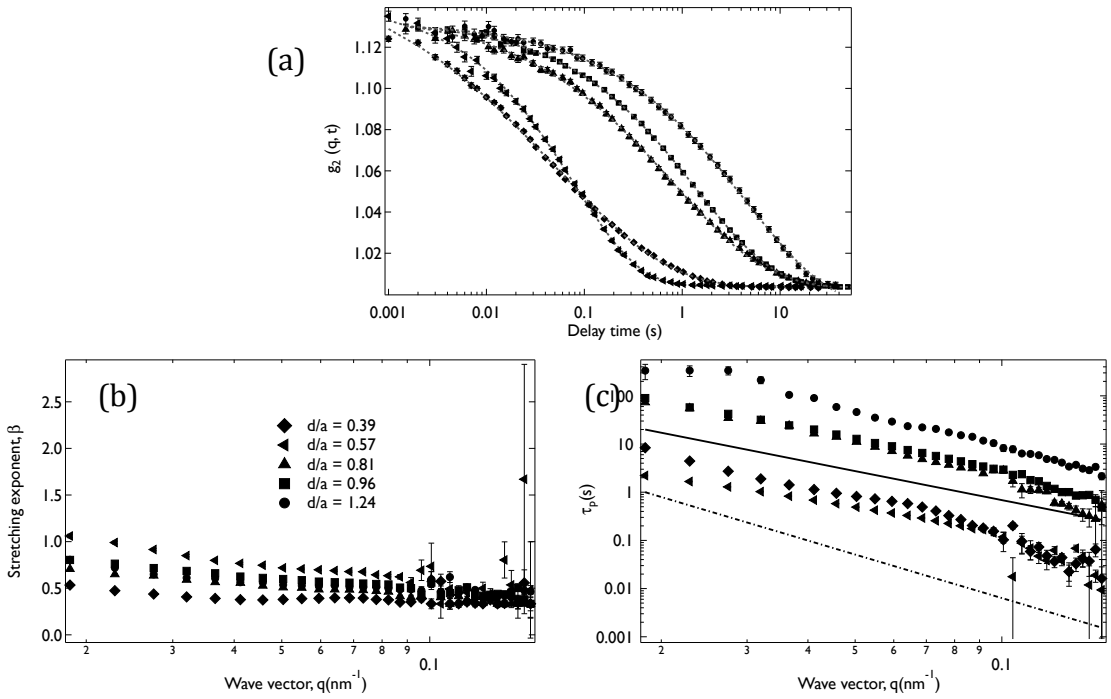

Figure B7. XPCS measurements of intensity autocorrelation curves for different wave-vectors for 1 vol% of 80 nm 10kDa PS-functionalized silica NPs in 20 MDa PS dissolved in DEP at different volume fractions (corresponding to different values of d/a). (a) Intensity autocorrelation functions can be fitted by stretched exponential fits (dashed grey lines) at q = 0.078 nm^{-1}, (b) β is the exponent for a stretched exponential fit to the intensity autocorrelation function and is < 1 for all samples at short wave-vectors. (c) Particle relaxation time, τ_p, plotted against wave-vector, q.

The dashed line indicates a q^{-3} scaling for subdiffusion and the solid line indicates a q^{-2} scaling for diffusion. Based on the scaling particles appear diffusive at longer length scales and subdiffusive at shorter length scales.

Table B4: Volume fraction (φ) and entanglement density (Z) of PS and the ratio of particle size to tube diameter (d/a) for 80 nm silica probes in PS-DEP solutions.

φ	Z	d/a
0.015	4.17	0.39
0.025	8.22	0.57
0.04	15.36	0.81
0.05	20.67	0.96
0.07	32.34	1.24

REFERENCES:

[1] Ma, K.; Mendoza, C.; Hanson, M.; Werner-Zwanziger, U.; Zwanziger, J.; Wiesner, U. Control of Ultrasmall Sub-10 nm Ligand-Functionalized Fluorescent Core–Shell Silica Nanoparticle Growth in Water. *Chem. Mater.* **2015**, *27*(11), 4119–4133.

[2] Hartlen, K. D.; Athanasopoulos, A. P. T.; Kitaev, V. Facile Preparation of Highly Monodisperse Small Silica Spheres (15 to >200 nm) Suitable for Colloidal Templating and Formation of Ordered Arrays. *Langmuir* **2008**, *24*(5), 1714–1720.

[3] Schübbe, S.; Cavelius, C.; Schumann, C.; Koch, M.; Kraegeloh, A. STED Microscopy to Monitor Agglomeration of Silica Particles Inside A549 Cells. *Adv. Eng. Mater.* **2010**, *12*(5), 417–422.